DEVELOPMENT OF EXPERIMENTAL INVERSION AND SIMULATION TECHNIQUES TO STUDY PROPELLER BLADE RESPONSE TO INFLOW DISTORTION

T.J. Mueller, D.F. Scharpf, S. Subramanian,
C.J. Sullivan and R.J. Minniti, III

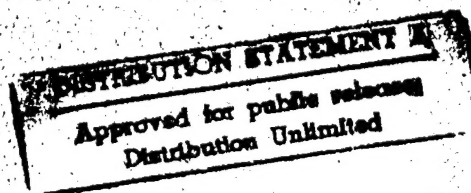## Hessert Center for Aerospace Research

Department of Aerospace and Mechanical Engineering

University of Notre Dame

Notre Dame, Indiana 46556

19951026 098

DEVELOPMENT OF EXPERIMENTAL INVERSION AND SIMULATION TECHNIQUES TO STUDY PROPELLER BLADE RESPONSE TO INFLOW DISTORTION

T.J. Mueller, D.F. Scharpf, S. Subramanian,
C.J. Sullivan and R.J. Minniti, III

UNDAS-FR-1493
February 1995

TABLE OF CONTENTS

FORWARD

INTRODUCTION

Marine propellers usually operate either in the non-uniform wake of a submarine or skewed flow under the stern of a surface ship. Therefore, the flow upstream of marine propeller blades is characterized by irregular patterns which are caused by various mean flow distortions due to the boundary layer growth on the hull of the ship, turbulent viscous wakes of upstream bodies (e.g., Hyun and Patel (1991)) or obstacles (e.g., Groves et al (1992)). Whether the inflow to the propeller is steady or unsteady, uniform or non-uniform, the flow over and downstream of the blades is unsteady. This unsteadiness can be due to a separation bubble near the leading edge of the blade, separated flow from the blade before the trailing edge, as well as tip and hub vortices. The unsteady flow over the blades produces unsteady hydrodynamic forces (i.e., excitations) which result in unwanted vibrations and noise. Inflow nonuniformities give rise to tonal and narrow band noise centered around the blade passing harmonics. Additional broad band signatures are superimposed due to turbulence-trailing edge interaction. Highly non-uniform and asymmetric inflows further exaggerate these effects.

Both theoretical and experimental research on the response of propellers, especially the unsteady force, in various flow conditions have been reported (Blake 1986, Chapter 12). Sevik (1974) was one of the first to investigate the unsteady force on propellers in turbulent flow. His model sought to predict thrust spectra for propellers with an isotropic turbulent approach flow. The predictions of this theory agree reasonably well with the broad band base of the measured response from water tunnel experiments. Boswell, Jessup and Kim (1981) studied the unsteady force on marine propellers in inclined and non-uniform velocity fields to help validate existing theories of Kerwin and Lee and others. Using Sevik's work as a base point, the theory was advanced considerably by Martinez and Weissmann (1990) and Martinez (1991), who included blade to blade effects in the theoretical modeling. This model evolved to predict the experimentally observed shifts in the peak response to a frequency greater than the blade passage frequency for isotropic turbulent approach flow. Jessup (1990) addressed the experimental verification of existing unsteady propeller lifting surface theory by measuring the unsteady force on propellers in turbulent flows in the David Taylor Research Center Water Tunnel. This effort concentrated on turbulent flows with wake harmonics of multiples of the blade passage frequency and advanced previous work done with wake harmonics at the blade passage frequency. A dynamometer equipped with strain gauges was used to determine the unsteady force spectra. Jiang, Chang and Liu (1991) also contributed to the theory. They followed Sevik's approach but included the rotational effect of the blade which was not included by either Sevik or Martinez. The results showed an improvement over previous theory in agreement with experiment, especially in the peak responses near the blade passage frequency. Theoretical research is continuing at Notre Dame on the propeller-gust problem (e.g.,Atassi and Subramanian (1991)).

1

Although much analytical research has been done in the area of noise generated by propellers in turbulent flows, very little experimental data exists to verify these theories. One of the problems with comparing these theories and experiments is that the majority of the experimental data is lacking in the physical quantities which characterize the turbulent or distorted inflow. The data that does provide the necessary quantities, i.e. turbulence intensities, length scales, and spectra, do not go beyond these fluid-mechanic measurements to understand the flow field aft of the rotor. The physical process by which the propeller alters this incoming flow and generates noise, especially for a turbulent inflow, is virtually untouched by previous researchers.

EXPERIMENTAL PROGRAM AT NOTRE DAME

The sources of noise from lifting surfaces experiencing unsteady pressures are well known, however, the magnitude of their relative contributions to the overall noise level is not. The difficulty is that many of the noise sources operate synergistically. This causes problems in decoupling the source mechanisms and identifying the dominant sources of rotor noise. Therefore, in order to predict the surface response, it becomes important to relate the aeroacoustic production to the characteristics of the flow field and the magnitude of the unsteady forces experienced by the surface. To this end, a series of experiments have been developed to expose a propeller or rotor to various known turbulent and non-uniform inflows and to investigate the characteristics of thin airfoils in unsteady lift conditions. Measurements of the resultant sound pressure levels and unsteady surface pressures are taken. Flow visualization and hot-wire measurements are used to characterize the non-uniform inflow which aid in the theoretical identification of noise sources and prediction of acoustical response.

Turbulent Inflows

The first experiments, by Scharpf and Mueller (1993 and 1995), exposed a four-bladed research propeller to uniform turbulent inflows. Appendix A contains a copy of Scharpf and Mueller, 1995. These experiments consisted of placing turbulence producing grids over the inlet of the Anechoic Wind Tunnel and measuring the radiated sound from the propeller. Extensive hot-wire measurements and flow visualization were used to characterize the inflow conditions. The results of this study were divided into two categories, discrete tone generation and broad-band noise generation.

Discrete Tone Generation

The measured turbulence length scales were found to be less than the length necessary for blade coupling and the radiation of tones at the blade-passage harmonics (BPHs). Because of this, the acoustic tones at the BPHs were attributed to stationary disturbances in the velocity field. The hot-wire spectra obtained downstream of the blades are the result of the velocity fluctuations in the plane directly behind the propeller. The dominant hot-wire frequencies in these spectra were at the

blade passage frequency because of the periodic nature of the wake. The fact that a high coherence did not exist between the hot wire and the microphone signals at the BPH despite the dominant hot-wire signal at this frequency in each of the individual spectra leads to the conclusion that the trailing edge effects were not responsible for generation of noise at the blade-passage frequency (BPF). Other evidence supporting this hypothesis was that the noise at the BPF was mainly due to the steady blade-loading which appears unsteady from the microphone frame of reference, (i.e., Gutin noise). Since the hot-wire signal was measuring the velocity fluctuations in the wake, it was not influenced whatsoever by the steady blade loading and therefore was not correlated with the noise at the BPF. For the clean flow (i.e., very low turbulence with no grids present) the entire blade span showed high coherence values at the first BPH, while the inflow turbulence reduced the coherence in the mid-span region.

The interaction of the frequency modes in the propeller wake were identified by the bicoherence measurements. From the clean flow experiments, the interactions between multiples of the BPF occurred near the hub and tip regions which indicated that the interactions in these regions were primarily non-linear. The low bicoherence values at multiples of the BPF in the mid-span region of the blade, ($r/R \approx 0.7$), indicate that very little of the energy transfer was due to nonlinear effects. If these coupling effects are viewed as the manner in which the flow leaves the blade trailing edges, then the resulting unsteady forces on the blades can be related to these flow interactions, and hence the hub and tip regions may be sources of noise at multiples of the BPF. The fact that the hot wire was not rotating with the blade however, indicates that the bicoherence values are a function of the flow directly behind the entire propeller disk, and not solely due to the passage of flow over the blade trailing edge.

Broad-Band Noise Generation

An increase in the integrated broadband Sound Pressure Level (SPL) of approximately 2 dB for every 1% increase in the turbulence was measured. From Figure 1, the slopes of the curves revealed the change in the radiated noise in each frequency band. For the same increase in turbulence the high-frequency bands experienced a much more rapid increase in the SPL than the low-frequency bands, but the magnitude of the SPL's in the low-frequency bands were at higher levels than those in the high-frequency bands. Assuming that the frequencies in the turbulence spectrum are responsible for the radiated noise at the same frequency, then the resulting higher SPL's in the low-frequency bands can be attributed to the large-amplitude fluctuations in the turbulence at those frequencies. These large-amplitude fluctuations cause the largest variation in the blade angle of attack and hence large fluctuations in the lift force.
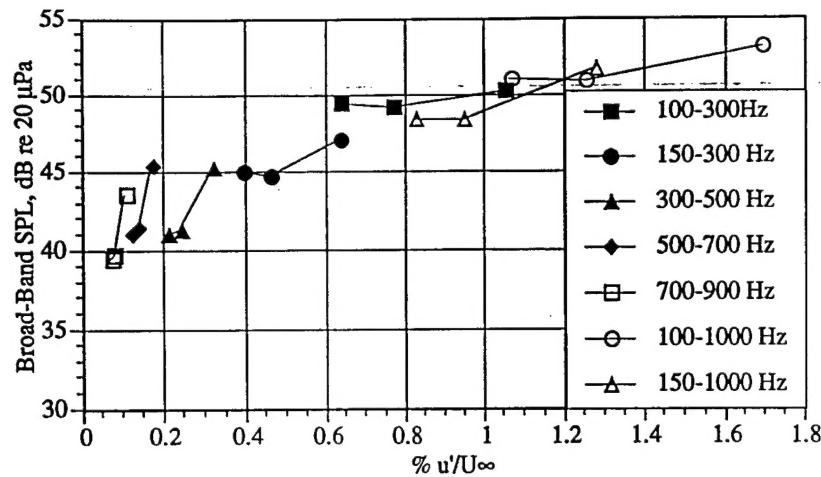
3

Figure 1. Integrated Broad-Band Sound Pressure Level as a Function of Inflow Turbulence for Selected Frequency Bandwidths.

Since the noise in question is broadband, it may be tempting to neglect the effect of the periodic cutting of the turbulent eddies by the propeller blades. The bicoherence measurements however, indicate that there is a certain amount of phase-coupling between the harmonics of the blade-passage frequency and the broadband frequencies in the wake flow. The influence that this coupling has on the fluctuating blade forces responsible for the noise radiation still remains in question. The decrease in this phase coupling as the turbulence was increased supports the notion that the BPHs do not constructively interact with the broadband frequencies. It should be stressed however that the exact relation between the bicoherence measurements and the blade forces has not been established. Also, the significance of the bicoherence measurements on the noise generation is based on the assumption that the bicoherence is related to the flow over the trailing edge of the propeller blades. No further bicoherence measurements are planned at the present time.

Cyclic Inflow Distortion

The turbulent inflow study was followed with experiments by Subramanian and Mueller (1993 and 1995). Appendix B contains a copy of Subramanian and Mueller, 1995 In these experiments non-uniform inflows were produced with cyclical distortions. The inflows were produced by covering the inlet of the tunnel with screens that contained regions of unrestricted flow equally spaced between regions of slightly restricted flow. The screens were constructed in an attempt to expose the four bladed propeller to sinusoidal variations in velocity as they rotated through the non-uniform inflow. The flow generators provided both a three-cycle and a four-cycle azimuthal variation of the mean velocity. The radiated sound pressure levels were measured and comparisons to theoretical predictions were made.

4

typically rise 10 to 20 dB above the broadband levels. A well-defined axisymmetric directivity exists only for the fundamental tone. Asymmetries in this fundamental directivity appear mostly at locations where the tonal value is low. In contrast, the higher harmonics have a random directivity.

Each screen flow has a unique fundamental harmonic directivity that is representative of the cycle number. The directivity from the three-cycle screen has a smooth decrease from downstream to upstream and has a scatter of 6 dB between the four azimuthal half-planes. This scatter is probably a result of contamination from the fourth mode, which can significantly alter the linear phase relation between the individual blade forces. The propeller radiation from the four-cycle screen has an axial dipole-type radiation that has very little scatter at off-plane regions. Along the propeller plane, the radiation from the four-cycle screen shows an asymmetry at 3600 RPM. It appears likely that the asymmetry at 3600 RPM is caused by the dissipation of one or more shear layers.

The propeller tonal levels due to the three-cycle and four-cycle screens have an excellent agreement with the theoretical trends both in magnitude and directivity, see Figure 2, for example. The noise levels fall within the theoretical spread of ± 3 dB at most locations. At the few locations where the experimental values lie outside the bounds, the discrepancy is well within the experimental uncertainty of ± 0.7 dB. This agreement is true for both propeller speeds.
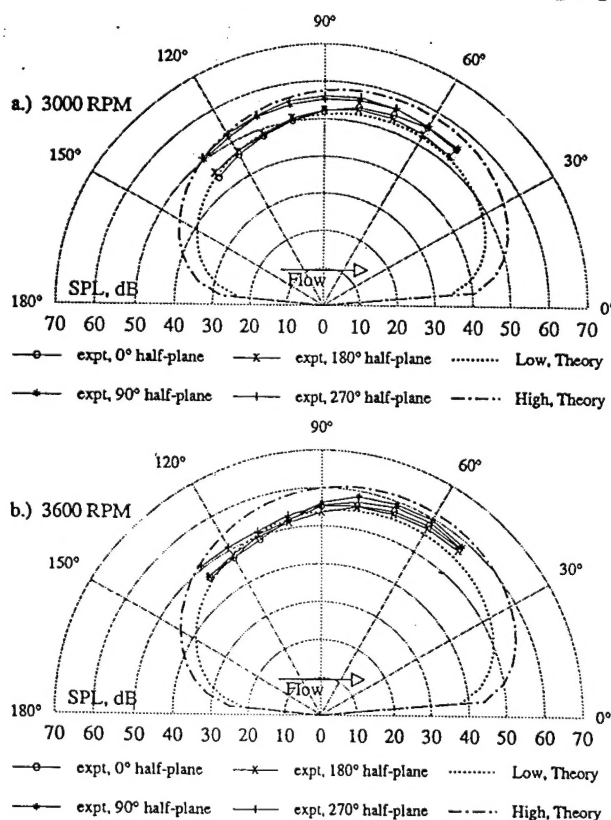

Figure 2.   Comparison bewtween Experiment and Theory for Three-Cycle Flow. (a) 3000 RPM (b) 3600 RPM.

5

THE INVERSE PROBLEM

The theoretical approach to the inverse gust problem of determining the characteristics of the inflow to an aerodynamic surface from its surface pressure response has received very little attention. Patrick and Atassi at Notre Dame along with Blake at DTRC (1994) have helped establish the theoretical basis for the inverse gust problem and the inverse acoustic problem and identified difficulties. The inverse acoustic problem of determining the unsteady pressure over an aerodynamic surface from the far field unsteady pressure was analyzed for compressible flow with a three-dimensional gust. The results showed exact reconstruction of the unsteady pressure for a periodic disturbance of a single frequency. Work on the experimental approach to the inverse problem is also in progress at Notre Dame. Sullivan and Mueller are currently developing experimental inversion techniques to use the unsteady propeller-blade surface pressure to determine the inflow distortion characteristics. In another experimental study, Minniti and Mueller are using a flat plate with a rotating inflow distortion in an attempt to validate the recent theoretical results of Patrick, Atassi and Blake (1994).

Propeller Experiments

A propeller dynamometer system has been developed for the experimental study of inversion techniques for the deduction of propeller flow field characteristics from propeller blade response. The features of this system (Figure 3) include of a Pacific Scientific high-torque DC servo motor, a system of 12 low-noise liquid mercury slip rings and high-precision bearings. The liquid mercury slip rings transfer the rotating signals from the propeller blade instrumentation to the non-rotating reference frame for sampling. Circulating chilled water serves to cool the slip rings and maintain the desired operating temperature.
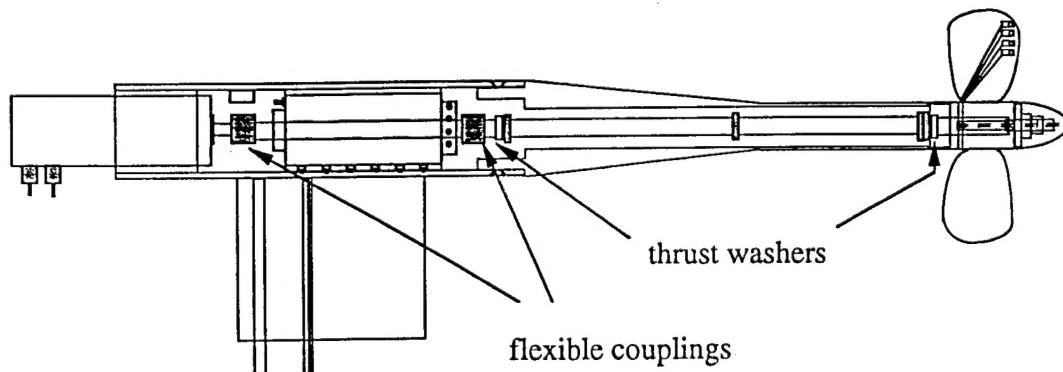

thrust washers

flexible couplings

Figure 3.   Propeller Dynamometer

6

Since the instrumentation of the propeller blades requires drilling holes in the blades, a method for the reproduction of the aluminum propeller provided by the DTRC was developed. A mold was constructed of the existing propeller using casting resin. From this mold, plastic propellers have been produced using a thin-wall casting resin. These propellers are of the same shape and size but of considerably less weight than the original, and allow for permanent modification during sensor installation. Two types of resin with different densities and strengths have been used to produce propellers with resonant frequencies in different ranges. This makes available a choice of which type of propeller is used in an experiment such that the resonant frequencies of the propeller are away from the frequencies of interest.

The propeller is instrumented with piezoelectric sensors that require the circuitry to be close to the sensor for minimal noise intrusion. A circuit board small enough to be incorporated into the dynamometer was developed for this purpose. It was determined that there would be sufficient space in the hollowed aluminum thrust collar (Figure 4a) to which the propeller is secured for the necessary circuits. An annular ring circuit board, as shown in Figure 4b), was designed and etched to receive the piezoelectric sensor circuits such that the necessary signal conditioning could be performed before the signal was sent to the slip rings.
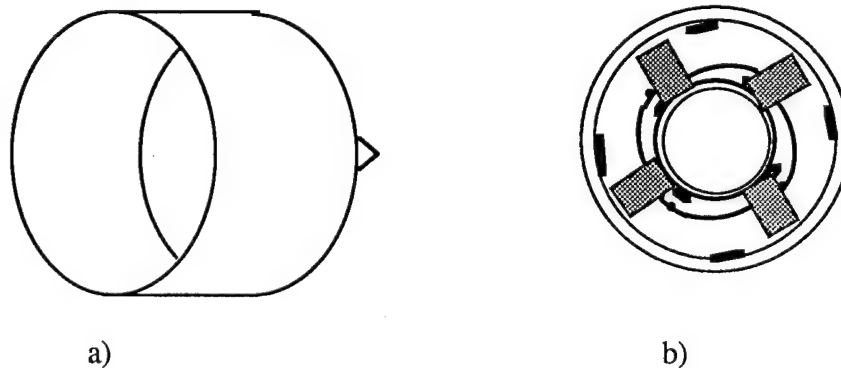

a)   b)

Figure 4. a) Aluminum thrust collar; b) Piezoelectric sensor interface circuit board

Piezoelectric Sensor/Circuit

The circuit developed for use with piezoelectric film can be called a *charge converter*. Utilizing a high input-impedance operational amplifier, a chip capacitor and two 1 GΩ resistors, the circuit was designed to be installed in a relatively small and spinning enclosure. The schematic for the circuit is shown in Figure 5a. The Analog Devices operational amplifier is electrometer grade and thus has a high input impedance. For the configuration used, it is listed as 0.8pF||10$^{15}\Omega$. Other important specifications include an open loop gain of 20,000 and an output resistance of 100Ω, typically. This is important in the verification of the low output impedance of the circuit. The frequency response is listed as 1MHz.

The circuit works as follows. Mechanical deformation of the piezoelectric film results in a build up of charge $\pm Q$ on the surface metalization of both sides of the film element (Figure 5b). This charge is linearly proportional to the strain and stress on the element and changes sign (+/-) with it. The operational amplifier used in this feedback configuration works to maintain the voltage and the current across its differential inputs at approximately zero. For each elemental difference in charge across the inputs of the operation amplifier, the op amp will feedback the appropriate charge such that no charge difference will exist across nodes p and n. In this way the charge across the piezoelectric sensor element will be applied across the feedback capacitor, resulting in a voltage equal to $2Q/C_F$. The feedback resistor serves to provide a decay time constant $R_F C_F$, whereby the output voltage will drain to zero. The corresponding high pass frequency for one half loss of power corresponds to $f_{hp} = 1/R_F C_F$. The resistor from p to common, R_G, serves to tie the output to ground by maintaining an input connection to ground. In the interest of utilizing the common-mode rejection feature of the operational amplifier, the positive input lead was isolated from ground. The voltage at the input nodes is thus $R_G * i_G$ and common AC noise, both of which are rejected. The output voltage then corresponds to the differential voltage of $2Q/C_F$ and a small DC component corresponding to $R_G * i_G$ which is removed by the AC-coupled input to the data acquisition board.
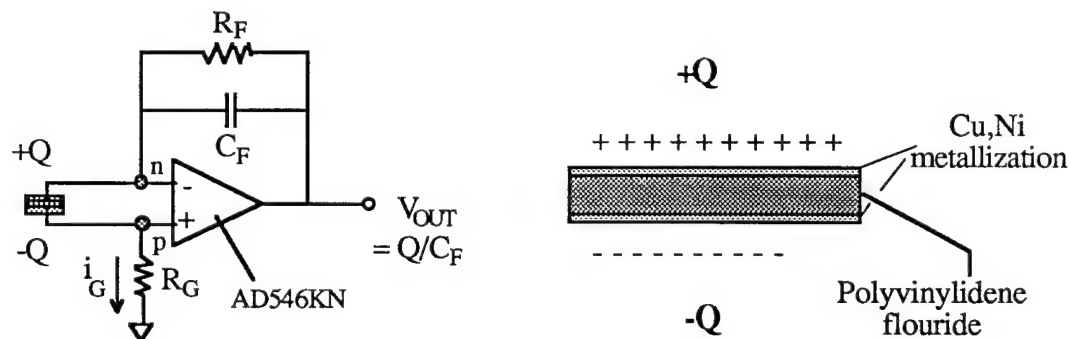

Figure 5 a) Charge conversion in circuit; b) Piezoelectric film cross section

Electrical noise is an issue in any experiment, especially where sensitive instrumentation is being used in close proximity to electromagnetic fields such as those generated by Pulse-Width-Modulated controlled DC servo motors. Special attention has been given to eliminate the sizable intrusion of noise from the servo motor onto the sensor signals. Great improvements in the signal-to-noise ratio have been achieved by a systematic study and application of shielding and elimination of ground loops. The motor has been physically insulated from the dynamometer to reduce

8

induced noise on the sensor circuitry. The motor wires, which carry high frequency and high current signals to the motor where isolated from the instrumentation wiring. The multi-conductor instrumentation wiring was replaced with coaxial cables to reduce the pickup of noise from the surroundings. An alternate method of controlling the motor was also developed to dramatically reduce its electro-magnectic interference noise. This careful and tedious work has resulted in an improvement in signal integrity by reducing electrical noise from levels of 0.4 volts peak-to-peak to less than 0.0001 volts and has allowed us to continue on to the main objective of the current research.

Signal processing developments have been achieved to facilitate the measurement of unsteady pressure using piezoelectric sensors with a frequency-domain calibration. Since the sensitivity of the piezoelectric sensor is not flat over all frequencies, an inverse filtering method was developed to transform the data taken by the sensor into what it would be with a flat response transducer. The raw signal from the piezoelectric sensor (see Figure 6a) is taken and decomposed into its complex Fourier representation, then this is multiplied by the calibrated sensitivity in the frequency domain. Finally an inverse Fourier transform is performed on the signal returning it to the time domain. The final signal is the equivalent signal for a calibrated, flat response transducer (see Figure 6b).

a) Raw Signal   b) Final Calibrated Signal
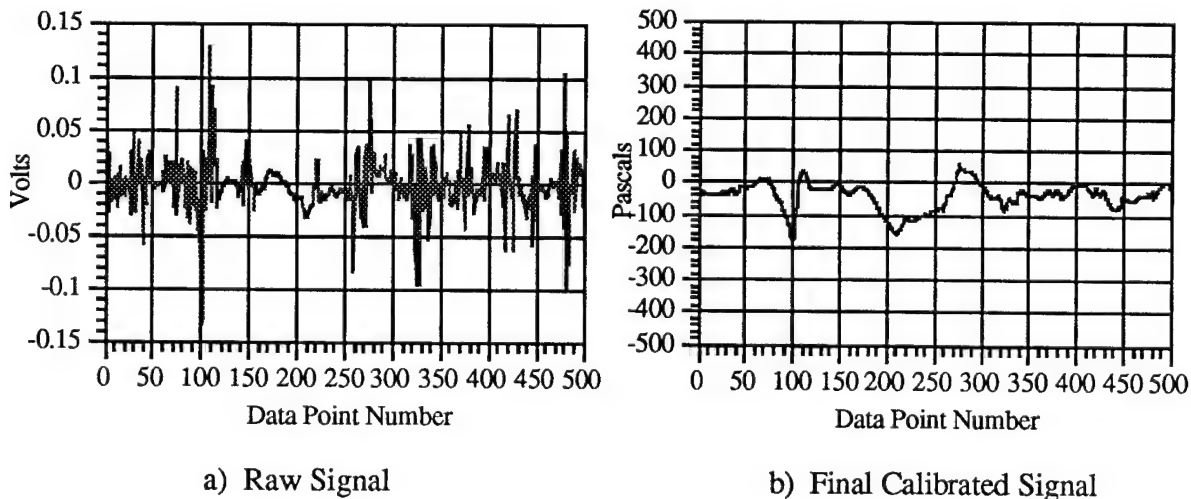
Figure 6.   Example of inverse filtering method to account for
                 piezoelectric sensor response.

Steps have been taken to remove the effect of vibration on the measurement of unsteady pressures by the piezoelectric sensors. A new mounting procedure was developed to insulate the sensors from vibration and any surface stress on the propeller blade. New propellers were constructed with a higher density epoxy such that resonant frequencies were moved away from the frequencies of interest. This facilitates the measurement of unsteady pressures for use in the inverse problem determination.

9

Propeller Flowfield Inversion

The opportunity for inversion of the propeller blade response to determine inflow distortion characteristics springs from the Sears function. It has been shown that for a flat plate in a sinusoidal gust normal to the plate with no spanwise variation of the gust, the unsteady lift per unit span may be related to the gust amplitude and phase by the equation

$$\frac{dL(k_1)}{dy_3} = \pi\rho c U_\infty \tilde{u}_2(k_1,\omega) S_e(k_1 c/2) e^{-i\omega t} \tag{1}$$

where L, $\tilde{u}_2$ and S_e are complex functions. The deduction of the complex gust, $\tilde{u}_2$, is found by simple manipulation of the equation.

$$\tilde{u}_2(k_1,\omega) = \frac{dL(k_1)/dy_3}{\pi\rho c U_\infty S_e(k_1 c/2) e^{-i\omega t}} \tag{2}$$

To include variations in spanwise wavelength of the incident gust, the variation may be written as (see Blake, 1986)

$$\frac{dL}{dy_3}(y_1,y_3,k_1,k_3,\omega) = 2\rho U_\infty \tilde{u}_2(k_1,k_3,\omega) S_{2D}(k_1 c, k_3 c) e^{+(k_3 y_3 - i\omega t)} \tag{3}$$

where S_{2D} is a two-dimensional Sears function. Blake reports the form given by several investigators for the pressure difference between upper and lower surfaces with the origin at the midchord.

$$\Delta p(y_1,y_3,k_1,k_3,\omega) = 2\rho U_\infty \tilde{u}_2(k_1,k_3,\omega) \sqrt{\frac{\frac{c}{2} - y_1}{\frac{c}{2} + y_1}} S_{2D}(k_1 c, k_3 c) e^{+(k_3 y_3 - i\omega t)} \tag{4}$$

For a given k_3, equation (4) is only a variation of equation (1) and is as easily invertable. Thus the successful inversion of this two-dimensional problem requires the local k_3 value. Dividing the propeller blade into spanwise strips and ignoring thickness variation, each section may be looked at as approximately a flat plate. Instead of the two-dimensional Sears function, which is a particular Green's function for its given system, we are looking for the Green's function of the blade. Using the radially adjacent sensors near the leading edge to help determine the local

k3 value, the local Green's function can be determined by experimental measurement of the pressure response of the blade and measurement of the complex gust. This information provided over an array of sensors and radial locations can then determine a strip Green's function for the entire blade. At a particular sensor location, y_3, the Green's function may be determined from

$$G_{y_3}(k_1 c)e^{+(\phi - i\omega t)} = \frac{\Delta p(k_1, \omega)}{\widetilde{u}_2(k_1, \omega)} \tag{5}$$

Placement of Sensors/Determination of k3

The initial investigation will determine the k_3 value for the gust on the blade. Modeling the blade section of interest as part of a flat plate, the signal from the sensors can be analyzed using cross-spectral techniques to determine the spanwise wavelength for the gust convecting along the chord. The distance between the sensors must be smaller than the wavelength in the y_3 direction (see Figure 7a). Otherwise the k_3 value will be fallacious. The *phase* between adjacent sensors can be determined using the cross-spectrum of their signal. And this in turn, along with their separation distance, will give the wavelength in the y_3 direction. If the sensor separation were larger than the actual wavelength, then results would show a phase lag that was off by a factor of $2\pi n$. This is the equivalent of aliasing in spatial sampling.
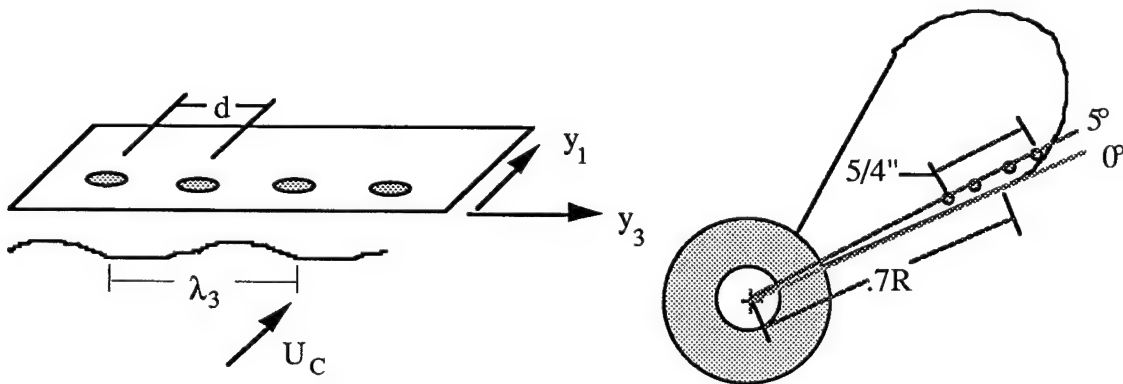

Figure 7. Spatial array of transducers in initial investigation of y_3 gust variation.
a) determination of wavelength in y_3 direction; b) current configuration of sensors on blade

The first tests are being performed with a sensor spacing of 3/8" spacing between the first and second sensor centers, 1/2" between the 2nd and 3rd and 3/8" between the third and fourth, as shown in Figure 7.b. This gives a range of spacings between specific sensors ranging from 3/8" to 1-1/4". Sensor positions were determined by centering the array on the .7R radial location and drawing a line parallel to the effective leading edge as shown in Figure 7.b. By varying the

11

spacing between the sensors (i.e. $\Delta r_{1,2} = 0.375"$, $\Delta r_{2,3} = 0.500"$), the minimum spatially determinable wavelength over the whole array becomes 0.125", a significant improvement over the 0.375" if the sensors were uniformly distributed at 3/8" apart.

Determination of Complex Gust

The determination of the complex gust from the blades reference frame will be done using hot-wire annemometry, specifically an X-wire probe and the IFA 100 annemometry system. By traversing the probe in a circumferential fashion and taking mean and standard deviations of the signal, both the mean velocity and turbulence intensity will be determined(Figure 8.a). The mean velocity over this circumference will then be mapped into gust of period 1/n (Figure 8b) for each radial location, maintaining the original form of the velocity variation, but converting it into the cyclical pattern that the blade would see. This will then be transformed into the Fourier domain for use in the determination of the local Green's function.
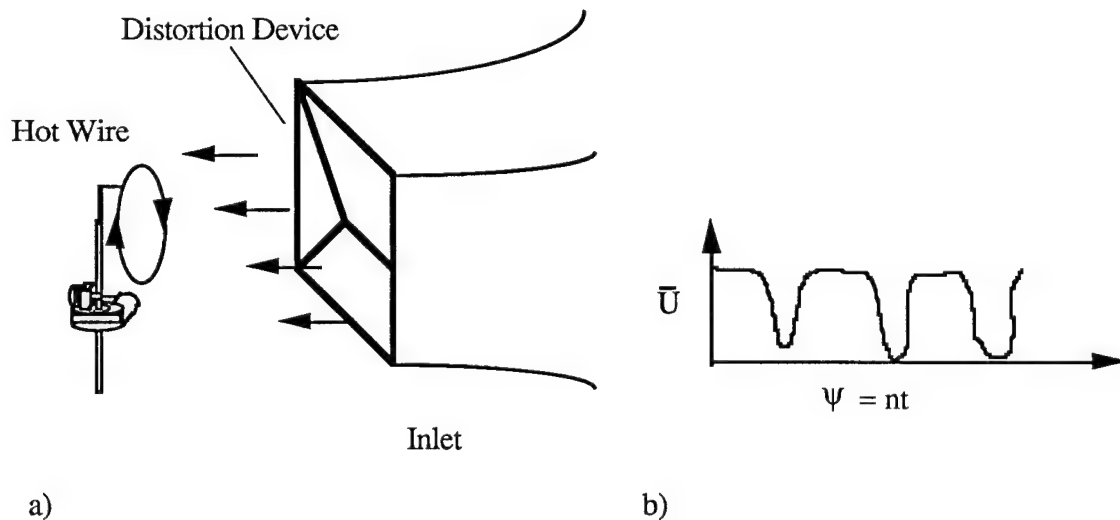
Distortion Device

Hot Wire

$\bar{U}$

$\psi = nt$

Inlet

a)   b)

Figure 8.   a) Circumferential hot wire configuration for determination of inflow
                       distortion; b) Mean velocity variation over one complete rotation

Preliminary Results

The calibration system has been developed utilizing a B&K intensity coupler, a B&K 1/2" microphone, a 4" Radio Shack® Woofer, and a brass horn section from a musical instrument.
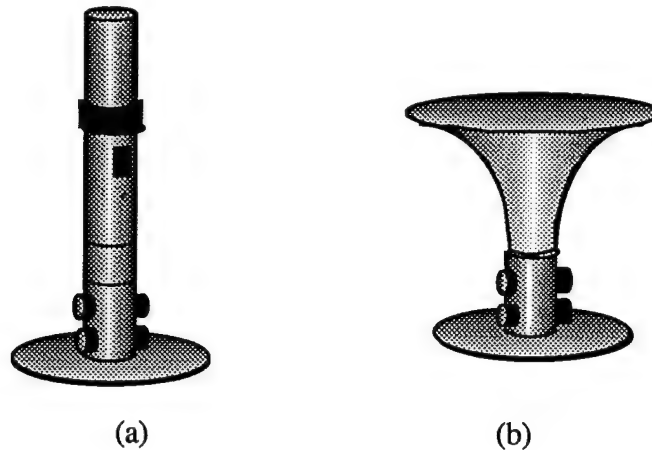
12

Figure 9.   (a) Standard Intensity Coupler Configuration with Pistonphone;
             (b) Configuration of calibration system using B&K Intensity Coupler and brass
             horn section .

The 4" woofer connected to a relatively large piece of aluminum which is in turn suspended from part of the microphone boom using some steel wire and a turnbuckle. A flat piece of cardboard, approximately 12" X 12", is fitted around the face of the speaker to increase its efficiency. The entire apparatus is then positioned above the intensity coupler/horn assembly shown in Figure 9 (b). A brass insert assembly was constructed to fit into one of the coupler's microphone ports, such that the surface of the tested piezo sensor is at the same distance from center as the microphone diaphragm. The piezo sensor mounts directly onto the inner insert of the brass assembly. The piece is inserted into the remaining portion of the brass assembly until it is fully seated. It is then backed out slightly (~1 mm) so that it is more isolated from structural vibration. This was discovered by trial and error. Calibrations were made initially on a sensor and circuit that were completely independent from the dynamometer. The results of this calibration showed the desired response. Next a calibration was performed on a sensor and circuit partially installed in the dynamometer. By partially installed, it is meant that the circuit *is* installed in the dynamometer and the sensor is connected to the circuit, but the sensor itself is not physically mounted to the propeller blade. Mounting of the sensor follows the calibration.

In the calibration process, a white noise electrical signal is sent to the 4" woofer through a Realistic® MPA-40 35 Watt P.A. Amplifier. The white noise signal is generated using a Brüel & Kjær ZI 0055 white noise generator. Due to the combination of speaker and the brass horn on the intensity coupler, actual white noise over the frequency range of interest is not generated. To compensate, the built-in graphic equalizer (three band) on the MPA-40 is adjusted to allow the maximum output at the lowest band while limiting the two higher band outputs. The output of the speaker is then adjusted such that the maximum sound level is achieved without saturating the input of the A2150 A/D board.

13

During the calibration process several spectral quantities are examined. Autospectra for the microphone and the sensor are taken, G_{xx} and G_{yy}, as well as the magnitude of the transfer function, $\sqrt{|H(f)|}$, the phase from the transfer function, θ, the coherence, γ^2, and the cross-spectrum, G_{xy}. From the coherence, the validity of the calibration at each frequency can be ascertained.
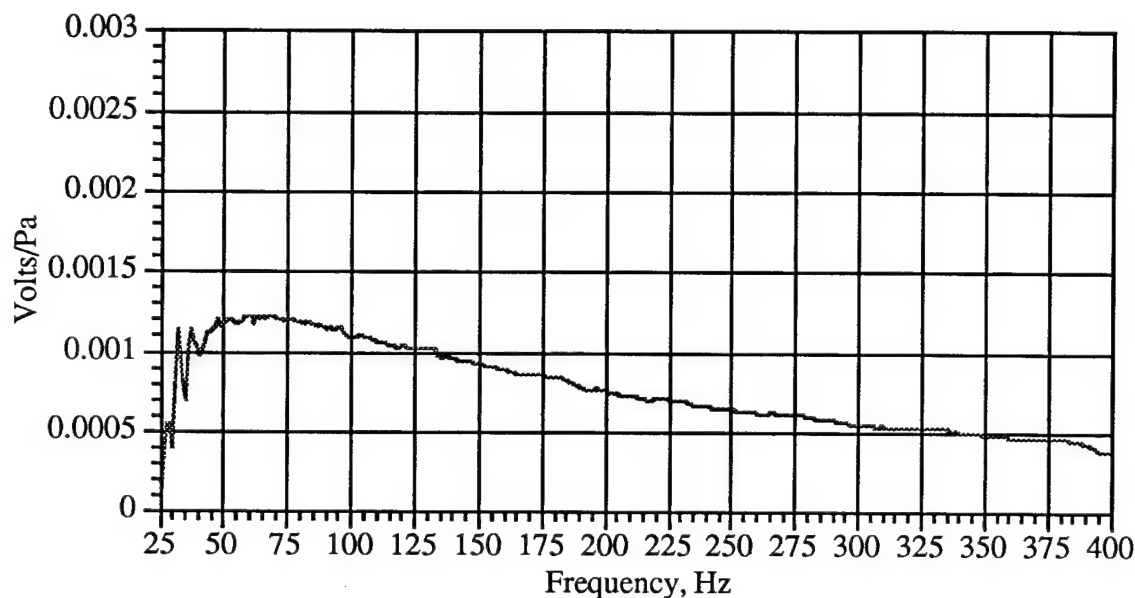

Figure 10.   Calibration of piezoelectric pressure transducer over frequency range of interest.

It can be seen from Figure 10 that over the range of interest (40 Hz to 400 Hz) that the sensor exhibits a fairly regular behavior in the magnitude of the transfer function. A spike can be observed at 60 Hz, which is due to the relatively poor signal-to-noise ratio at *that*   frequency during the calibration with white noise. The phase difference between the microphone and the sensor/circuit combination can be seen in Figure 11. The phase is particularly regular, over the region of interest, though not constant (40 Hz to 400 Hz). With both the phase and amplitude of the transfer function determined, the signal conditioning necessary for conversion of the piezo signal into pressure information can be made.

region of interest, though not constant (40 Hz to 400 Hz). With both the phase and amplitude of the transfer function determined, the signal conditioning necessary for conversion of the piezo signal into pressure information can be made.
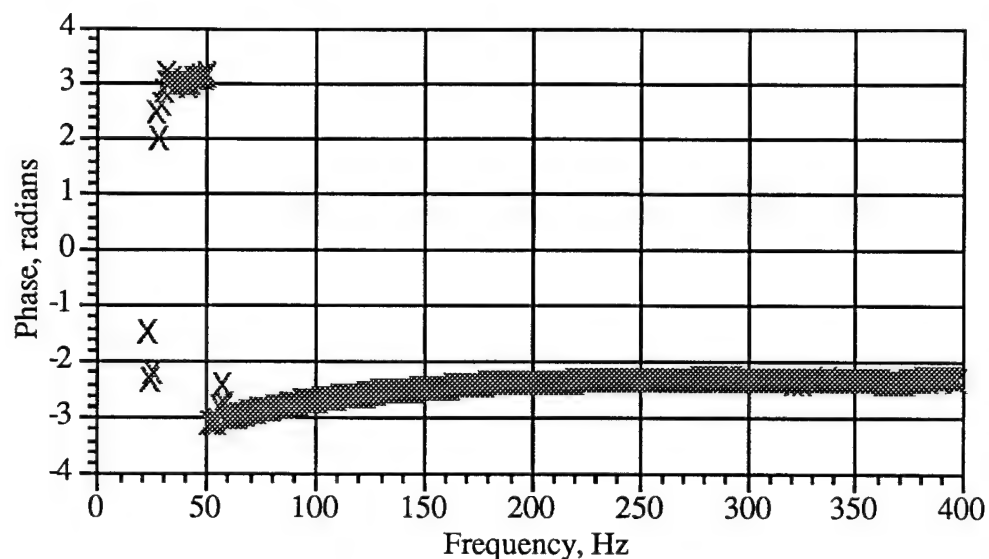

Figure 11   Phase difference between piezoelectric pressure transducer and 1/2" B&K microphone.

The coherence, as mentioned, is useful for qualifying the calibration. The coherence for this calibration is shown in Figure 12.
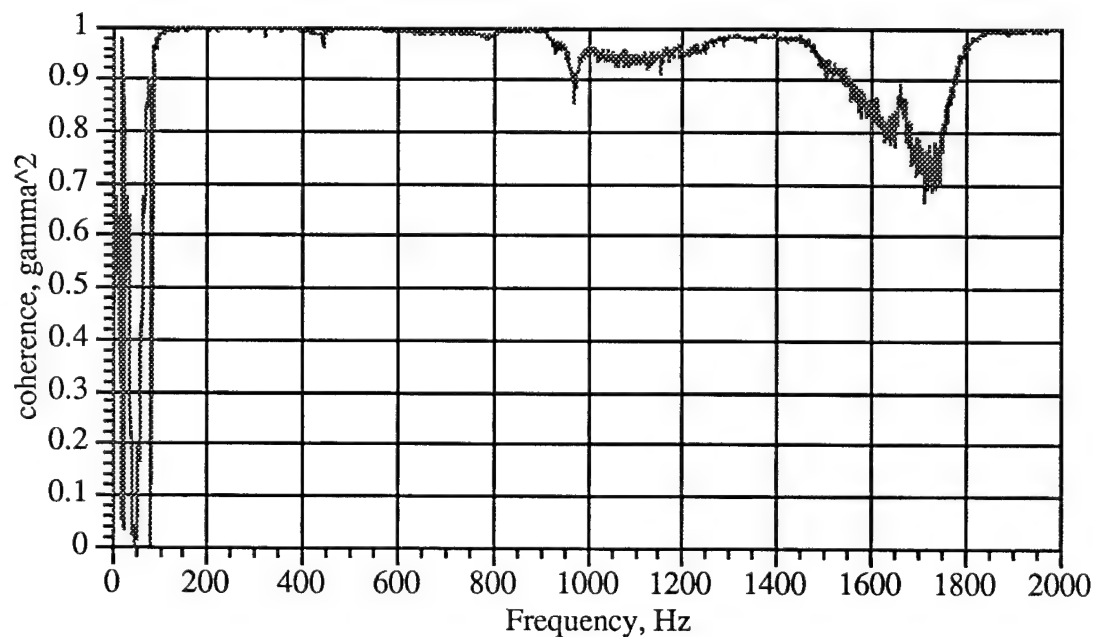

Figure 12.   Coherence, g^2, of microphone and piezoelectric film sensor/circuit for calibration.

Calibrations were made on a number of days and the results compared. The calibrations proved to be consistent within acceptable limits. It should be noted that where coherence levels are calculated to be low, the calibration source level may not be high enough for an accurate calibration. In these regions, individual sine wave pressure signals have been generated to measure the sensitivity of the piezoelectric transducer.

Identification of the major natural frequencies of the propeller blade *in-situ* is completed. With the major natural frequencies identified, care is taken not to run the propeller in a configuration where these natural modes are excited. Outputs of a piezoelectric transducer mounted on the blade and an accelerometer in the hub were analyzed during vibration test to determine these natural frequencies. The system was excited by an impulse from a hammer and the response was recorded and analyzed. As can be seen by Figure 13 the natural frequencies were identified to be 179 Hz and 237 Hz.
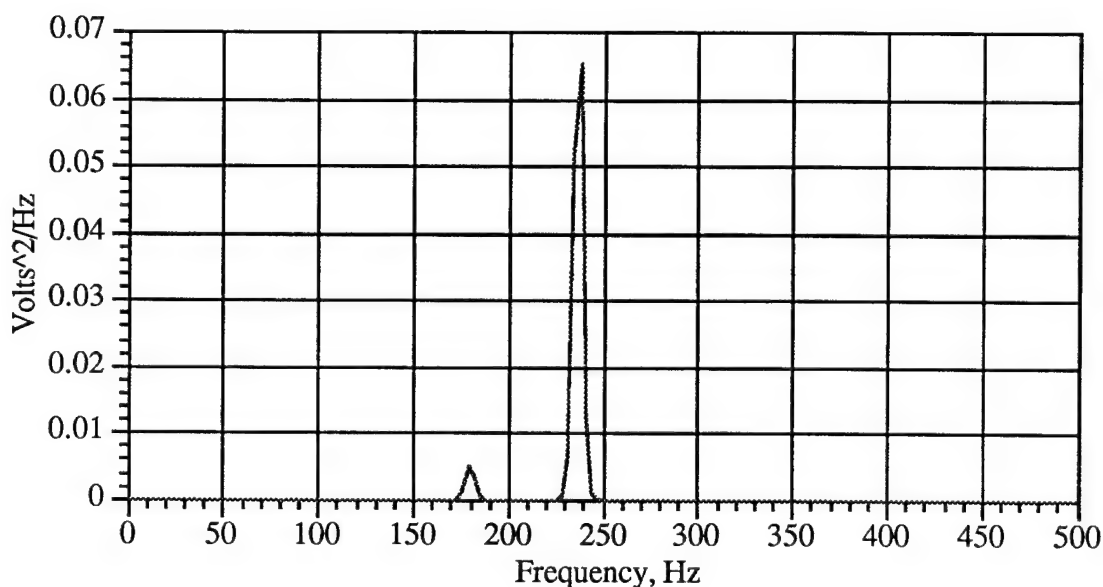

Figure 13.   Vibrational spectrum on propeller blade at 0.575 R location in response to impulse input.

This essentially gives us a map of frequencies to avoid. At these frequencies the output of the piezoelectric transducer can be saturated by vibration induced voltages. The natural modes will be excited to some degree regardless of the experimental configuration, but operating away from these frequencies, we are reasonably assured that the vibration level is kept to a minimum and will have less influence on the integrity of the pressure measurement.

Initial experiments have been conducted using a three-cycle flow distortion device developed by Subramanian and Mueller (1993) (see Figure 14). Using alternating straw sections, a three-cycle distortion is created of higher and lower velocity regions. With this installed

upstream of the propeller, each blade on the propeller experiences a flow distortion at a frequency of three times the shaft rate. Data has been taken and analyzed to provide a base to develop the experimental techniques for the inverse problem.
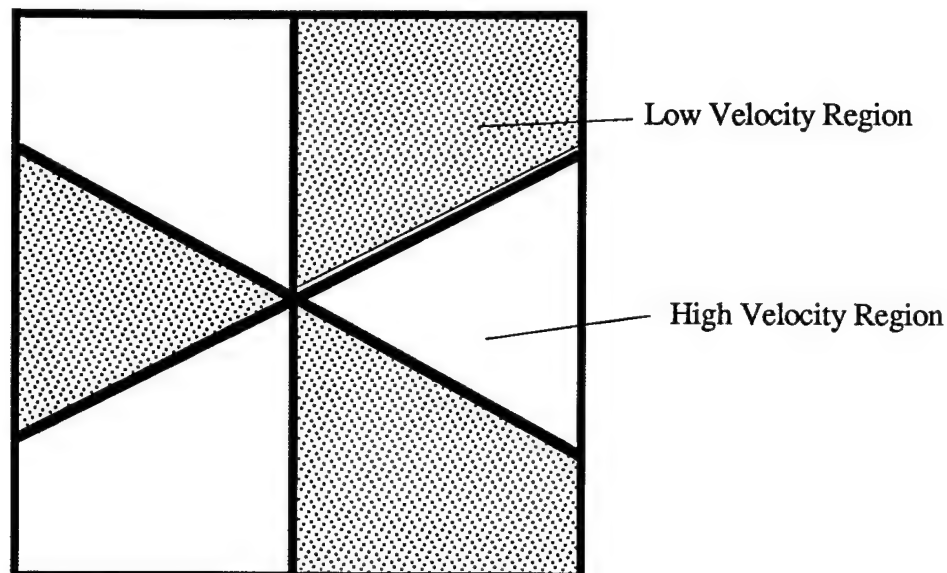

Figure 14.   Three-cycle flow distortion device, view from downstream.
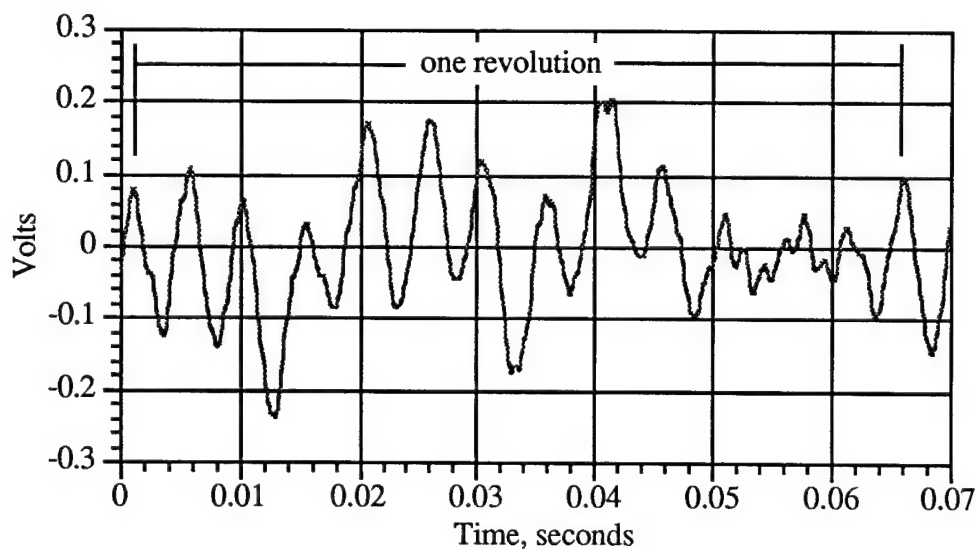

Figure 15.   Raw phase-lock averaged time signal from piezoelectric sensor at 0.575R location in three-cycle test.

Signal analysis techniques have been developed to reduce the influence of vibration and ambient electrical noise on pressure measurements. By phase-lock averaging a number of ensembles of the piezo transducer output (see Figure 15), portions of the signal that do not exhibit coherency with the blade position are attenuated. This includes 60 Hz ambient electrical noise as well as the

17

portion of the piezoelectric transducer signal which results from the natural frequencies of vibration of the system. As long as the rotational rate of the propeller is not a sub-harmonic of one of these frequencies, this portion of the signal will be attenuated. Figure 16 shows the autospectral density function of a phase-lock averaged signal. Both were techniques utilized the same triggering method.
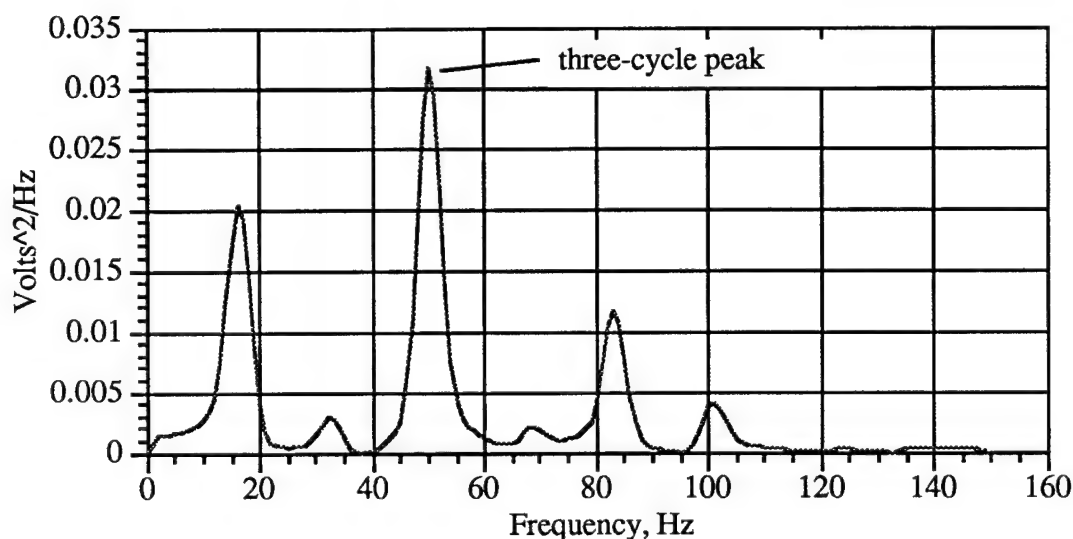

Figure 16.   Ensemble-averaged autospectral density function of piezoelectric sensor output for 3-cycle, 1000 RPM configuration.

The amplitude of the peak at the vibrational frequency of 237 Hz is reduced by this signal processing method. Also, since we are interested in distortions in the mean flow, the phase-lock averaging provides a more desirable measurement of the blade pressure fluctuations, since it is a measurement of the mean pressure at each rotational location.

Using the calibration shown in Figure 10, rms pressure values were determined for the frequencies of interest. For example using the three-cycle frequency of 51 Hz, the amplitude was determined to be approximately 45 Pa. Estimates using Sears function and some basic assumptions were in agreement with this value.

CONCLUDING REMARKS

Work up to this point has been successful in design, construction, and demonstration of the experimental apparati and methods necessary for the inversion of propeller inflow flow fields from pressure measurements on the blades. Vibration measurements have successfully identified the vibrational modes of the propeller blade and have been an integral part of this necessarily methodical investigation. A calibration system was developed, demonstrated and employed on sensors in use in this investigation. Initial pressure measurements of the propeller in a three-cycle

flow distortion have demonstrated the success of all of the previous steps taken to arrive at this point in the investigation.

Efforts are currently underway to expand the current data base to include additional types of distortions. Hot wire measurements of the flow field are forthcoming to provide the necessary upstream information for the determination of the blade Green's function. This along with the additional pressure measurements in the complement of distorted flow fields will provide all of the necessary information for demonstration of propeller flow field inversion.

REFERENCES

Atassi, H. M. and Dusey, M. P., "Acoustic Radiation From a Thin Airfoil in Nonuniform Subsonic Flows," *Prepared for* AIAA 13th Aeroacoustics Conference, October 22-24, Tallahassee, FL, 1990.

Blake, W.K., Private Communications, 1992.

Blake,W.K., Mechanics of Flow-Induced Sound and Vibration, Volume I and Volume II, *Applied Mathematics and Mechanics,* Vol 17-I and 17-II, Academic Press, 1986.

Boswell, R.J., Jessup, S.D., and Kim, K., "Periodic Blade Loads on Propellers in Tangential and Longitudinal Wakes", Propellers '81 Symposium, Society of Naval Architects and Marine Engineering, Virginia Beach, Virginia, 181-202, 1981.

Fujita, H. and Kovasznay, S. G., "Unsteady Lift and Radiated Sound from a Wake Cutting Airfoil," *AIAA Journal,* Vol. 12, No. 9, pp. 1216-1221, 1974.

Groves, N.C., Jiang, C.W., and Liu, Y.N., "Turbulence at the Stern of an Axisymmetric Model With and Without Removable Appendages, DTRC/SHD-1355-03, January 1992.

Hyun, B-S., and Patel, V.C., "Measurements in the Flow Around a Marine Propeller at the Stern of an Axisymmetric Body", Experiments in Fluids , Part I, Circumferentially-Averaged Flow, Vol. 11, pp. 33-44, 1991. Part II, Phase-Averaged Flow, Vol. 11, pp. 105-117, 1991.

Jessup, S.D., "Measurement of Multiple Blade Rate Unsteady Propeller Forces", DTRC-90/015, May 1990.

Jiang, C.W., Chang, M.S., and Liu, 5., "The Effect of Turbulence Ingestion on Propeller Broadband Thrust", DTRC-SHD-1355-02, December 1991.

Kim, K.H. and Fleeter, S., "Compressor Blade Gust Response to Attached Flow Forcing Functions," Published in Unsteady Aerodynamics, Aeroacoustics, and Aeroelasticity of Turbomachines and Propellers edited by H.M. Atassi, Springer-Verlag, 1993, pages 433-451.

Martinez, R., "Numerical Predictions of Thrust Frequency Spectra for the New Penn State Model Propeller Operating in Homogeneous Isotropic Turbulent Flow, " Final Report U-1954-381.2, David Taylor Research Center, May 1991.

Martinez, R., Weissmann, K., "Spatial-Domain Analysis of the Thrust on a Propeller Cutting Through Isotropic Turbulence," Final Report U-1894-358.47, David Taylor Research Center, December 1990.

Mueller, T.J., Scharpf, D.F., et. al, "The Design of a Subsonic Low-Noise, Low Turbulence Wind Tunnel for Acoustic Measurements", to be presented at the AIAA 17th Aerospace Ground Testing Conference, Nashville, TN, July 6-8, 1992.

Patrick, S. M., Atassi, H. M., and Blake, W. K., "Inverse Problems in Unsteady Aerodynamics and Aeroacoustiscs", to be presented at Symposium on Active Control of Vibration and Noise, 1994 International Mechanical Engineering Congress and Exposition, Chicago, IL, 6-11 Nov, 1994.

Scharpf, D.F. and Mueller, T.J. "An Experimental Investigation of the Sources of Propeller Noise Due to Turbulence Ingestion", UNDAS-FR-1783, University of Notre Dame, 1993.

Scharpf, D.F. and Mueller, T.J., "An Experimental Investigation of the Sources of Propeller Noise Due to the Ingestion of Turbulence at Low Speeds", accepted for publication in Experiments in Fluids, 1995

Sears, W. R. . "Some Aspects of Non-Stationary Airfoil Theory and Its Practical Application," *Journal of the Aeronautical Sciences*, Vol. 8, pp. 104-108, 1941.

Sevik, M., "Sound Radiation from a Subsonic Rotor Subjected to Turbulence", Fluid Mechanics, Acoustics, and Design of Turbomachinery, Part II, pp. 493-511, 1974.

Subramanian, S, Mueller, T.J. and Atassi, H.M., "Experimental and Computational Studies on Propeller Noise Due to Inflow Distortion", UNDAS-FR-1783-A, University of Notre Dame, April 1993

Subramanian, S. and Atassi, H.M., "Acoustic Radiation from a Propeller Blade Encountering a High Frequency Gust", Symposium on Flow Noise Modeling, Measurement and Control, ASME Winter Annual Meeting, Atlanta, Georgia, December 1-6, 1991.

Subramanian, S. and Mueller, T.J., "An Experimental Study on Propeller Noise Due to Cyclic Flow Distortions", accepted for publication by The Journal of Sound and Vibrations , 1995.

APPENDIX A

AN EXPERIMENTAL INVESTIGATION OF THE SOURCES OF PROPELLER NOISE

DUE TO THE INGESTION OF TURBULENCE AT LOW SPEEDS

by

Daniel F. Scharpf
Noise Engineering Laboratory
Boeing Commercial Airplane Group
Seattle, WA 98124-2207

and

Thomas J. Mueller
Hessert Center for Aerospace Research
Department of Aerospace and Mechanical Engineering
University of Notre Dame
Notre Dame, IN 46556

NOMENCLATURE

$b^2(f_k, f_l)$	Bicoherence
$B(k,l)$	Bispectrum
B	Number of Blades
c	Speed of Sound
C_T	Thrust Coefficient $= \dfrac{T}{\rho n^2 D^4}$
D	Propeller Diameter
E[ ]	Expected Value
f	Frequency, Hz
$G_{xx}(f)$	One Sided Autospectral Density Function.
$G_{xy}(f)$	One Sided Cross-spectral Density Function.
J	Advance Ratio, $J = U/nD$
j,k	Fourier Component Indices
m	Grid Mesh Length
M_o	Rotational Mach number at a Radial Location $M_o = 2\pi nr/a_o$
M_c	Axial Convection Mach Number
n	Rotational Speed, Revolutions per Second
r	Propeller Radial Location
R	Propeller Radius
R_e	Reynolds Number
T	Propeller Thrust
U_∞	Freestream Velocity
U_i	Induced Axial Velocity from Propeller
u', w'	RMS of Fluctuating Velocity, $u' = \sqrt{(U-u)^2}$
$X(f)$	Fourier Transform of x(t)

Symbols

$\gamma_{xy}^2(f)$ Coherence Function, $\gamma_{xy}^2(f) = \dfrac{|G_{xy}(f)|^2}{G_{xx}(f)\,G_{yy}(f)}$

φ Observer Angle, Measured from Propeller Thrust Direction

λ_f Longitudinal Eulerian Dissipation Length Scale

Λ_f Longitudinal Eulerian Integral Length Scale

ρ Air Density

θ Blade Azimuthal Location

INTRODUCTION

The spectra of the radiated noise from typical rotors consists of broadband noise with superimposed peaks at the blade-passage frequency and higher harmonics. The radiation of harmonics, or tones, is due to the periodic loading on the blades as a result of interactions with the flow or a periodicity inherent in the operation of the rotor. Broadband noise radiation is the result of the passage of the boundary layer over the trailing edge which causes unsteady loading on the blades as well as acoustic scattering from the trailing edge. When non-uniform flow is introduced upstream of a rotor, the unsteady forces increase resulting in higher noise levels. The sources of this noise and the physics involved in the interaction between the inflow and blades has not yet been fully understood, especially at low speeds. In an effort to increase this understanding, detailed measurements of the aerodynamics *and* acoustics involved in this phenomenon were performed.

The noise generated by inflow disturbances can result in the radiation of both broadband and discrete tones depending upon the structure of the turbulence entering the rotor. If the turbulent eddy is long enough it may be cut by more than one blade, which results in blade coupling and the generation of tones near the blade passage. If the eddies are too small to be cut more than once by any of the blades, the result is an induced angle of attack at that particular rotor radius and azimuthal location. As the blade rotates this phenomenon results in random blade loadings which radiate broad-band sound.

George and Kim [1977] indicate that these small eddies generate high-frequency blade loadings modulated to give wide side-bands around each blade-passing harmonic. If however, the eddy is longer, such that it cannot pass through the propeller plane without

being cut by at least two blades, an unsteady force will be generated on these blades resulting in the radiation of sound at the blade-passage frequency.

The effect of the interaction between a rotor and inflow turbulence has also been studied by many other researchers, e.g. Chandrashekhara [1971a,b], Sevic [1974], Mugridge [1976], Aravamudan and Harris [1979], and Trunzo, Lakshminarayana, and Thompson [1981], each of which have improved upon previous analytical estimation schemes, or provided more data from which to substantiate the prediction methods. The problem however, is that there is a serious lack of comprehensive acoustic *and* flow-field measurements from which to verify or identify problems with the prediction methods. Because of the simplifications that can be made concerning the characteristics of the flow, most of the experimental and analytical work has attempted to focus on isotropic turbulence. Also, due to the relatively low noise levels associated with low tip- and inflow speeds, most of the previous experimental work was concentrated near tip Mach numbers of 1.0.

Experimental Facility and Equipment

All of the data presented here was performed in the Notre Dame Anechoic Wind Tunnel. A schematic of the facility is shown in Figure 1. For a complete description of the facility see Mueller et. al. [1992a and b] and Scharpf [1993]. The facility is equipped with 2-ft. fiberglass acoustic wedges, which allow a low-frequency cut-off of 150 Hz in the microphone measurement region. For the present research the open-jet wind tunnel was configured with a 4 ft. jet length which issued from a contraction exit area of 2 ft. square. The propeller was an aluminum, four-bladed, 10-in. diameter U.S. Navy marine propeller, #3714, which was supplied by the David Taylor Research Center. At r/R = 0.7, the

pitch/diameter ratio was 1.262 and the chord was 2.71 in. A freestream velocity of 33 ft/s and rotational speed of 3000 RPM was used for all of the data presented.

All data acquisition and instrumentation control was performed with a Macintosh IIfx computer equipped with National Instruments data-acquisition boards. Both single- and X-wire hot-wire measurements were performed with Dantec probes and a TSI IFA 100 anemometer system. Microphone measurements were performed with a type 4181 Brüel and Kjær, 1/2-in. condenser microphone and a B&K type 2807 preamplifier. Further amplification and signal conditioning utilized the capabilities of the IFA 100.

Aerodynamic Characteristics of Turbulence Grids

The turbulence-generating grids were constructed from circular wooden dowels arranged to form square-meshes. These grids were placed upstream of the propeller at the exit plane of the wind-tunnel contraction. The turbulence ingested by the propeller was characterized by measuring length and time scales, turbulence intensities, and spectral content. The time scales were determined by integrating the autocorrelation curve from the hot-wire measurements. By multiplying the time scale by the freestream velocity, (i.e. assuming Taylor's hypothesis), the integral length-scales were calculated. The micro-scales were calculated from the osculating parabola from the autocorrelation curves. Table 1 gives the grid dimensions and associated flow properties for each of the grids at the propeller test location.

TABLE 1

TURBULENCE GRID DIMENSIONS AND FLOW CHARACTERISTICS

Mesh Spacing, (in.)	Rod Diameter, (in.)	Grid Solidity	Re_m (U_∞=33 ft/s)	Re_d (U_∞=33 ft/s)	% u'/U_∞	% w'/U_∞	$\Lambda_{f, (in.)}$	$\lambda_{f, (in.)}$
1	0.19	0.27	14,000	2600	3.0	2.7	0.37	0.12
1.26	0.35	0.34	18,000	4800	3.7	3.4	0.44	0.15
3	0.5	0.33	52,000	7000	5.5	5.1	0.34	0.14
Clean Section	—	—	—	—	0.24	0.19	3.24	0.60

It should be noted that the propeller tends to stretch the eddies as they are drawn into the rotor plane. Hanson [1975] showed that this phenomenon results in large changes in the turbulence properties. Stretching of the turbulent eddies was investigated by measuring the length scales 6 inches in front of the propeller for each of the grids. These measurements were not possible for the clean-flow case due to the imposed periodicity from the propeller which contaminated the autocorrelation curve. The high turbulence levels generated by the grids however, dominated the flow and hence negated this periodic effect. Any stretching of the length scales due to the effect of the propeller was not evident from these measurements. Stretching of the eddies may have occurred closer to the propeller plane but were not investigated due to the size of the probe and the aforementioned periodic effects.

Flow Visualization

Since the range of blade-chord Reynolds numbers never exceeded 160,000, there was the possibility of the existence of a separation bubble on the upper surface of the blades. Surface flow-visualization was accomplished by spraying a thin layer of naphthalene over the entire propeller. Sublimation of the naphthalene would first occur where the air was moving the fastest, thus creating flow patterns on the blade surfaces. Figure 2 is an image of the propeller blade for a clean inflow condition which shows evidence of boundary-layer transition by the existence of periodic striations near the leading edge that extended in the chord-wise direction. Similar naphthalene patterns seen on rotating disks, cones, spheres, and swept wings have been identified by previous researchers, (Reed and Saric [1989]) to be evidence of cross-flow instabilities in the boundary layer. The wavelength of these instability patterns on the blade surface was calculated to be approximately 0.3 inches. Evidence of a leading edge vortex was seen to extend from the hub to the tip along the upper and lower surfaces near the leading edge of the blades. Similar evidence of this leading-edge vortex structure was seen by Tillman and Simonich [1991] who used surface-oil flow-visualization on a propfan.

Propeller Wake Surveys

The wakes of propellers operating in axial flow-fields have been documented by Tillman and Simonich [1991], Hyun and Patel [1991], Hanson and Patrick [1990] and Favier, Ettaouil, and Maresca [1989], by the hot-wire technique. In each of these investigations multiple rotations of the sensor(s) were necessary. For the present measurements a single-wire probe was employed which posed problems since the hot wire signal was contaminated by cross-flow velocities. Because of this, errors in certain regions of the wake, namely the tip-vortex region, were unavoidable due to the highly three-dimensional structure of the flow. By orienting the sensor as shown in Figure 3 such that it was tangent to the azimuthal velocity-component and normal to the axial direction, the

added cooling-effect from the azimuthal component was reduced. The error in these measurements was therefore mainly due to the added cooling from the radial velocity-component, (which was typically less than the azimuthal component except in regions near the tip vortex and close to the hub). Errors in the measurement of the mean and fluctuating axial-velocity components were estimated to be 12% and 15%, respectively near the mid-span regions

Measurements performed in the propeller wake were phase-locked with the propeller rotation such that each data sample corresponded to the azimuthal location of a blade, and each revolution corresponded to an ensemble for averaging. In this manner, mean and fluctuating axial velocities were measured which could be related to a specific propeller blade-location.

Based on actuator-disk analysis (McCormick [1979]), the propeller-induced velocity, U_i, was calculated from Equation 2.

$$\frac{U_\infty + U_i}{U_i} = \frac{T}{2\rho A_{disk}} \tag{1}$$

From performance measurements by Asson [1990] a value of the thrust coefficient, C_T = 0.3, was measured at the present operating condition; $J = 0.8$. The resulting induced velocity was then calculated to be $U_i = 4.4$ ft/s which was only a 13% increase over the freestream velocity. Figure 4 shows the measured axial velocity at 1/8-inch downstream of blade trailing edge from hub, ($r/R = 0.3$), to tip, ($r/R = 1.0$) for probe locations 45° before the passage of a blade. From this figure, the induced velocity was approximately 30% higher than the freestream for most of the radial locations and decreased to a value equal to the freestream at $r/R = 1.2$. The error bars in the figure denote the added cooling effect of the radial and tangential components ($\pm$ 12%). The convective velocity through the

propeller plane for the grid-flows were measured to be between $1.3U_\infty$ and $1.35U_\infty$ which were comparable to the measurements from the clean inflow case.

The way the propeller effected the turbulence as it was convected through the propeller plane was also examined. Due to the nature of the free jet, the magnitude of these fluctuations increased as the shear layer was approached from the jet center-line. The phase-locked axial-velocity fluctuations behind the propeller are shown in Figure 5 at an azimuthal location of 15° before the passage of a blade for the clean flow condition.

It can be seen from Figure 5 that the fluctuations have increased as a result of being passed through the propeller plane, and tend to approach the freestream values beyond the propeller disk. When turbulence was introduced upstream of the propeller (see Figure 6) the magnitude of the fluctuations in the propeller wake were below the incoming turbulence levels but then increased to the freestream values outside of the propeller disk.

The variation in the turbulence level across the propeller plane can be viewed as a chord-wise variation in the propeller frame of reference. Likewise, the variation in the radial direction contributes to the overall dissimilarity in the velocity distribution seen by the entire blade, and hence contributes to the unsteady blade loading and consequently the radiated broad-band noise.

Auto-Bicoherence Measurements

Bicoherence measurements were taken in the wake of the propeller in order to provide information concerning the frequencies involved in the wake interactions near the blade trailing edges. The autobicoherence is defined as:

$$b^2(f_j, f_k) = \frac{|\ B(f_j, f_k)\ |^2}{E[\ |\ X_j X_k\ |^2\ ] \cdot E[\ X_m]}, \quad 0 \leq b^2 \leq 1 \qquad (2)$$

where,

$$B(f_j, f_k) = E[\ X_j X_k Y_m^*], \quad m = j+k \qquad (3)$$

The bicoherence can be interpreted as a measure of the phase coherence between three spectral components due to nonlinear wave-coupling. If three spectral components are nonlinearly coupled, then a phase coherence will exist between them and the value of the bicoherence will be nonzero. Since the *phase* coherence is what drives the magnitude of the bicoherence, wave triads that satisfy the resonant condition, $f_j + f_k = f_m$, but are not phase-coupled will yield a bicoherence of zero. For a more detailed description of the bicoherence the interested reader is referred to Kim and Powers [1979], and Miksad, Jones and Powers [1983].

It should be noted that since the measurements presented here were performed at a single point they reflect the possibility of three different interactions. (Two-point measurements, i.e. the cross bicoherence are capable of determining the direction of energy transfer between phase coupled waves; see e.g. Hajj, Miksad and Powers [1993], and Thomas and Chu [1991].) These interactions include a sum interaction, where waves at f_k and f_l interact to generate a third wave at their sum, $f_j + f_k = f_m$, and two difference interactions; $f_m - f_k = f_j$ or, $f_m - f_j = f_k$.

The auto-bicoherence measurements in the wake of the propeller were performed with a single-wire probe at a distance of 0.12 inches behind the blade trailing edges for a number of radial locations. Because of the demanding computational requirements, the frequency resolution of the bicoherence measurements was limited. Sampling was synchronized with the passage of a single blade and data was acquired at a rate of 2000 Hz

for 128 samples and 50 ensembles which resulted in a frequency resolution of $\Delta f =$ 15.625 Hz.

Figure 7 shows the auto-bicoherence results for the clean inflow. Near the hub, r/R = 0.3, the patterns of high bicoherence indicate that the blade-passage harmonics are phase coherent with the broad-band frequencies. For example, the horizontal pattern at f_k/BPF = 1 indicates that a sum interaction may be the cause of the high coherence between the blade-passage frequency and all of the frequencies between f_j/BPF = 1 to 4 which interact to generate the frequencies at f_j/BPF = 2 through 5. The possible difference interaction implies that the broad-band frequencies from f_j/BPF = 2 to 5 interact with the blade-passage frequency to generate the lower broad-band frequencies at f_j/BPF = 1 to 4. The intersection of these lines at the blade passage harmonics also show that the there is a strong coherence between all of these harmonics.

High bicoherence values indicate that the wave coupling is due to nonlinear interactions within the wave triad. The vertical and horizontal lines at the blade passage harmonics show values as high as $b^2(1, 1) = 0.99$. For f_j/BPF = 1, 2 and 3, the bicoherence maintained values of $b^2 \approx 0.8$, 0.7, and 0.5 respectively, illustrating diminishing coherence between blade-passage harmonics and the broadband frequencies. This trend also occurred for the coherence between all of the blade-passage harmonics.

The high bicoherence values of the blade-passage harmonics at r/R = 0.3 may be related to the secondary corner flow that was seen from the flow visualization. As the distance from this secondary flow structure increases, the wake that is shed from the central region of the blade-span provides much less phase coherence than the highly organized vortex structure in the hub and tip regions. This is illustrated in Figure 7 b) for r/R = 0.7. While some traces of the coherence between all of the interactions at r/R = 0.3 can still be

seen, the dominant broadband interactions only persist for f/BPF=2 and 3. The maximum coherence in this region is $b^2(2, 2) = 0.6$ which indicates a weakening of the phase-coherent interactions from the r/R = 0.3 location. This is especially true for the blade-passage frequency which was the dominant interaction mode at r/R = 0.3. At r/R = 0.7, b^2 ≈ 0.1 for the broad-band interactions, and the harmonic interactions have dropped to $b^2(1, 1) = 0.22$, $b^2(2, 1) = 0.40$, and $b^2(3, 2) = 0.22$.

Once the tip of the blade is reached the bicoherence values increase once again due to the strong influence of the tip vortex. At all of the harmonic intersections, the bicoherence had a value of $b^2 = 1.0$. The blade-passage frequency /broadband interactions at $(f_j, 1)$ show b^2 ≈ 0.9, for $1 < f_j < 3$, and b^2 ≈ 0.8, for $3<f_j<4$. The effect of the tip vortices is therefore seen to provide a clearly nonlinear interaction-mechanism between the blade-passage harmonics and the broad-band frequencies.

When the auto-bicoherence is measured outside of the propeller disk, as seen in Figure 7 d), the broadband interaction patterns were no longer present. Instead, the nonlinear interaction regions were reduced to those which occur between the blade-passage harmonics and also with the sub-harmonics, $(i+\frac{1}{2})$BPF. A possible explanation for this may be the mutual effect of the helical vortices that, due to some type of induction/pairing, are generating frequencies at the subharmonics.

The most significant change in the results of the bicoherence measurements due to the turbulent inflow were seen in the broadband bicoherence patterns. Figure 8 shows the bicoherence for the grid mesh of 3 inches at radial locations of r/R = 0.3, 0.7, 1.0, and 1.2. Near the hub, (r/R = 0.3), bicoherence values of $b^2(f_k, f_l) = 0.95$ were present at the blade-passage harmonic intersections. The coherence between these modes and the broadband frequencies were significantly reduced compared to the clean-flow condition.

As the tip was approached the coherence between the blade-passage harmonics remained, albeit at a lower level, ($b^2(f_k, f_l) \approx 0.8$), than at r/R = 0.3. When the blade tip was reached all of the broadband interaction patterns were gone, indicating that the only phase coherence that remained was at the harmonics of the blade-passage frequency. At r/R = 1.2 the maximum bicoherence value at was 0.16 indicating that all of the interactions between the frequencies were independent from one another.

The trends illustrated in the data for the 3-inch mesh were representative of the effects of the other grids; i.e. decreasing coherence levels corresponding to increasing inflow-turbulence levels.

The difference between the wakes from the clean inflow and the turbulent inflow can therefore be distinguished not only in terms of their intensity, but also by their phase relation with the generation mechanism, namely the propeller blades. For the clean flow, the broad-band frequency interactions are highly phase-coherent with the blade-passage frequency and the higher harmonics near the hub and tip regions. Because of this, the unsteady loading on the blades, which is a function of the passage of the unsteady flow over the blade trailing edges, is therefore phase-coupled with the dominant modes in the flow, i.e. the blade-passage frequency and harmonics.

The turbulent inflow however, is not affected in the same manner. With this high energy flow, the blade passage harmonics were unable to impose any significant phase coherence with the broad-band frequencies of the incoming turbulence. Thus, the broad-band, high-energy flow passing through the propeller plane remained as a series of independent modes. This independence results in a shedding pattern which adds to the random, unsteady blade loadings.

Propeller Acoustic Measurements

The radiated noise from the propeller was measured at a distance of 75 inches (15 propeller radii), for angles of $\varphi = 45°$ - 135° and 225° - 315° as shown in Figure 9. All measurements shown are in 10 Hz constant bandwidths with errors in the measured SPL's estimated to be ± 0.3 dB.

While the noise produced by the shear layers of the open jet was always at least 10 dB below the level of the propeller noise, the bearing noise for the clean-inflow case contaminated the acoustic spectrum at frequencies greater than 1000 Hz. Also, the blade-passage harmonics for this condition were only about 2 to 3 dB above the broad-band level which made the directivity patterns at these frequencies difficult to assess. Figure 10 shows a typical acoustic spectra for $\varphi = 60°$.

Integration of the broad-band levels were performed over a bandwidth from 150-1000 Hz after extracting the tones at multiples of the shaft rotational speed from the spectrum and replacing these values by the average of the two neighboring side bands. By performing this operation comparisons between the overall broadband sound-pressure levels from the turbulent inflow conditions were possible. The directivity patterns for the propeller noise due to clean inflow is shown in Figure 11 for the broad-band noise, blade-passage frequency and the first two harmonics. Slight deviations between the directivity patterns on either side of the propeller have been attributed to stationary disturbances in the flow that result in radiation of tones at the blade passage harmonics. These disturbances that occur at particular locations in the flow are seen as periodic variations in the rotating reference frame of the propeller. Since these disturbances are not cyclic in the circumferential direction, the propeller blades only experience them at fixed rotational

locations, hence rendering the directivity due to this noise-generating mechanism asymmetric with respect to the inertial reference frame. This conclusion is substantiated by the fact that the broad-band directivity, which is caused by the random blade forces, is symmetric on either side of the propeller.

Typical spectra for the grid-induced propeller noise are shown in Figure 12 for the 3-inch mesh grid at $\varphi = 90°$. Tones were seen at multiples of the blade-passage frequency for each azimuthal location, but did not follow any specific trend. The varying levels of these tones have been attributed to the aforementioned stationary-disturbance effect. The effect of the random flow-fluctuations can be seen in the spectra near $f/\text{BPF} = 2$ where a "hump" exists that grew in size as the turbulence level was increased. Also, the smooth spectrum compared to the clean flow condition can be attributed to the effect of the random blade loadings caused by the inflow turbulence. The frequency at which this smoothing occurs has been estimated by Homicz and George [1974] to be:

$$\frac{f}{n} \approx \frac{B(1 + M_0/M_c)}{2(1 - M_0\cos\varphi)} \tag{4}$$

By letting the convective velocity be $1.3U_\infty$ as determined from the wake surveys, and letting $r = R_{\text{tip}}$, the approximate frequency at which the smoothing of the spectrum was predicted to be was between 410 and 464 Hz.

The directivity patterns for the 3-inch mesh grid are shown in Figures 13 for the integrated broad-band levels, blade-passage frequency, and first two harmonics. The directivity patterns at the blade-passage frequency show higher sound-pressure levels aft of the propeller plane, while the first and second harmonics show a lobed pattern with minimum value occurring at the plane. Similar patterns which extend around the front of an isolated helicopter rotor measured by Stainer [1969], show that the magnitude of the SPL reaches a maximum on the axis of the rotor. This pattern has been described by

Morfey [1973], Wright [1969], and Lowson and Ollerhead [1969] to be caused by unsteady lift effects . The relative levels between the broadband noise from each of the grid flows are shown in Figure 14. In each of these cases, the higher levels were directed in the upstream direction, with a local minimum occurring at the plane (with the exception of the clean flow condition which did not exhibit this minimum).

The effect of increasing inflow turbulence has been shown to cause corresponding increases in the broadband noise levels. In the present experiments, the axial length scales were approximately the same for each of the grids at the propeller location. Because of this, any variations in the radiated noise were primarily a function of the turbulence intensity. The manner in which the turbulence spectrum interacted with the propeller to generate sound was examined by plotting the integrated broadband sound-pressure levels as a function of different frequency bandwidths as shown in Figure 15. For each of these bandwidths, the sound-pressure level increased with increasing turbulence. The *rate* at which this occurred however was a function of the bandwidth. In the low frequency range from 150 - 300 Hz, the increase in turbulence had the least effect on increasing the propeller noise. In the mid range of frequencies, from 300 to 900 Hz, the increasing turbulence resulted in an increase of approximately 2.5 dB for every 1% increase in turbulence intensity. Since an increase of 3 dB corresponds to a doubling of the acoustic power, this is a substantial increase in the radiated noise for a moderate increase in turbulence.

In order to examine which frequencies from the turbulence spectra influenced the different acoustic frequencies, the turbulence intensity was calculated from the energy spectrum using Parseval's theorem over the same intervals as the acoustic spectrum. The results of these calculations are shown in Figure 16. From this figure the slope of the curves were seen to decrease as the frequencies increased. The high-frequency turbulence

therefore had a much more significant effect on the broad-band noise in the corresponding bandwidth. Turbulence associated with low frequencies did not cause the radiated noise at these frequencies to increase as rapidly.

Cross Spectrum Between Velocity Fluctuations in Propeller Wake and Radiated Sound

To relate the propeller noise to the velocity fluctuations in the propeller wake, cross-spectral density measurements between the hot wire and the microphone were made. These were performed with the microphone at $\varphi = 120°$ and the hot wire at $r/R = 0.3, 0.4, \ldots 1.2$. Data were simultaneously sampled and the raw voltages used in the data reduction to arrive at the coherence function, γ_{xy}^2.

Figure 17 shows the coherence between the hot-wire and microphone signals at various hot-wire radial locations for the clean inflow condition. The highest coherence level consistently occurred at the first blade-passage harmonic (i.e., 2 BPF) for each of the hot-wire radial locations except at $r/R = 1.2$. From this figure a general decrease in the coherence is seen for all radial locations as the blade-passage harmonic increases.

By viewing the coherence function for each blade-passage harmonic the contribution from each radial location can be seen as illustrated in Figure 18. For the blade-passage frequency the coherence function has maxima near the hub and tip which supports the bicoherence measurements which indicated a weakening of the harmonic interactions in the mid-span region of the blade, and also tonal noise generation at the hub and tip. The noise generated at twice the blade-passage frequency showed a strong coherence with the velocity fluctuations near the hub which decreased toward the tip. For $f = 3\text{BPF}$, the coherence is again highest at $r/R = 0.3$ and 0.9, as was the case for the fundamental,

indicating that the hub and tip regions of the wake are more closely associated with the noise at the BPH' s than the rest of the blade section.

The cross-spectra for the turbulent inflow condition were measured in the same manner as the clean inflow case. The results from these measurements showed reduced coherence between the fluctuating velocities in the propeller wake and the radiated sound at the blade passage harmonics due to the inherently random nature of the incoming flow, as compared to the clean-flow condition. Figure 19 shows the coherence between the hot-wire and microphone signals for the 3-in. grid. As the inflow turbulence levels increased the coherence, γ^2, at the higher blade-passage harmonics was reduced. As with the clean flow, the highest coherence existed at twice the blade-passage frequency for all of the turbulence levels.

The distributions of the coherence along the blade span are shown in Figure 20 for the 3-inch mesh grid. As the turbulence level increased the coherence across the span at the blade-passage frequency decreased. Compared to the clean inflow case, the first blade-passage harmonic also showed a general decrease in the coherence across the span for all of the turbulence levels. The tip region still showed the highest coherence due to the strength of the tip vortex. Across the span however, the flow became dominated by the incoming random turbulence which caused a decrease in γ^2 for the majority of the blade.

DISCUSSION OF RESULTS

Since the measured grid-turbulence length scales were found to be less than the length necessary for blade coupling, tones in the acoustic spectrum have been attributed to stationary disturbances in the velocity field.

The cross-spectra measurements between the hot-wire and microphone signals showed high coherence at the first blade-passage harmonic (i.e., 2 BPF) and lower levels at the blade-passage frequency. It should be stressed that the hot-wire spectra is the result of the velocity fluctuations in the plane directly behind the propeller. The fact that a high coherence did not exist between the hot wire and the microphone at the blade-passage frequency despite the dominant signal at this frequency in each of the individual spectra leads to the conclusion that the trailing edge effects were not responsible for generation of noise at the blade-passage frequency. For the clean flow, the entire blade span showed high coherence values at the first harmonic, while the inflow turbulence reduced the coherence in the mid-span region.

Autobicoherence measurements from the clean-flow experiments showed regions of high coherence between the harmonic frequencies near the hub and tip regions indicating that the interactions in these regions were primarily non-linear. The low bicoherence values at multiples of the blade-passage frequency in the mid-span region of the blade indicate that very little of the energy transfer was due to nonlinear effects. If these coupling effects are viewed as the manner in which the flow leaves the blade trailing edges, the resulting unsteady forces on the blades would therefore be related to these flow interactions, and hence the hub and tip regions would be sources of noise radiation at the blade-passage harmonics. Further measurements with a hot wire that is rotating with the blades is needed to verify this assumption.

Since the noise in question is broadband, it may be tempting to neglect the effect of the periodic cutting of the turbulent eddies by the propeller blades. The bicoherence measurements however, indicate that there is a certain amount of phase-coupling between the harmonics of the blade-passage frequency and the broadband frequencies. The influence that this coupling has on the fluctuating blade forces responsible for the noise

radiation still remains in question. The decrease in this phase coupling as the turbulence was increased supports the notion that the blade-passage harmonics do not constructively interact with the broadband frequencies. It should be stressed however that the exact relation between the bicoherence measurements and the blade forces has not been established. Also, the significance of the bicoherence measurements on the noise generation is based on the assumption that the bicoherence is related to the flow over the trailing edge of the propeller blades.

The effect of the inflow turbulence on the radiated noise showed that for the same increase in turbulence the high-frequency bands experienced a much more rapid increase in the noise levels than the low-frequency bands. Assuming that the frequencies in the turbulence spectrum are responsible for the radiated noise at the same frequency, the higher noise levels in the low-frequency bands can be attributed to the large-amplitude fluctuations in the turbulence at those frequencies. These large-amplitude fluctuations cause the largest variation in the blade angle of attack and hence large fluctuations in the lift force.

CONCLUSIONS

The acoustic spectrum consisted of tones which were superimposed on a broadband spectrum. These two noise elements were separated and the possible source mechanisms were identified. The generation of tones at multiples of the blade-passage frequency were due to three mechanisms: 1.) Steady blade loadings which resulted in noise at the blade-passage frequency, 2.) The cutting of large scale eddies that were passed through the propeller plane in the clean flow condition which resulted in harmonics of the blade-passage frequency, and 3.) Periodic, fluctuating forces due to stationary disturbances in the incoming flow field. The hub and tip regions appear to be the most probable sources of the tone-generation.

The effect of inflow turbulence, as shown by the surface-flow visualization, was seen to make the instabilities less and less intensive in the boundary layer on the blades as the turbulence intensity increased. In terms of the broadband noise generation, an increase in the integrated broadband sound-pressure level of approximately 2 dB for every 1% increase in turbulence was measured. While this increase was much stronger for the high frequency noise, the SPL's at the low frequencies were at much higher levels. This was attributed to the large-magnitude fluctuations in the low-frequency turbulence spectrum.

ACKNOWLEDGMENTS

REFERENCES

Aravamudan, K. S. and Harris, W.L., " Low Frequency Broadband Noise Generated by a Model Rotor," *Journal of the Acoustical Society of America*, Volume 66(2), August, 1979, pp. 522 - 533.

Asson, K. M., " The Development of an advanced Dynamometer System to Experimentally Determine Propeller Performance ", Masters Thesis, University of Notre Dame, Notre Dame, IN, 1990.

Batchelor, G. K., and Townsend, A.A., " Decay of Isotropic Turbulence in the Initial Period," *Proceedings of the Royal Society of London*, Series A, Volume 193, 1948, pp.539 - 558.

Chandrashekhara, N., (b) " Sound Radiation From Inflow Turbulence in Axial Flow Fans," *Journal of Sound and Vibration*, Volume 19, Number 2, 1971, pp. 133 - 146.

Favier, D., Ettaouil, A., and Maresca, C., " Numerical and Experimental Investigation of Isolated Propeller Wakes in Axial Flight," *Journal of Aircraft*, Volume 26, No. 9, September 1989, pp.837 - 846.

George, A. R., and Kim, Y. N., " High-Frequency Broadband Rotor Noise," *AIAA Journal*, Volume 15, Number 4, 1977, pp. 538 - 545.

Hajj, M. R., Miksad, R. W., and Powers, E. J., " Fundamental-Subharmonic Interaction: Effect of Phase Relation ", Journal of Fluid Mechanics, Volume 256, 1993, pp. 403 - 426.

Hanson, D. B., " Measurement of Static Inlet Turbulence," AIAA Paper 75-467, Hampton Virginia, 1975.

Hanson, D. B. and Patrick, W. P., " Investigation of the Near Wake of a Propfan," *Journal of Aircraft*, Volume 26, No. 6, 1990, pp. 536 - 542.

Homicz, G. F., and George, A.R., " Broadband and Discrete Frequency Radiation from Subsonic Rotors," *Journal of Sound and Vibration*, Volume 36(2), 1974, pp.151 - 177.

Hyun, B-S., and Patel, V. C., " Measurements in the Flow Around a Marine Propeller at the Stern of an Axisymmetric Body Part 1: Circumferentially-Averaged Flow," *Experiments in Fluids*, Volume 11, 1991, pp. 33 - 44.

Kim, Y. C., and Powers, E.J.," Digital Bispectral Analysis and Its Application to Nonlinear Wave Interactions, " *IEEE Transactions on Plasma Science*, Vol. PS-7, No. 2, June 1979, p.120 - 131.

Lowson, M. V. and Ollerhead, J. B., " A Theoretical Study of Helicopter Noise," *Journal of Sound and Vibration*, Volume 9, pp. 197 - 222.

McCormack, B. W., Aerodynamics, Aeronautics, and Flight Mechanics, © 1979, by John Wiley and Sons.

Miksad, R. W., Jones, F. L. and Powers, E. J., "Measurements of Nonlinear Interactions During Natural Transition of a Symmetric Wake," *Physics of Fluids*, Vol. 26, No. 6, June 1983.

Morfey, C. L., "Rotating Blades and Aerodynamic Sounds," *Journal of Sound and Vibration*, Volume 28 No. 3, 1973, pp.587 - 617.

Mueller, T.J., Scharpf, D.F., Batill, S.M., Strebinger, R.B., Sullivan, C.J., and Subramanian, S., (a) " The Design of a Low-Noise, Low-Turbulence Wind Tunnel for Acoustic Measurements," 17th AIAA Ground Testing Conference, Nashville, Tennessee, July 6 - 8, 1992, AIAA Paper No. 92-3883.

Mueller, T.J., Scharpf, D.F., Batill, S.M., Strebinger, R.B., Sullivan, C.J., and Subramanian, S., (b) " A New Low Speed Wind Tunnel for Acoustic Measurements," *European Forum on Wind Tunnels and Wind Tunnel Test Techniques*, Southampton University, United Kingdom, September 14 - 17, 1992.

Mugridge, B. D., " The Noise of Cooling Fansused in Heavy Automotive Vehicles," *Journal of Sound and Vibration*, Volume 44, No. 3, 1976, pp.349 - 367.

Reed, H. L. and Saric, W. S., " Stability of Three-Dimensional Boundary Layers," *Annual Review of Fluid Mechanics*, Volume 21, pp. 235 - 284, 1989.

Scharpf, D. F., " An Experimental Investigation of the Sources of Propeller Noise Due to Turbulence Ingestion," Ph.D. Dissertation, University of Notre Dame, Notre Dame, IN, 1993.

Sevic, M., " Sound Radiation From a Subsonic Rotor Subjected to Turbulence," *Fluid Mechanics, Acoustics, and Design of Turbomachinery*, Part 2, edited by B. Lakshminarayana, W. R. Britsch, and W. S. Gearhart, NASA SP 304, 1974, pp. 493 - 511.

Stainer, N. J., An Experimental Investigation into Rotational Noise for a Low Solidity Rotor, M.Sc. Dissertation, University of Southampton, 1969, From Morfey,C. L., 1973.

Thomas, F. O., and Chu, H. C., (a), "Measurement of Nonlinear Wave Coupling and Energy Transfer in Planar Jet Shear Layer Transition," AIAA Paper 91-0314, 29th Aerospace Sciences Meeting, Jan 7 - 10, 1991, Reno, Nevada.

Thomas, F. O., and Chu, H. C., (b), " Experimental Investigation of the Nonlinear Spectral Dynamics of Planar Jet Transition," *Physics of Fluids*, A3 (6), June 1991, p. 1544 - 1559.

Tillman, T. G., and Simonich, J. C., " Hot Wire Measurements Downstream of a Propfan," *Journal of Propulsion*, Vol. 7, No. 5, Sept. - Oct. 1991, pp.776 - 783.

Trunzo, R., Lakshninarayana, B., and Thompson, D. E., " Nature of Inlet Turbulenceand Strut Flow Disturbances and Their Effect on Turbomachinery Rotor Noise," *Journal of Sound and Vibration*, Volume 76 Number 2, 1981, pp. 233 - 259.

Wright, S. E., " Sound Radiation From a Lifting Rotor Generated by Asymmetric Disk Loading," *Journal of Sound and Vibration*, Volume 9, 1969, pp. 223 - 240.
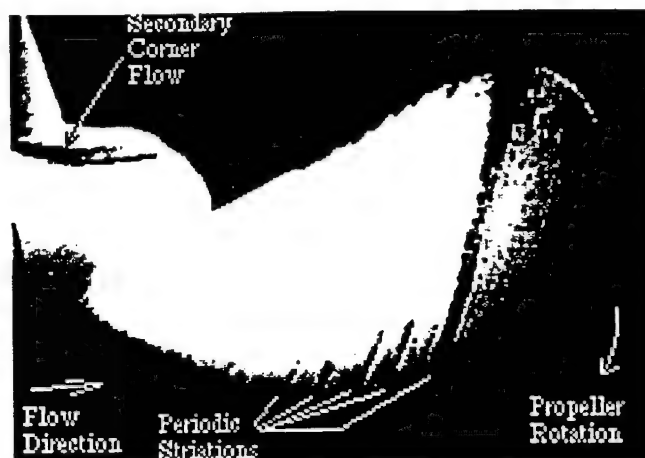
List of Figures
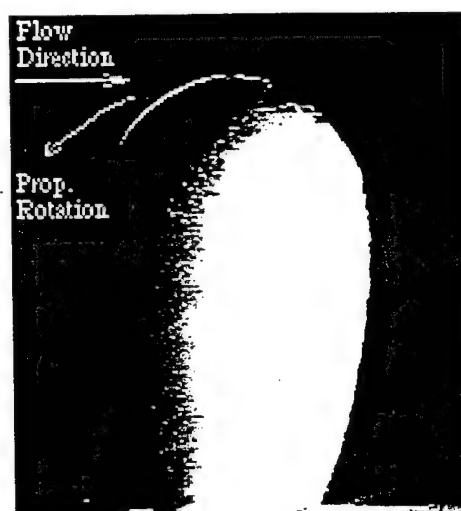
a) Top View

b) Side View

Figure 1.   Schematic of Notre Dame Anechoic Wind Tunnel.

a)

b)

Figure 2.   Naphthalene Surface Flow-Visualization of Propeller on Clean Flow, U_∞ = 33 ft/s, 3000 RPM, a) Suction Side of Blade, b) Pressure Side of Blade.
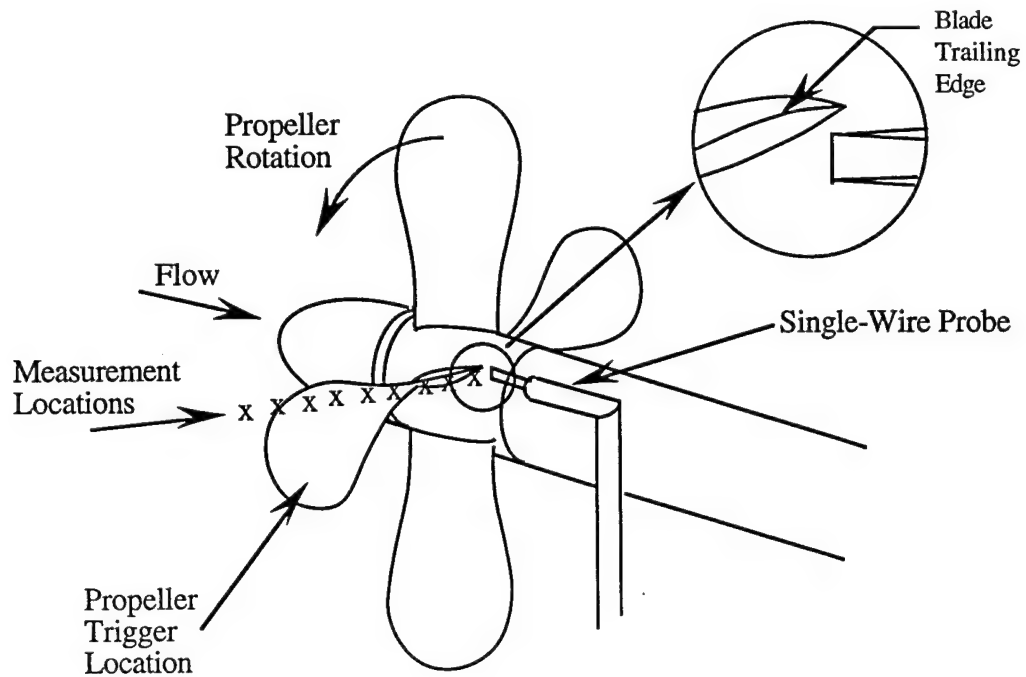
Figure 3.   Schematic of Hot Wire Arrangement Behind Propeller for Phase-Locked Wake Measurements.
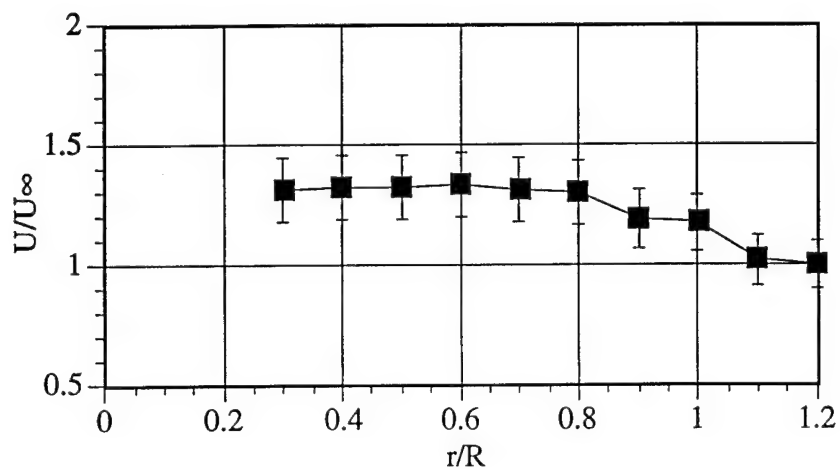
Figure 4.   Convective Velocity as a Function of Radial Location 45° Before the Passage of Blade at 1/8-inch Downstream of Blade Trailing Edge for Clean Inflow.
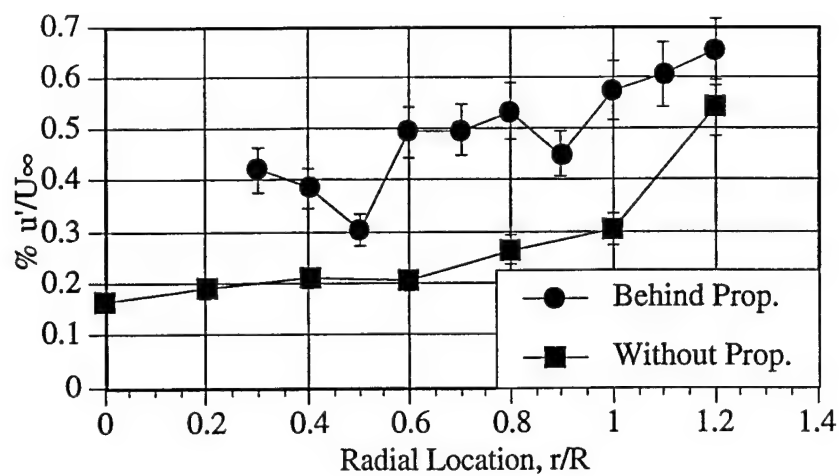
Figure 5.   Axial Velocity Fluctuations at Propeller Location for Clean Flow Without
Propeller and Clean Flow in the Wake of the Propeller at 15° Before the
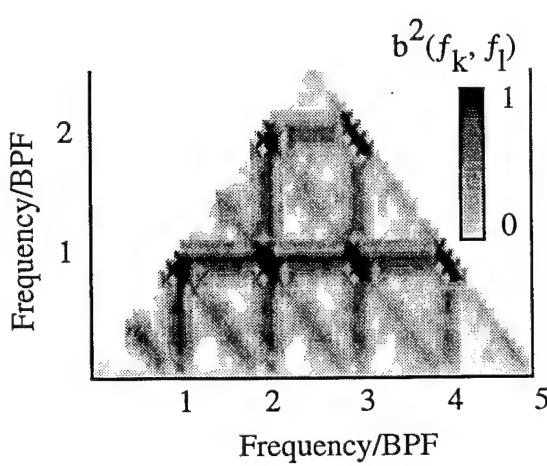Passage of a Blade.
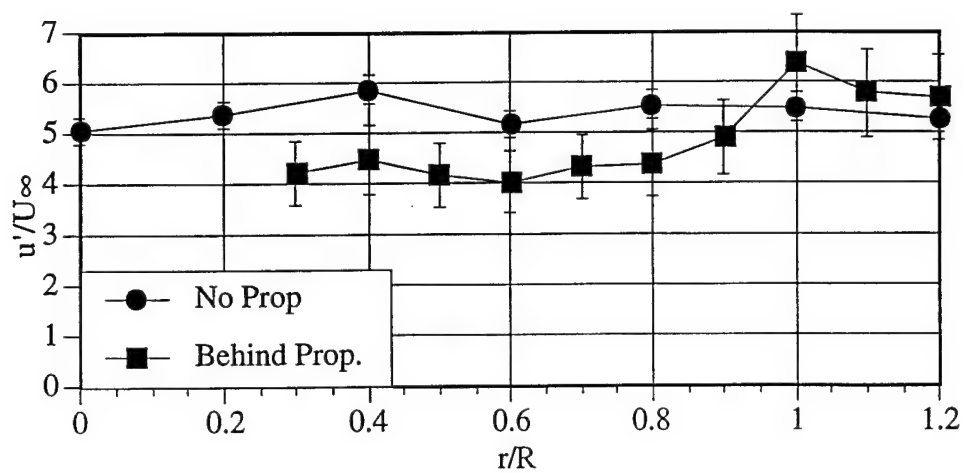
Figure 6.   Radial Variation of Axial Velocity Fluctuations 1/8-in. Behind Propeller at 15° Before Passage of Propeller Blade for m = 3", u'/U_∞ = 5.5%.
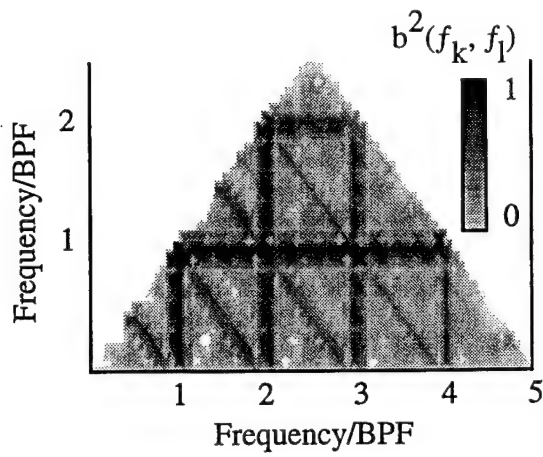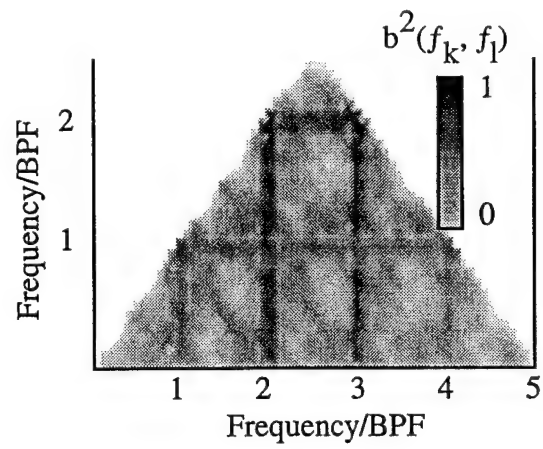
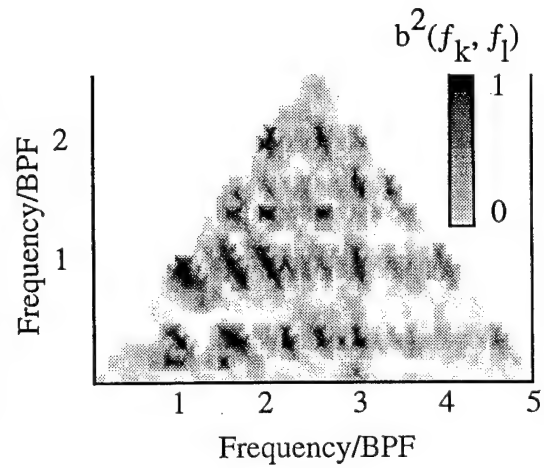Figure 7. Auto-Bicoherence of Propeller Wake for Clean Flow Taken at x/R = 0.025, 3000 RPM, U_∞ = 33 ft/s, a) r/R = 0.3, b) r/R = 0.7, c) r/R = 1.0, and d) r/R = 1.2.
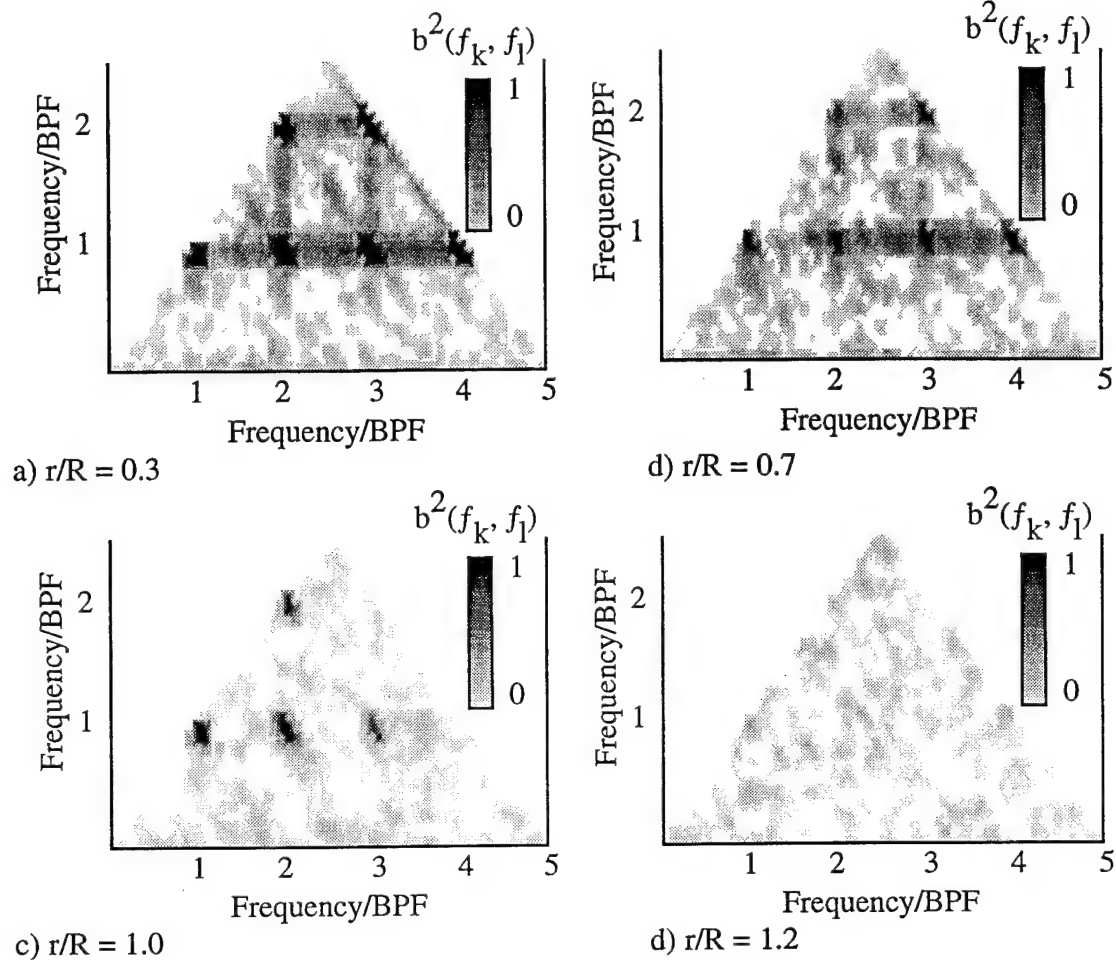
Figure 8.   Auto-Bicoherence of Propeller Wake for Turbulent Inflow Taken at x/R = 0.025, m = 3 in., 3000 RPM, U_∞ = 33 ft/s, a) r/R = 0.3, b) r/R = 0.7, c) r/R = 1.0, r/R = 1.2.
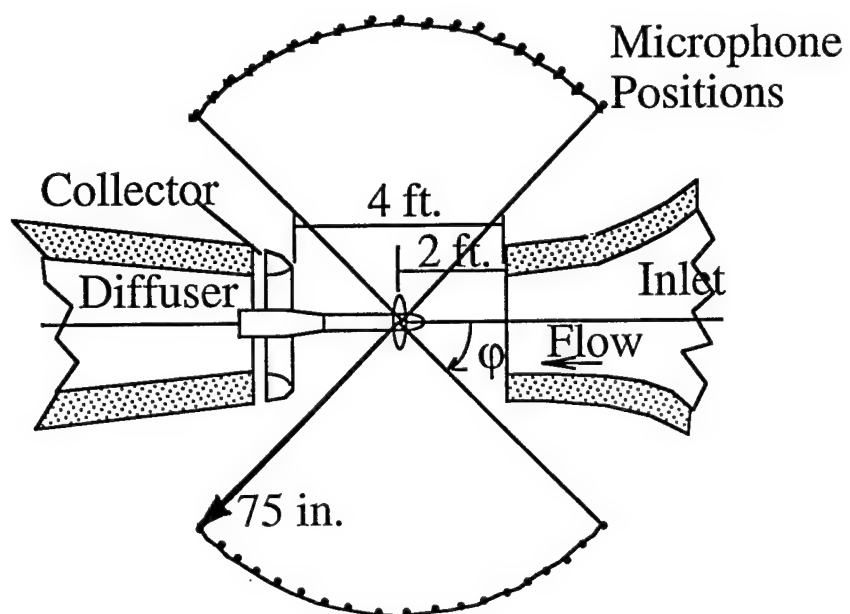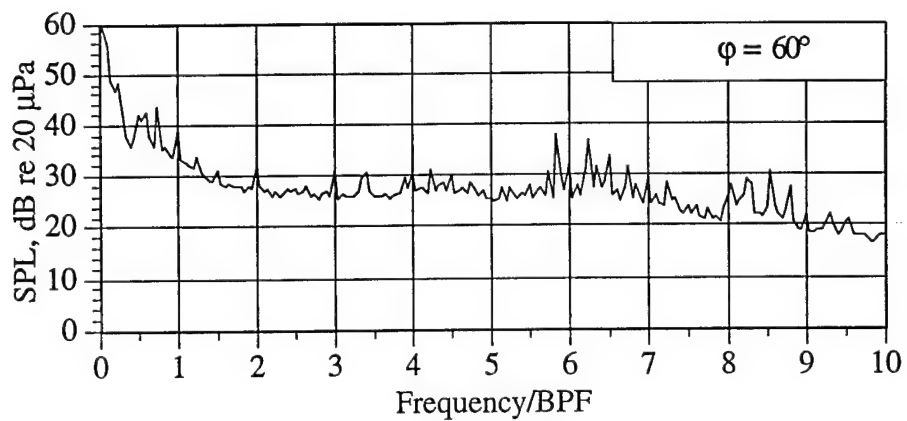
Figure 9.   Microphone Measurement Locations

Figure 10.   Sound Pressure Level Spectrum for Propeller with Clean Inflow; $U_\infty = 33$ ft/s, 3000 RPM, $J = 0.8$, $\varphi = 60°$.
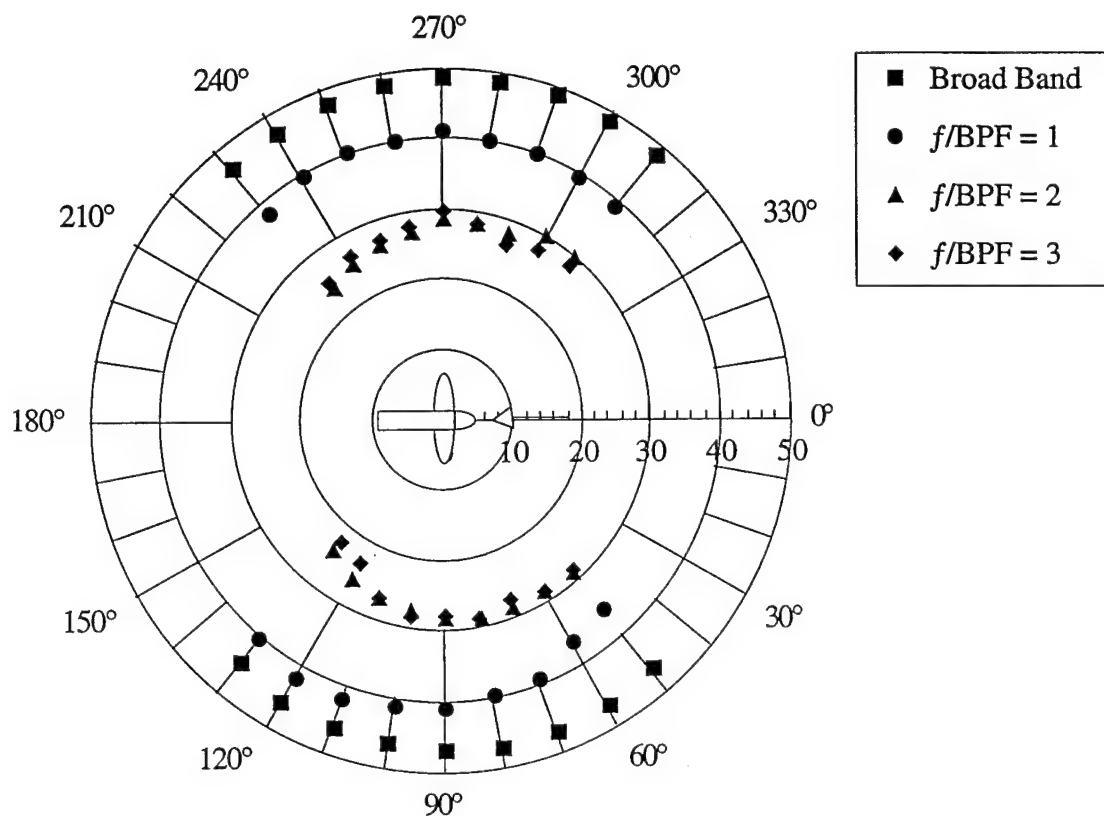
Figure 11.   Sound Pressure Level Directivity for Propeller with Clean Inflow, $U_\infty = 33$ ft/s, 3000 RPM, Microphone at 75" from Center Line.
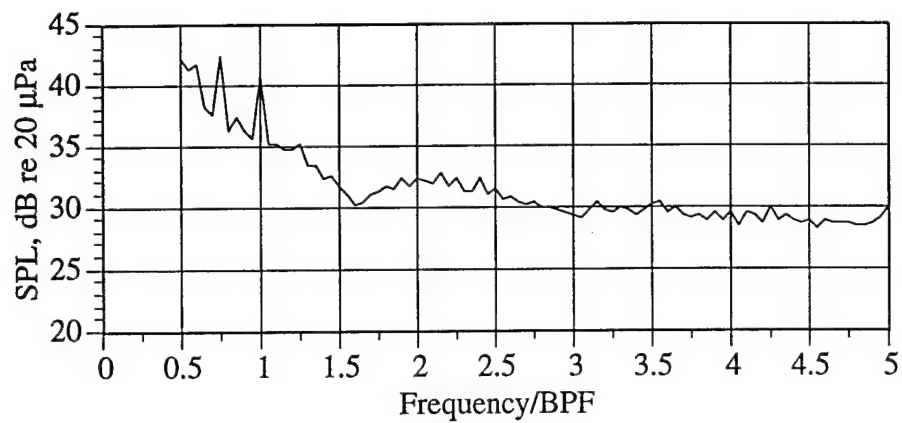
Figure 12. Sound Pressure Level Spectra Measured in 10 Hz Constant Bandwidths for $U_\infty = 33$ ft/s, 3000 RPM, $\varphi = 90°$, m =3 in., u'/U_∞ 5.5 %.
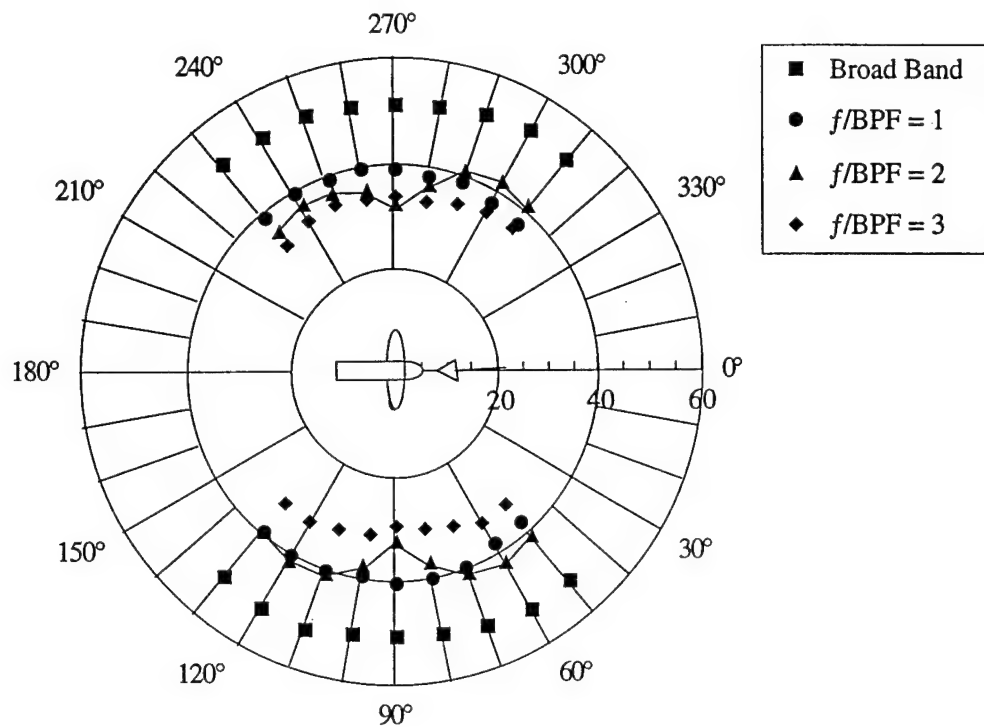
Figure 13.   Sound Pressure Level Directivity of Propeller Noise with Turbulent Inflow
From Grid Mesh = 3 in.
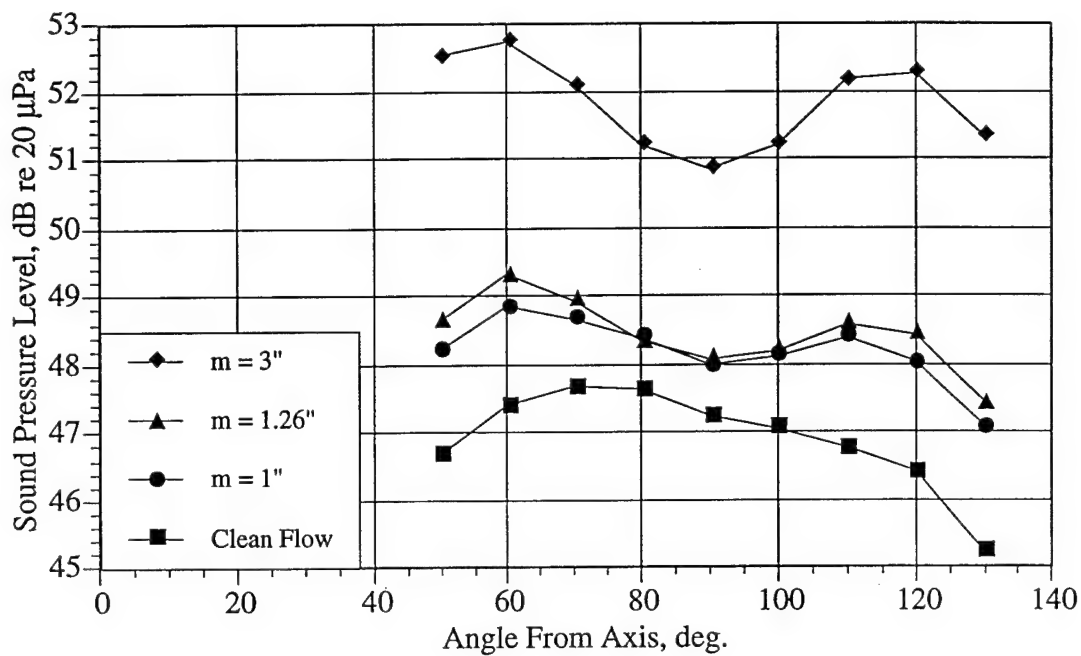
Figure 14.   Integrated Broad Band Sound Pressure Levels (150 - 1000 Hz), of Propeller Noise for Each Flow Condition, $U_\infty = 33$ ft/s, 3000 RPM.
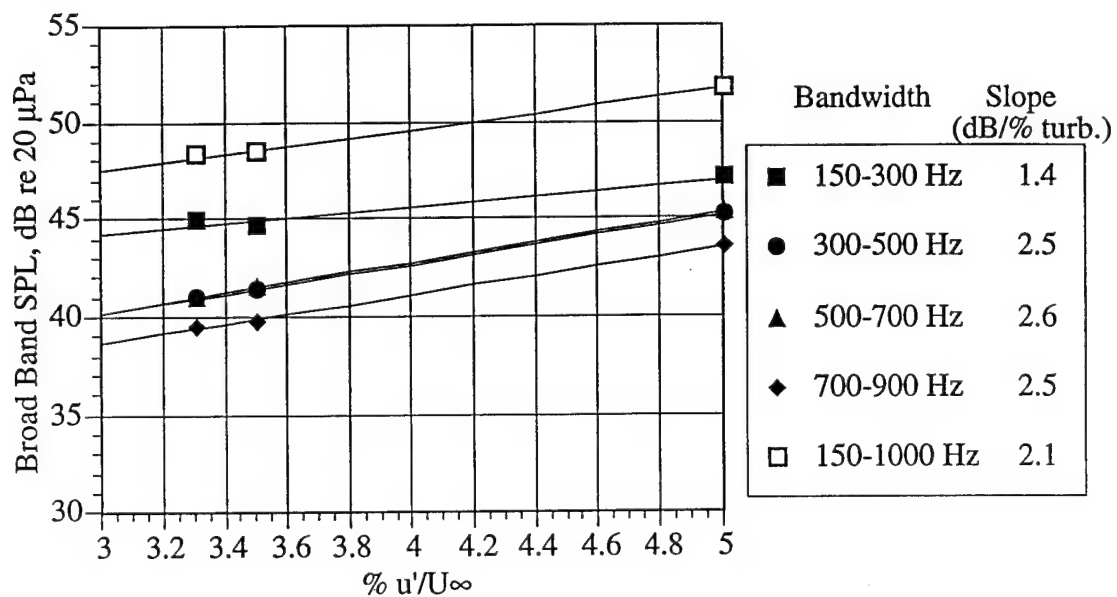
Figure 15.   Integrated Broad-Band Sound Pressure Level in Selected frequency Bands
as a Function of Inflow Turbulence, U_∞ = 33 ft/s, 3000 RPM, φ=120°.
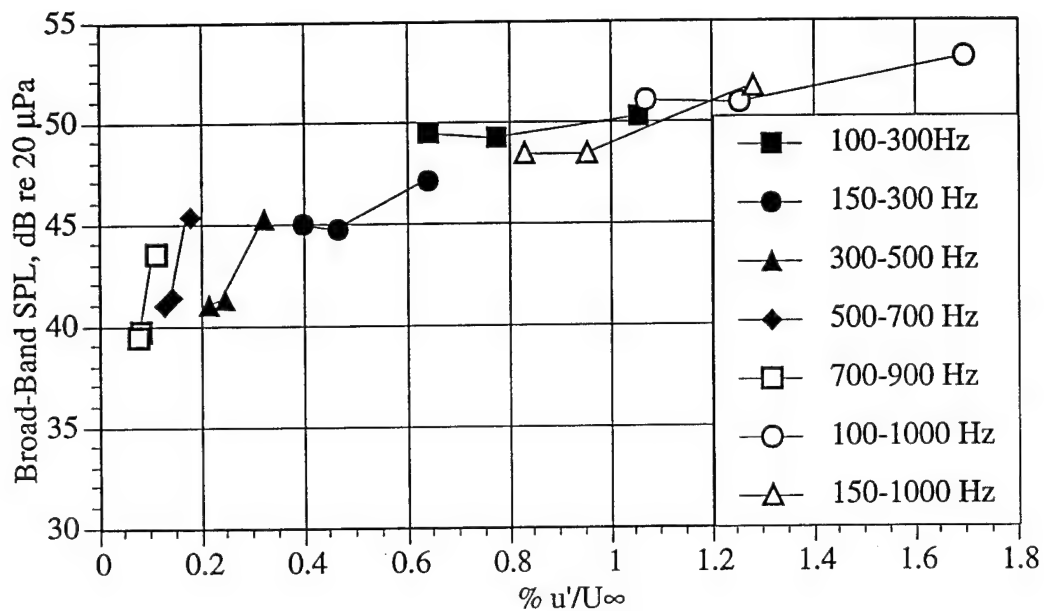
Figure 16.   Integrated Broad-Band Sound Pressure Level as a Function of Inflow
              Turbulence for Selected Frequency Bandwidths.
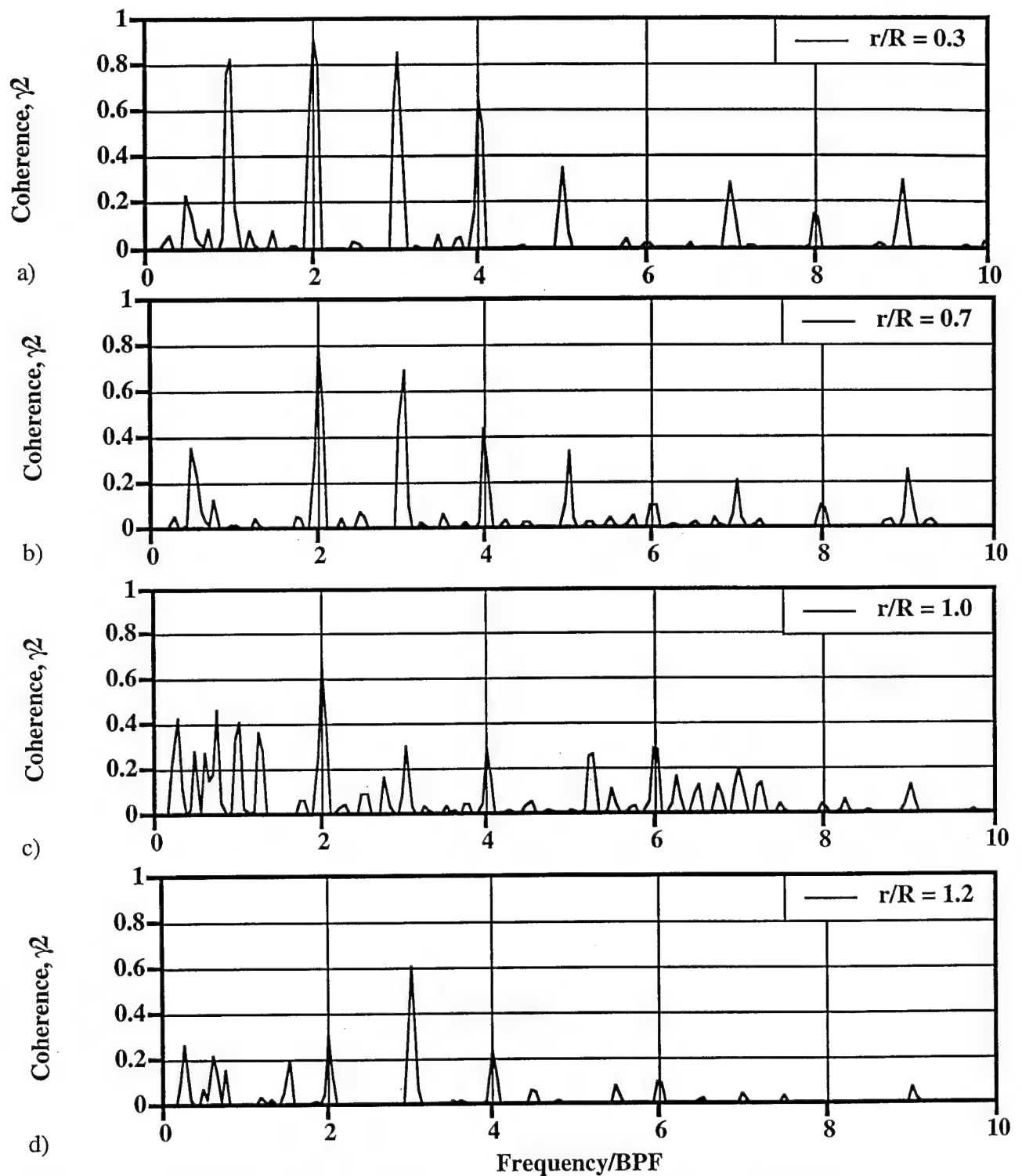
Figure 17.   Coherence Function Spectra for Hot-Wire/Microphone Measurements with Clean Inflow . U_∞ = 33 ft/s, 3000 RPM, Microphone at r/R = 15, ϕ = 120°, and Hot-Wire Locations in Propeller Wake at x/R = 0.025 and a) r/R = 0.3, b) r/R = 0.7, c) r/R = 1.0, and d) r/R = 1.2

Figure 18   Coherence Function at Each Blade-Passage Harmonic for Hot-Wire/Microphone Measurements with Clean Flow for Microphone at a Radial Distance of r/R = 15, φ = 120°, and Hot-Wire Locations in Propeller Wake at x/R = 0.025 and r/R = 0.3 - 1.2.
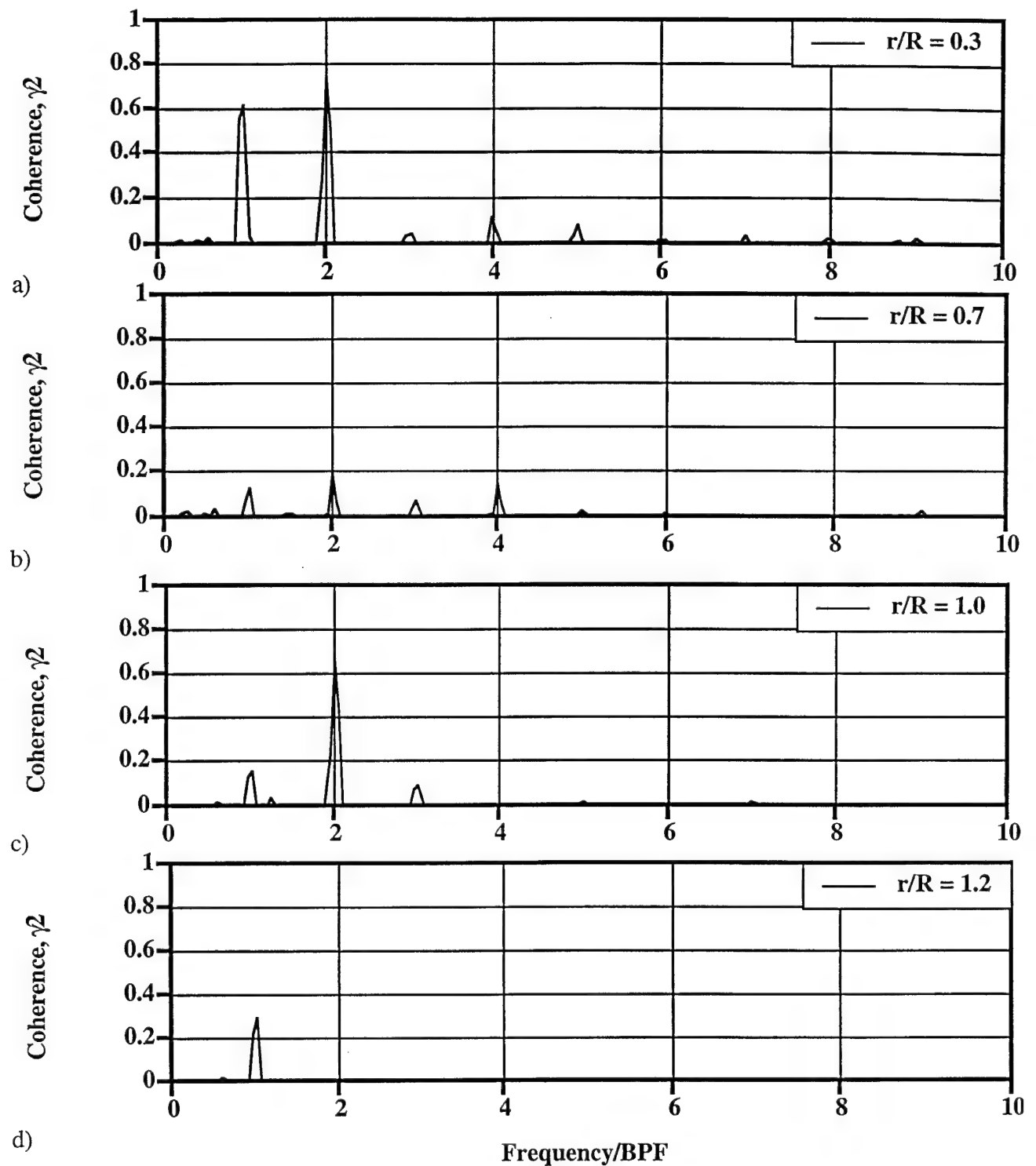
Figure 19.   Coherence Function Spectra for Hot-Wire/Microphone Measurements with Turbulent Inflow from Grid m = 3 in., U_∞ = 33 ft/s, 3000 RPM, Microphone at r/R = 15, ϕ = 120°, and Hot-Wire Locations in Propeller Wake at x/R = 0.025 and a) r/R = 0.3, b) r/R = 0.7, c) r/R = 1.0, and d) r/R= 1.2
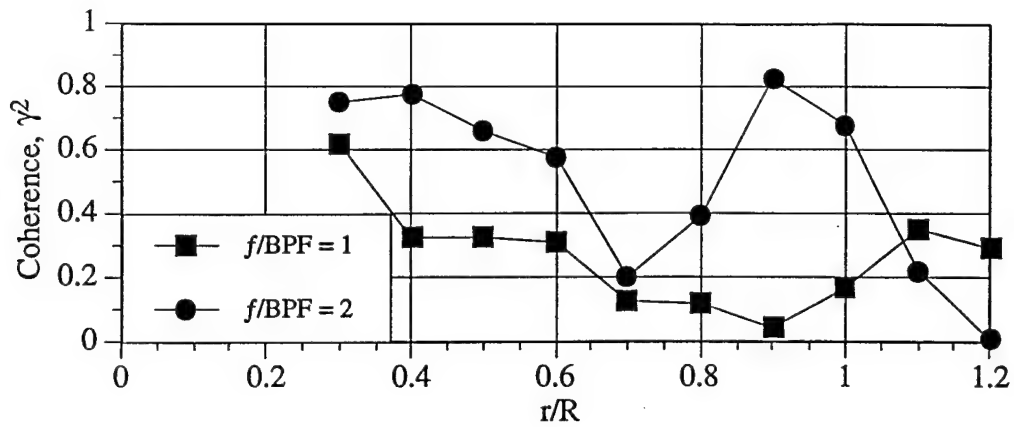
b)

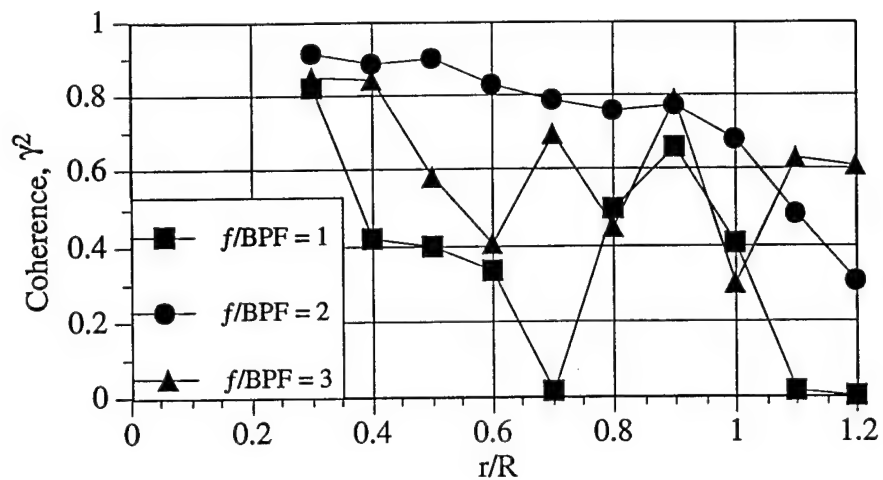Figure 20.   Coherence Function at BPF and 2BPF, for Hot-Wire/Microphone Measurements for Turbulent Inflow as a Function of Radial Location, r/R. $U_\infty = 33$ ft/s, 3000 RPM, m = 3 in., $u'/U_\infty = 5.5\%$.

APPENDIX B

AN EXPERIMENTAL STUDY ON PROPELLER NOISE DUE TO CYCLIC

FLOW DISTORTIONS

by

Srinivasan Subramanian
Aeroacoustics and Vibration
Carrier Corporation
P.O. Box 4808, Carrier Parkway
Syracuse, NY 13221

and

Thomas J. Mueller
Hessert Center for Aerospace Research
Department of Aerospace and Mechanical Engineering
University of Notre Dame
Notre Dame, IN 46556

SUMMARY

Large-scale non-uniformities in the approach flow to a propeller result in periodic unsteady blade forces that radiate tonal noise at the blade passing frequency and its higher harmonics. The current research experimentally investigates the free-field directivity of a four-bladed propeller interacting with matched and mismatched cyclic distortions. The study employs non-uniform flow generators that provide a three-cycle and four-cycle azimuthal distortion of the flow-field. As the inflow distortions contain just one dominant Fourier mode, a well-defined axisymmetric free-field directivity exists only for the fundamental tone. Higher harmonics, originating from small-scale flow gradients, have a random directivity. An extensive comparison of the measured tonal noise levels with the theoretical predictions shows an excellent agreement both in magnitude and directivity.

1. INTRODUCTION

In recent years, rotor noise control in engineering systems has become an active area of research. As a broad classification, rotor noise can be divided into two major categories: self-noise and interaction noise. A form of self-noise known as Gutin noise [1] is caused by the periodic rotation of the steady blade forces and can be neglected at low tip speeds. As opposed to self-noise, interaction noise is parasitic and is caused by incoming turbulence and non-uniformities in the approach flow. These inflow disturbances create a fluctuating pressure field around the rotating blades, leading to the radiation of acoustic waves to the far-field. While small-scale turbulence results in narrowband and broadband unsteady blade forces, flow distortions give rise to periodic force histories. These periodic unsteady forces result in tonal noise radiation at the blade-passing frequency and its higher harmonics [2,3].

Research in the sixties and seventies focused on obtaining analytical formulations for this propeller aeroacoustic problem. Lowson [4,5] provided analytical solutions for the far-field directivity of a free-field rotor operating in a distorted flow. Wright [6,7] employed a modal approach to solve the same problem. Both analyses treated the inflow distortion as a linear superposition of azimuthal Fourier modes, the modal value being equivalent to the number of cycle excursions. Their results established the critical dependence of the far-field tonal noise on the matching between the blade number and the inflow distortion Fourier modes. For modes that match integer multiples of the blade number, the individual blade forces vary in phase. Due to the rotation of the tangential force component, only the axial force component

radiates to the far-field, and the propeller acoustic directivity is equivalent to that of a system of axial dipoles. For modes that are mismatched with integer multiples of the blade number, the individual blade forces have a linear phase relation as they move through the cyclic disturbance, and the far-field radiation is subjected to inter-blade cancellations. When the mismatched value is equal to one, however, the changing direction of the tangential force component negates its linear phase variation, causing it to radiate as an in-phase dipole along the propeller plane [Wright,6]. This dipole radiation from the unsteady tangential forces interacts with a quadrupole-type radiation from the unsteady axial forces, producing a skew in the dipole directivity. The unsteady axial forces radiate like a quadrupole since their net phase is zero, and total cancellation is incomplete in the far-field only due to the existence of a path-difference. These analytical results of Lowson and Wright have been employed in conjunction with linear unsteady aerodynamic theories such as Sears [8] to provide theoretical predictions for the far-field noise levels.

As opposed to the extensive research in theoretical and computational work on flow distortion noise, experimental studies of the far-field directivity is limited to inflow distortions that typically have multiple azimuthal Fourier modes. Most experiments have been conducted in fans, compressors, and high-speed propellers where stators, inlet guide vanes, and pylons have served as wake-producing upstream devices. Tyler and Sofrin [9] conducted experiments on the acoustic radiation from an axial compressor. Their classical findings identified mismatching the number of stator vanes and rotor blades as a powerful method of noise control. Mugridge [10] studied the noise radiation from an automobile cooling fan operating behind a

radiator. The inflow distortion was measured by a hot-wire anemometer attached to the blade. The radiated noise was measured at three locations and found to be in good agreement with theory. Kobayashi and Groeneweg [11] studied the noise radiation of a JT15D turbofan engine due to wakes from upstream rods. The first set of experiments utilized a symmetric arrangement of the rods in the azimuthal direction. The wakes were assumed to have a gaussian-type characteristic, and this was related to the measured overall sound power. A second set of experiments introduced localized wakes in the flow-field through a cylindrical probe attached to the duct housing. The radiated sound power was found to be proportional to the immersion length of the probe.

Block and Gentry [12] conducted an extensive study on propeller tonal noise radiation due to pylon-wake interaction. The experiments were performed in a low-speed anechoic wind tunnel and employed several pylon arrangements in front of the high-speed propeller. The radiated noise was mapped over a range of 110° in the spherical direction and 340° in the azimuthal direction. This exhaustive mapping, necessitated by the asymmetric nature of the wake, showed the azimuthal directivity to be asymmetric as well. Borchers and co-workers [13] studied the tonal radiation from a propeller interacting with the wake of an airfoil. The airfoil was placed directly upstream of the propeller and extended from the bottom of the wind tunnel to the propeller centerline. The free-field measurements indicated a sharp increase in the tonal noise levels. The directivity was found to be highly skewed towards the direction the propeller rotated as it passed the wake.

The inflow distortions created in these experiments were mostly gaussian-type

wakes from upstream devices and contained multiple Fourier modes. The free-field directivity therefore was not axisymmetric and in some cases possessed a high degree of asymmetry. In contrast, little work has been done on the acoustic radiation from inflow distortions that have only one dominant Fourier mode. Such sinusoidal cyclic distortions have been extensively employed for measuring unsteady blade forces on marine propellers operating in water tunnels [12,13]. These experiments have successfully correlated the measured unsteady shaft forces to the amplitude of the cyclic inflow distortion. However, no such comparison exists for the acoustic radiation from cyclic disturbances, partly because of the difficulty in creating aerial flow distortions that have only one dominant cycle.

The objective of this research was to conduct a fundamental experimental study on the acoustic radiation of a low-speed propeller interacting with matched and mismatched cyclic distortions. Emphasis was placed on two basic case studies: one that matched the blade number and produced in-phase axial dipole radiation, and one that mismatched the blade number and yielded in-phase tangential dipole radiation. To quantify the azimuthal variation of the two cycles, mean velocity profiles were obtained using hot-wire anemometry. Acoustic measurements in an anechoic environment provided the free-field magnitude and directivity of the radiated tonal noise. The magnitude and directivity of this tonal noise radiation was then correlated with the measured velocity profiles through quantitative predictions from theory [16].

2. EXPERIMENTAL TEST FACILITY

The experiments were conducted in a low-speed, free-jet anechoic flow facility located at the University of Notre Dame. The facility consists of a open-jet wind tunnel enclosed within an anechoic chamber (9.1m x 7.3m x 3.6m) and has a free-jet length of four feet (1.22 m). The tunnel provides a low-turbulence, laminar free-jet at the inlet exit for speeds ranging from 3 m/s to 20 m/s. Calibrations with a white-noise generator established an anechoic region where the acoustic levels observed the required free-field decay for frequencies above 150 Hz. All experiments were carried out at speeds around 12.7 m/s (Mach number=0.03), and thus the acoustics did not require any correction for shear-layer refraction effects. For more details regarding the design, construction, and calibration of this facility, the reader is asked to consult Mueller et al [15,16].

The experimental test propeller employed for the current study is a four-bladed marine propeller developed by David Taylor Ship Research and Development Center. The propeller has an expanded area ratio of 0.451, a tip diameter of 0.2504 m (hub diameter = 0.05 m), and is coded as Prop 3714 in the U.S. Naval Propeller listings. Table 1 provides the section properties of the test propeller. The propeller was driven at a constant speed (resolution = ±0.01 RPM) by a dynamometer system that consisted of a brushless servomotor and a Linear Variable Differential Transformer. A complete description of the dynamometer system can be found in Asson [19].

2.1 NON-UNIFORM FLOW GENERATORS

As outlined in the introduction, the goal of this research was to build non-

uniform flow generators that will provide a single sinusoidal distortion of the axial flow velocity. Figure 1(a) illustrates the design features. A square wooden box is split into equi-angular sectors by some mechanical means. If such a section is filled with straws in alternating sectors, the disproportionate pressure drop will cause the fluid through any two adjoining sectors to exit with different speeds. If care is taken to ensure that each alternating sector has the same blockage, the exiting flow will be a set of circumferential jets wherein alternate sectors have the same flow speed. With increasing distance from the inlet exit, the velocity profile at a given radius may appear similar to two-dimensional jet mixing, yielding an inflow distortion that has a dominant Fourier mode of order p.

Based on the above design, a three-cycle and a four-cycle generator were constructed. The 0.197 m long flow generators utilized 0.003 m thick aluminum plates for separating the various compartments in the square wooden box. A straw size of 0.005 m diameter was chosen to fill the straw sectors. Once filled, the straws were tightly packed and held in place by fiberglass screens both at the front and back. The two flow generators were then attached to the inlet by means of guide-bolts. The complete screen configurations are shown in Figures 1(b) and 1(c).

2.2 DATA ACQUISITION EQUIPMENT

The data acquisition for the current research was conducted with a Macintosh IIfx computer. The boards employed for sampling the aerodynamic and acoustic signals were standard A/D converters built by National Instruments, Inc. The incoming signals were first sampled at the desired frequency and then post-processed

in the computer. The details of the software development can be found in Scharpf [20].

A single hot-wire sensor, mounted on a three-dimensional traversing unit, was employed for quantifying the non-uniform variation of the axial flow velocity. The calibration of the single wire was conducted prior to the installation of the flow generator. The hot-wire anemometry was performed with a TSI IFA 100 Intelligent Flow Analyzer model 158. The acoustic measurements employed a B&K 0.0127 m (0.5 inches) condenser microphone type 4181. The microphone was traversed through a rotating boom arrangement at a given radius from the propeller. The microphone signal was first high-passed at 10 Hz to remove the low-frequency noise and then low-passed at 5.5125 kHz for anti-aliasing. The signal was then post-processed to narrow-band, constant-bandwidth spectra with a resolution of 10 Hz. The tones at the blade-passing frequency and higher harmonics occupied the central frequency of their corresponding bands. Prior to the acoustic measurements, the microphone was calibrated using a B&K microphone calibrator, pistonphone type 3541.

The uncertainty in the mean velocity measurements was ±0.2 m/s. The uncertainty in the acoustic spectrum level was ±0.70 dB.

3. EXPERIMENTAL PROCEDURE

3.1 TEST CONDITIONS

As the aerodynamic and acoustic measurements were not carried out at the

same time, the non-uniform flow-field needed to be referenced at a suitable location. Since the distortions introduced by the screen underwent rapid mixing at the core regions, a downstream centerline location was chosen to reference the flow-field. All experiments—aerodynamic and acoustic—were carried out after referencing the flow velocity to 12.7 m/s at a downstream distance of 0.381 m from the screen center. The propeller was positioned at a distance of 0.508 m from the flow generator (see Figure 2(a) for details). This corresponded to a distance of four propeller radii. The propeller was operated at two speeds—3000 RPM and 3600 RPM. Based on the reference velocity of 12.7 m/s, these speeds corresponded to advance ratios of 1.0 and 0.83 respectively.

3.2 MEASUREMENT LOCATIONS

As the primary concern of the aerodynamics was the azimuthal variation of the axial flow velocity, circumferential mean velocity profiles were obtained at the propeller plane along radial locations of 0.2, 0.4, 0.6, 0.8, 1.0, and 1.2 times the propeller tip radius. For the radial positions of $0.2R_t$, $0.4R_t$, and $0.6R_t$, the resolution of the azimuthal angle was six degrees. For the outer radii of $0.8R_t$, $1.0R_t$, and $1.2R_t$, an increment of five degrees was chosen to provide a better resolution. These two increments were adequate to quantify a three or four-cycle azimuthal variation in the mean velocity.

The measurement points for the acoustics, shown in Figure 2(b), were located on the horizontal plane OXZ. θ is the azimuthal angle measured from the positive Z-axis along the direction of propeller rotation. ϕ is the spherical angle measured

from the downstream axis $O\vec{\prime}X$. The acoustic measurements were obtained along ϕ at a radius of 1.9 m $(15.0R_t)$ on both sides of the propeller axis. This provided the propeller noise directivity along the azimuthal half-planes of $\theta = 0°$ and $\theta = 180°$. To obtain the directivity along the plane XY, the screens were reattached to the inlet after *rotating* them by 90° against the direction of propeller rotation. Figures 3(a) and 3(b) show the frontal view of both cycle screens and their two orientations. In the second orientation, the shaded region—labeled as *Side One* in Figure 2(a)— faced the positive Z-axis and enabled the directivities to be obtained along the azimuthal half-planes of $\theta = 90°$ and $\theta = 270°$. Since the propeller radiation may not be axisymmetric due to possible contamination from other Fourier modes, the azimuthal four half-planes provided the means of ascertaining the departure from axisymmetry. These contaminating modes alter the unique phase relation between the individual blade forces, thus leading to azimuthal asymmetries in the directivity.

4. RESULTS AND DISCUSSION—AERODYNAMICS

The aerodynamic results in this section discuss the azimuthal variation of the mean velocity and its spatial Fourier transform. As radiation at the fundamental harmonic predominantly originates from modes that are close to the blade number, the modal analysis focuses on the third, fourth, and fifth modes. All velocities and Fourier amplitudes are non-dimensionalized by the volume average velocity, V_a, that is representative of the total flow rate through the circular area of radius $1.2R_t$.

4.1 THREE-CYCLE AERODYNAMICS

Figure 4 shows the results of the measurements taken at the six radial positions corresponding to the propeller plane location. The progressive radial change in the mean velocity profile is apparent. As the radius increases, the shear layers become well-established and separate the low-velocity from the high-velocity regions. The low-velocity and the high-velocity regions are also equal in area. Since the straw-sections occupy fifty per cent of the total inlet area, this result is to be expected.

A spatial Fourier decomposition of the flow-field showed the relative dominance of the third mode at all the radii. Though other modes were also present in the flow-field, they were much weaker in magnitude and showed a random radial variation in phase. Particular attention was focused on possible contamination by the fourth mode due to its strong acoustic coupling with the blade number. Figure 5 compares the radial variations of the three Fourier modes—3, 4 and 5. The amplitude of the third mode linearly increases with radius and reaches a value of 0.08 at the outer radii. The phase remains a constant except at $0.2R_t$ where it deviates due to mixing. The fourth mode has a nearly constant amplitude of 0.02 at all the radii while the phase changes by over eighty degrees. Though this indicates a possible contamination of the acoustic signature, the influence will probably be weakened by the changing modal phase. The fifth mode has a radial variation in amplitude and phase that is quite similar to the fourth mode. However, its weaker acoustic coupling makes it an unlikely candidate for a strong influence on the fundamental tone radiation.

4.2 FOUR-CYCLE AERODYNAMICS

Figure 6 shows the mean velocity profiles obtained from the four-cycle screen at the propeller plane location. There is a considerable change in the azimuthal profiles from the inner regions to the outer radii. This is evident at the $0.2R_t$ radius where one of the four cycles has dissipated. With increasing radius, this cycle starts to reappear in the azimuthal profile. The profiles at the outer radii look very much like four equal-amplitude square pulses. This symmetry contrasts with the three-cycle screen where each cycle had a distinct size and shape. The outer profiles also display sharp kinks that are probably due to local shear effects.

The azimuthal Fourier decomposition showed the dominance of the fourth mode at all radial locations excepting the $0.2R_t$ radius where it had been superseded by the third mode. Other modes displayed random behavior both in amplitude and phase. Figure 7 shows the radial variations of the third, fourth and fifth modes. The fourth mode, with the exception of the $0.2R_t$ location, has a linear increase in amplitude with radius and attains a value close to 0.07 at the propeller tip location. The phase stays constant close to 90 degrees except again at the $0.2R_t$ location where dissipation leads to a change of phase. This phase of 90 degrees is a result of screen orientation with respect to the reference axis OZ. The other two modes—three and five—have significantly smaller amplitudes at the outer radii. The weak presence of these two modes, coupled with their low acoustic coupling, indicates that these modes will not affect the fundamental harmonic directivity except possibly at the propeller plane.

5. RESULTS AND DISCUSSION—ACOUSTICS

Acoustic spectra were obtained at the measurement locations shown in Figure 2(b). Figures 8(a) and 8(b) compare the propeller noise spectra taken with the clean flow with those obtained with the screens. There is a clear difference in the broadband levels of the two spectra. Moreover, distinct tonal harmonics appear only in the spectra with the screens. The tones are seen to rise well above the broadband level.

Since the tones represent radiation from periodic unsteady blade forces, any discussion of their directivity must first establish the height of these tones above the broadband spectrum. The broadband levels are created by aperiodic blade forces that are a result of turbulence or other random interactions. Once a harmonic spike disappears into the broadband level, the spectrum level at that frequency loses its significance in any discussion of a tonal directivity plot. To emphasize this distinction, all tonal directivity plots are referenced by their local broadband levels.

5.1 FUNDAMENTAL DIRECTIVITY FROM THREE-CYCLE FLOW

Figure 9(a) compares the four directivities obtained at the azimuthal half-planes of $0°, 90°, 180°$ and $270°$ for a propeller speed of 3000 RPM. There is a smooth decrease in the tonal level from downstream to upstream, and this decrease is seen on all four half-planes. The decrease is about 6 dB for the $90°, 180°$ and $270°$ azimuthal half-planes and 8 dB for the $0°$ azimuthal half-plane. Though such a reduction from downstream to upstream is expected from theory due to the interaction between the axial unsteady forces and the tangential unsteady forces, it can be seen that

the reduction does not take place equally along all azimuthal half-planes. At a spherical angle of 130°, the four directivities have a scatter of 6 dB. Moreover, the azimuthal half-planes 90° and 270° have higher noise levels at all spherical angles. This asymmetry in the radiation is likely a result of the unequal cycle shapes seen earlier in the mean velocity profiles. A departure from a pure cyclic disturbance results in a departure from a linear phase variation between the individual blade forces. Consequently, azimuthal asymmetries occur in the directivity. As the Fourier analysis of the mean velocity profiles had indicated a weak presence of the fourth mode, the asymmetry can be attributed to its strong influence. Moreover, such an influence will be more pronounced at regions of lower tonal intensity, as seen in the present case.

Figure 9(b) shows the same directivity at 3600 RPM. The tone levels have increased by 2 to 3 dB along all four azimuthal half-planes. Again, all four directivities decrease from downstream to upstream, but the reduction is stronger in comparison to 3000 RPM. The bulk of this reduction, 7 to 8 dB, takes place from the propeller plane to upstream. The four directivities also have a smaller scatter—around 3 to 4 dB. Since the directivities at the two speeds don't display the same level of asymmetry, it appears that the asymmetries could also be due to changes *induced* by the propeller to the oncoming flow. Any creation or dispersion of distortions in the flow-field will correspondingly introduce or remove asymmetries in the acoustic directivity. It appears that small but distinct changes introduced by the propeller may account for the observed directivity differences between the two rotational speeds.

5.2 FUNDAMENTAL DIRECTIVITY FROM FOUR-CYCLE FLOW

The fundamental tonal directivity at 3000 RPM is shown in Figure 10(a). The tonal magnitudes are seen to rise well above the background and have higher noise levels than seen in the case of the three-cycle screen. There is a sharp reduction of 15 dB from the off-plane regions to the propeller plane. At the propeller plane location, the tones occupy only 1-2 dB above the broadband level. The directivity pattern is symmetric both with respect to the propeller axis as well as the propeller plane and thus constitutes a dipole whose axis is aligned with the propeller axis of rotation. This dipole-type radiation has a slight skew in the downstream direction for the azimuthal half-planes of 180° and 270°. This skew is probably a result of slight differences between the individual cycles. The four directivities are within a scatter of 2 dB at all spherical locations. This symmetry in the radiation appears to be a direct result of the symmetry in the four-cycle mean velocity profile.

As seen in Figure 10(b), the profile at 3600 RPM also has an axial dipole-type directivity but with a few significant differences. The tonal levels are higher everywhere. There is also a clear asymmetry in the directivity patterns at the propeller plane. While the tonal level at this location has increased for $\theta = 0°$, the level at $\theta = 90°$ has decreased. This asymmetry was verified more than once and indicated that it could be a result of a possible change in the inflow with increase in the propeller speed. Since this change affected only two of the four azimuthal locations, it was hypothesized that the propeller—operating at 3600 RPM—may have weakened one of the four cycles. Such an erosion will have a greater effect at

the propeller plane due to the low tonal intensity at that location but will have a lesser effect at off-plane regions.

5.3 HIGHER HARMONIC DIRECTIVITY

Unlike the fundamental tone, the directivity of the higher harmonics did not follow any distinct pattern for both screens. Figures 11(a) and 11(b) show the directivity at the second harmonic for a propeller speed of 3000 RPM. The large scatter in the directivity plots indicate that these tones are radiated due to the propeller's interaction with small-scale velocity gradients in the flow-field. Such random gradients were seen to occur in the mean velocity profiles at the outer radii. While such sharp gradients will also cause radiation at the first harmonic, the amplitudes are not strong enough to affect the fundamental tonal radiation due to the dominant Fourier mode.

6. COMPARISON WITH THEORY

As outlined in the introduction, the measured harmonics from each screen were employed in a theoretical formulation to provide the magnitude of the radiated noise. The theoretical predictions use the airfoil analyses of Atassi [1984] and provide a lower and upper bound for the unsteady blade forces. The far-field noise levels are calculated using the classical results of Lowson and Wright. The spread between the lower and upper acoustic bounds is $\pm$ 3 dB. While both bounds have been calculated using two-dimensional unsteady aerodynamic theory applied in a strip-wise sense, the lower bound includes a quasi-steady correction for the effect of the

tip vortex. A more detailed account of the theory can be found in Subramanian [16] and Subramanian and Atassi [21]. The experimental data from all four azimuthal half-planes have been included in the comparison.

Figure 12(a) shows the comparison at 3000 RPM for the three-cycle screen. The measured tonal levels are seen to lie within or close to the predicted bounds for all four azimuthal half-planes. A few experimental points lie outside the bounds, but these are still close to one of the two bounds and are within the experimental uncertainty of $\pm$ 0.7 dB. The spherical directivity at $\theta = 180°$ follows the theoretical curve at nearly all angular locations. Figure 12(b) shows the comparison at 3600 RPM. Once again, the experimental values fall within the bounds at most angular locations. Interestingly, all four directivities are seen to have a sharper drop from downstream to upstream than the theoretical curves.

Figure 13(a) shows the comparison at 3000 RPM for the four-cycle flow. The experimental points fall within the theoretical curves for all four azimuthal half-planes except at the location corresponding to the propeller plane. The theoretical prediction for the sound pressure level at this location is zero pascals. Practically, a tone will always be present due to small-scale distortions in the flow-field. Elsewhere, the magnitude of the tone is considerably higher and falls within the predicted bounds. Figure 13(b) displays the comparison for an RPM of 3600. Two of the four experimental directivities, $\theta = 180°$ and $\theta = 270°$, follow the theoretical directivities closely. While the directivity at $\theta = 90°$ has a slight deviation close to the propeller plane, the directivity at $\theta = 0°$ has a significantly higher noise level at the same location. This asymmetry has already been attributed to the erosion of one of the

four cycles. Aside from this deviation at the propeller plane, the four-cycle propeller radiation is also seen to agree with the theoretical trends.

7. CONCLUSIONS

An experimental study on the acoustic radiation of a propeller interacting with cyclic distortions has been conducted. A four-bladed propeller was operated in three and four-cycle inflow distortions to study the tonal noise radiation arising from matched and mismatched distortions. In each distortion case, the amplitude of the dominant cycle linearly increases with radius while the phase remains a constant. Other cyclic modes also exist in the flow-field but are well below the amplitude of the dominant cycle. The acoustic spectra from this interaction contain dominant tones at the blade-passing frequency and its higher harmonics. The fundamental tones typically rise 10 to 20 dB above the broadband levels. A well-defined axisymmetric directivity exists only for the fundamental tone. Asymmetries in this fundamental directivity appear mostly at locations where the tonal value is low. In contrast, the higher harmonics have a random directivity.

Each screen flow has a unique fundamental harmonic directivity that is representative of the cycle number. The directivity from the three-cycle has a smooth decrease from downstream to upstream and has a scatter of 6 dB between the four azimuthal half-planes. This scatter is probably a result of contamination from the fourth mode, which can significantly alter the linear phase relation between the individual blade forces. The propeller radiation from the four-cycle has an axial

dipole-type radiation that has very little scatter at off-plane regions. Along the propeller plane, the radiation from the four-cycle shows an asymmetry at 3600 RPM. It appears likely that the asymmetry at 3600 RPM is caused by the dissipation of one or more shear layers.

The propeller tonal levels due to the three-cycle and four-cycle screen have an excellent agreement with the theoretical trends both in magnitude and directivity. The noise levels fall within the theoretical spread of $\pm$ 3 dB at most locations. At the few locations where the experimental values lie outside the bounds, the discrepancy is well within the experimental uncertainty of $\pm$ 0.7 dB. This agreement is true for both propeller speeds.

ACKNOWLEDGMENTS

REFERENCES

[1] L. Gutin 1948 *NACA Technical Memorandum* NACA 1195. On the Sound Field of a Rotating Propeller ; translated from the Russian paper L. Gutin 1936 *Phys. Z. Sowjetunion* **9**. Uber Das Schalfeld Einer Rotierenden Luftschraube.

[2] C.L. Morfey 1973 *Journal of Sound and Vibration* **28**, 587-617. Rotating Blades and Aerodynamic Sound.

[3] W.K. Blake 1986 *Mechanics of Flow Induced Sound and Vibration* (two volumes), Volume 17, Applied Mathematics and Mechanics, Academic Press, Inc.

[4] M.V. Lowson and J.B. Ollerhead 1969 *Journal of Sound and Vibration* **9**, 197-222. A Theoretical Study of Helicopter Rotor Noise.

[5] M.V. Lowson 1970 *Journal of the Acoustical Society of America* **47**, 371-385. Theoretical Analysis of Compressor Noise.

[6] S.E. Wright 1969 *Journal of Sound and Vibration* **9**, 223-240. Sound Radiation from a Lifting Rotor Generated by Asymmetric Disk Loading.

[7] S.E. Wright 1971 *Journal of Sound and Vibration* **17** 437-498. Discrete Radiation from Rotating Periodic Forces.

[8] W.R. Sears 1941 *Journal of Aeronautical Sciences* **8**, 104-108. Some Aspects of Non-stationary Airfoil Theory and Its Practical Applications.

[9] J.M. Tyler and T.G. Sofrin 1962 *Society of Automotive Engineers Transactions* **70**, 309-332. Axial Flow Compressor Noise Studies.

[10] B.D. Mugridge 1976 *Journal of Sound and Vibration* **44**, 349-367. The Noise from Cooling Fans Used in Heavy Automotive Vehicles.

[11] H. Kobayashi and J.F. Groeneweg 1980 *AIAA Journal* **18**, 899-906. Effects of Inflow Distortion Profiles on Fan Tone Noise.

[12] P.J.W. Block and G.L. Gentry, Jr 1986 *NASA Technical Paper 2609.* Directivity and Trends of Noise Generated by a Propeller in a Wake.

[13] I.U. Borchers, R. Scholten and B.W. Gehlhar 1986 *AIAA 10th Aeroacosutics Conference, 86-1928.* Experimental Results of the Noise Radiation of Propellers in Non-uniform Flows.

[14] R.J. Boswell, S.D. Jessup and K. Kim 1981 *Propellers '81 Symposium*, Society of Naval Architects and Marine Engineering, Virginia Beach, Virginia, 181-202. Periodic Blade Loads on Propellers in Tangential and Longitudinal Wakes.

[15] S.D. Jessup 1990 *Research and Development Report*, DTRC-90/015, Ship Hydromechanics Department, David Taylor Research Center, Bethesda, Madison. Measurement of Multiple Blade Rate Unsteady Propeller Forces.

[16] S. Subramanian 1993 *Ph.D. Dissertation*, University of Notre Dame, Notre Dame, Indiana. Experimental and Computational Studies on Propeller Noise Due to Inflow Distortion.

[17] T.J. Mueller, D.F. Scharpf, S.M. Batill, R.B. Strebinger, C.J. Sullivan, and S. Subramanian 1992 *Seventeenth AIAA Ground Testing Conference*, AIAA

92-3883, Nashville, Tennessee. The Design of a Low-Noise Wind Tunnel for Acoustic Measurements.

[18] T.J. Mueller, D.F. Scharpf, S.M. Batill, R.B. Strebinger, C.J. Sullivan, and S. Subramanian 1992 *European Forum on Wind Tunnels and Wind Tunnel Test Techniques*, Southampton University, United Kingdom. A New Low Speed Wind Tunnel for Acoustic Measurements.

[19] K.M. Asson 1990 *Master's Thesis*, University of Notre Dame, Notre Dame, Indiana. The Development of an Advanced Dynamometer System to Experimentally Determine Propeller Performance.

[20] D.F. Scharpf 1993 *Ph.D. Dissertation*, University of Notre Dame, Notre Dame, Indiana. An Experimental Investigation of the Sources of Propeller Noise due to Turbulence Ingestion.

[21] S. Subramanian and H.M Atassi—To be Submitted to *Journal of Fluids Engineering*. Acoustic Radiation from a Loaded Propeller Operating in Low-speed, Non-uniform Flows.
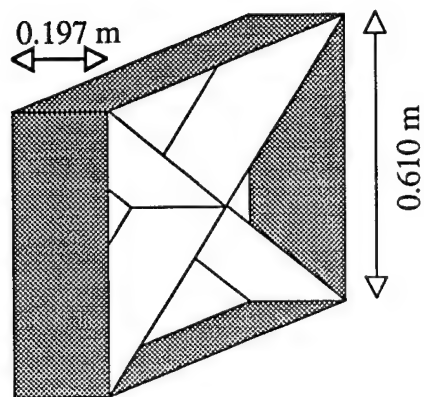
a.) Flow Generator
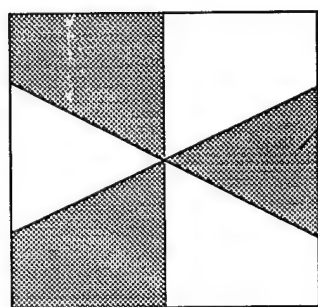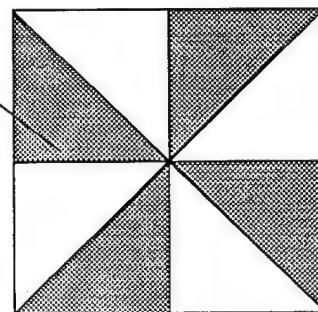
b.) Three-cycle screen   c.) Four-cycle screen

Figure 1: Schematic of Non-uniform Flow Generator.   (a) Flow Generator. (b) Three-cycle Screen. (c) Four-cycle Screen.
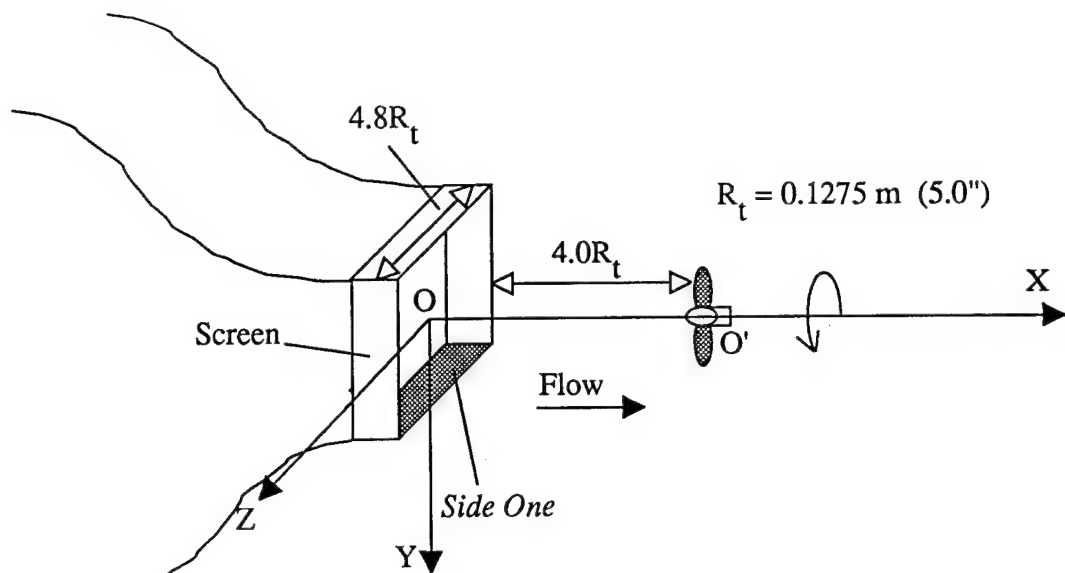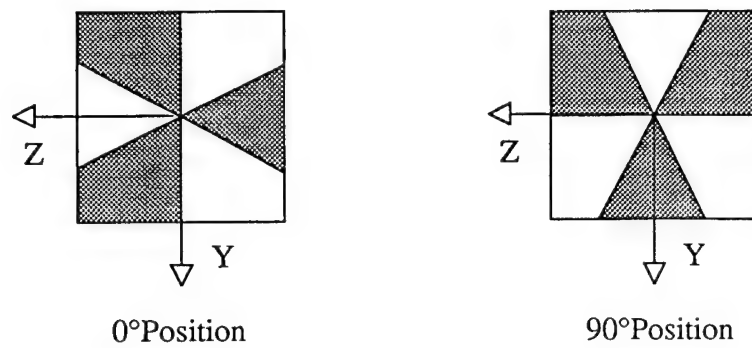
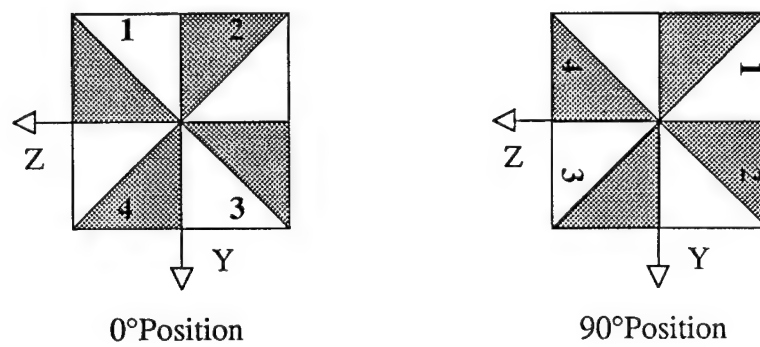a.) Experimental Arrangement
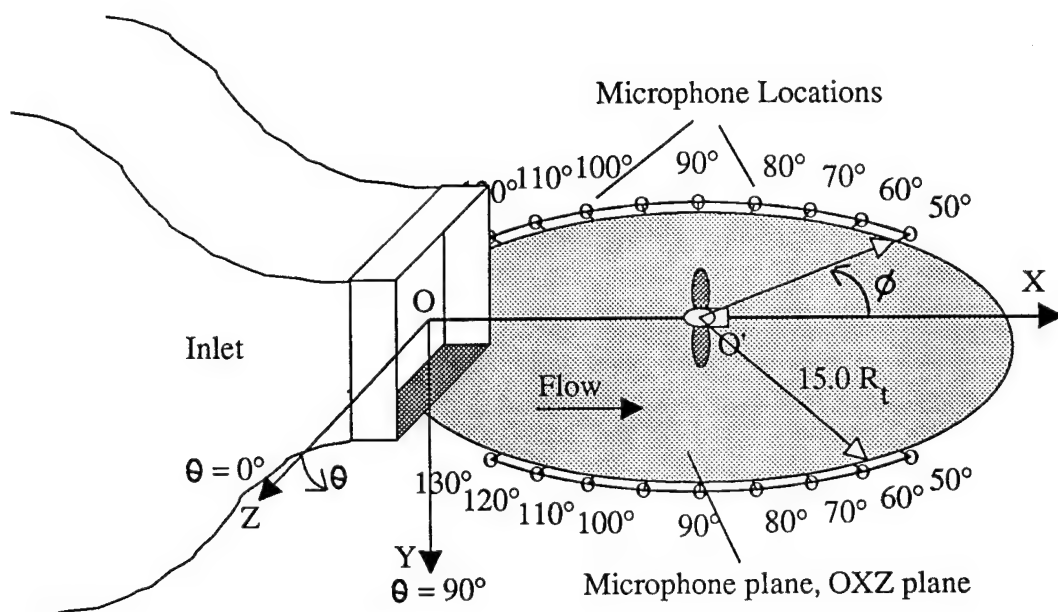
b.) Microphone Locations

Figure 2: Experimental Set-up. (a) Experimental Arrangement. (b) Microphone Locations.

a.) Three-cycle screen

b.) Four-cycle screen

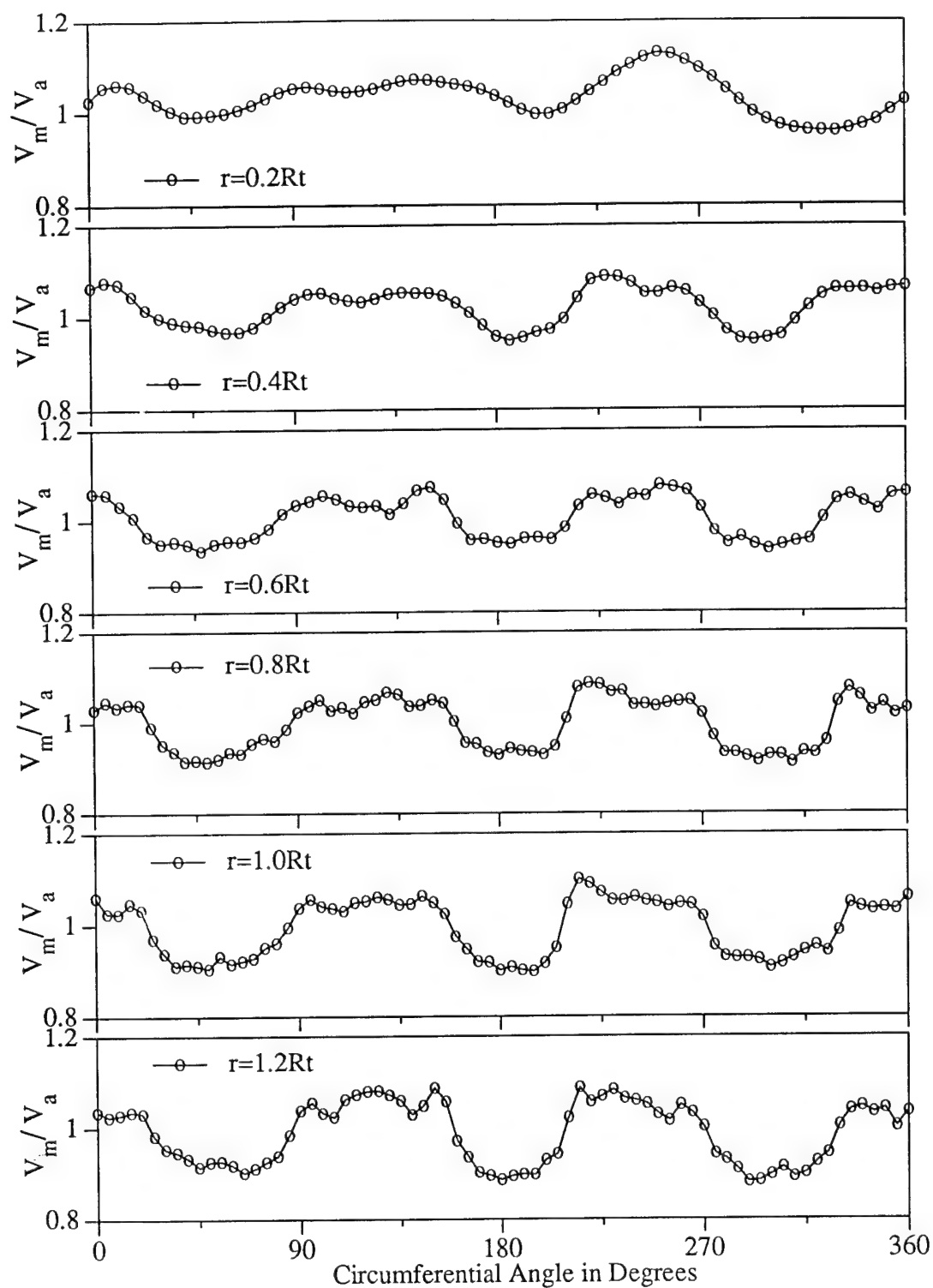Figure 3: Screen Orientations for Acoustic Measurements.   (a) Three-cycle Screen. (b) Four-cycle Screen.

Figure 4: Three-cycle Screen Flow: Mean Velocity Profiles at the Propeller Plane.
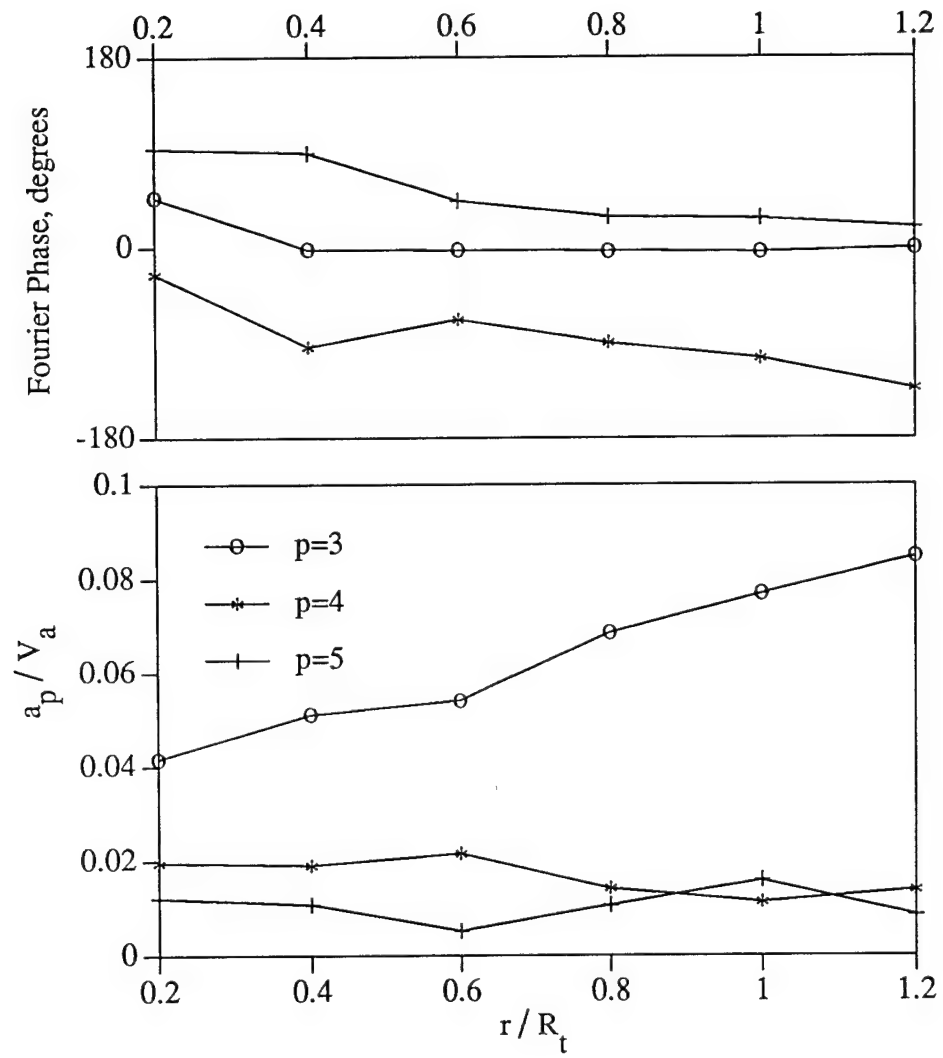
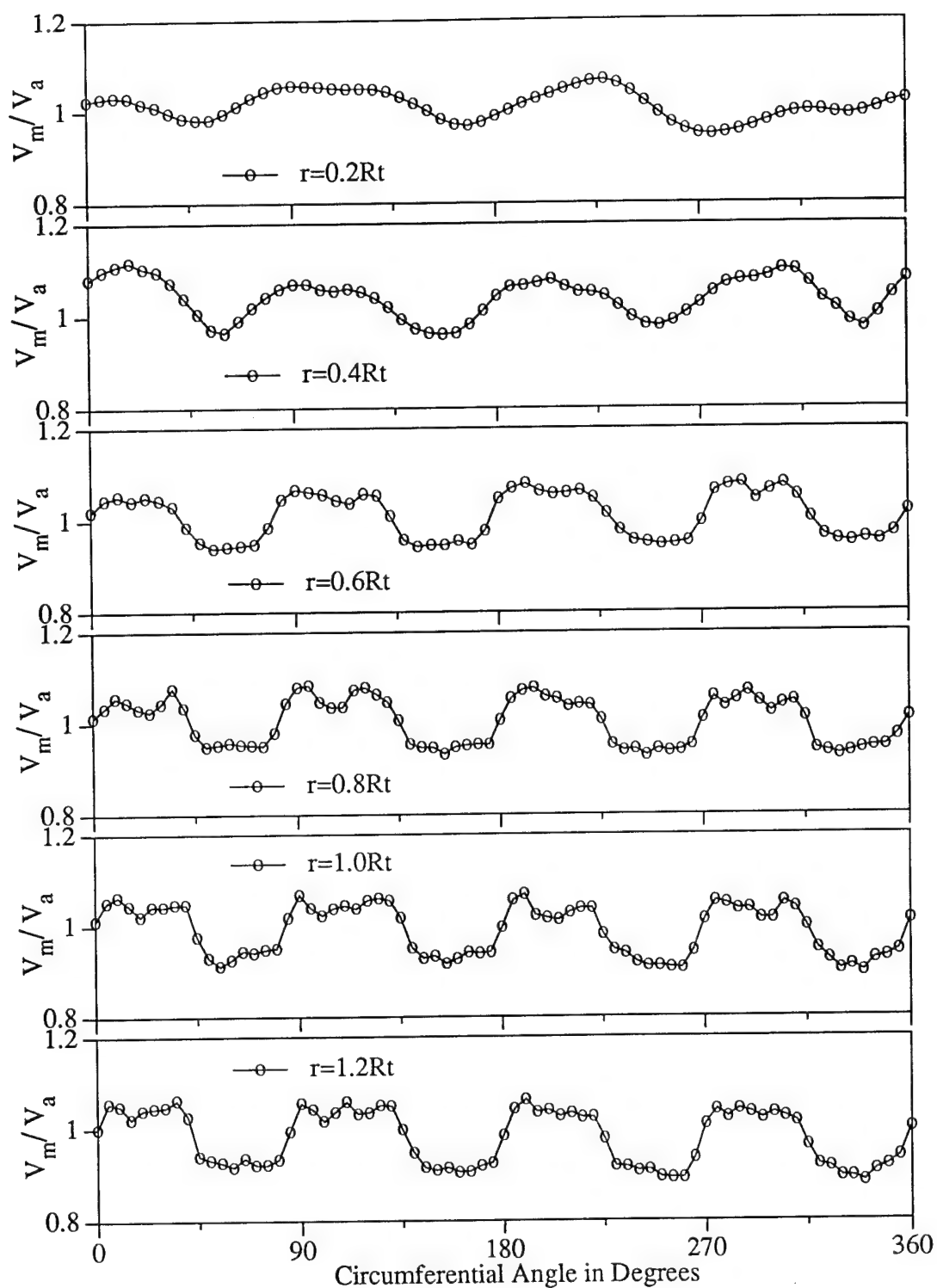Figure 5: Three-cycle Screen Flow: Radial Variation of the Fourier Modes.

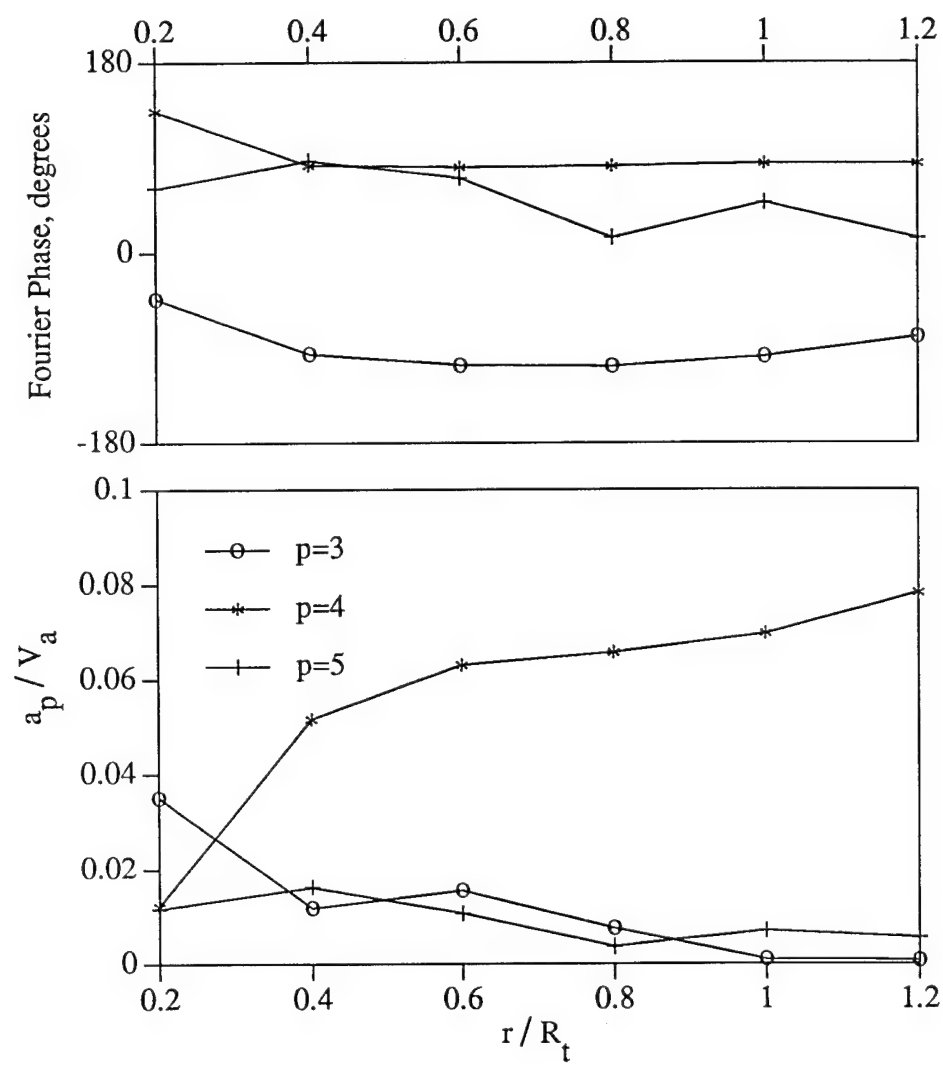Figure 6: Four-cycle Screen Flow: Mean Velocity Profiles at the Propeller Plane.

Figure 7: Four-cycle Screen Flow: Radial Variation of the Fourier Modes.
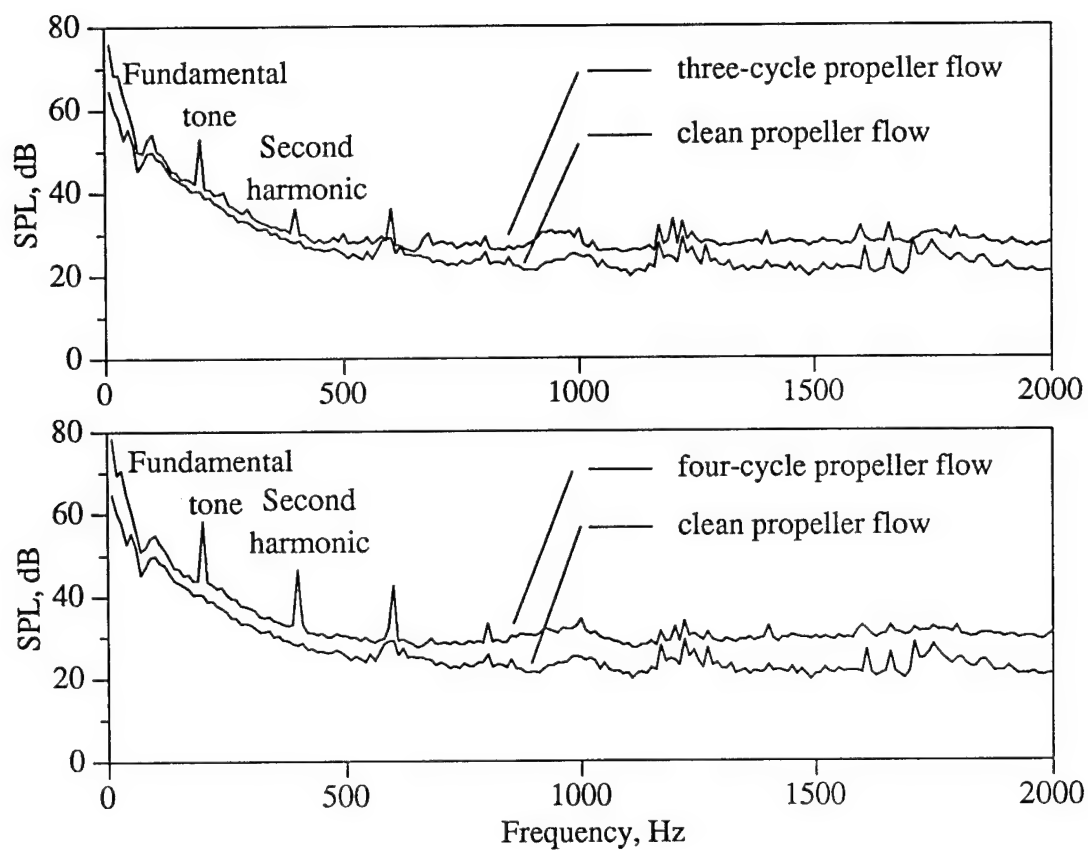
Figure 8: Propeller Noise Spectra with and without the Screens.   (a) Three-cycle Screen. (b) Four-cycle Screen.
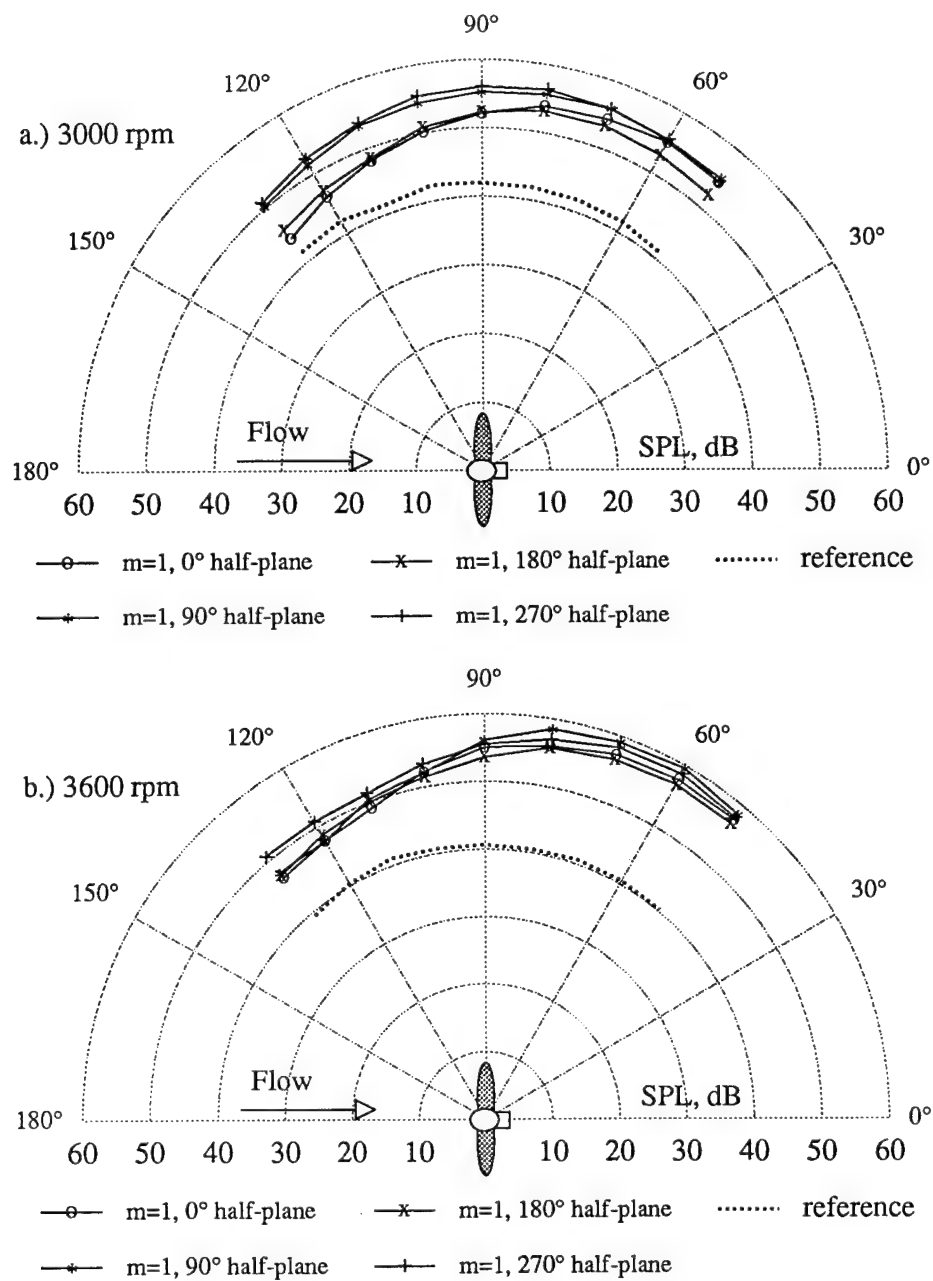
Figure 9: First Harmonic Directivity due to Three-cycle Flow.   (a) 3000 RPM. (b) 3600 RPM.
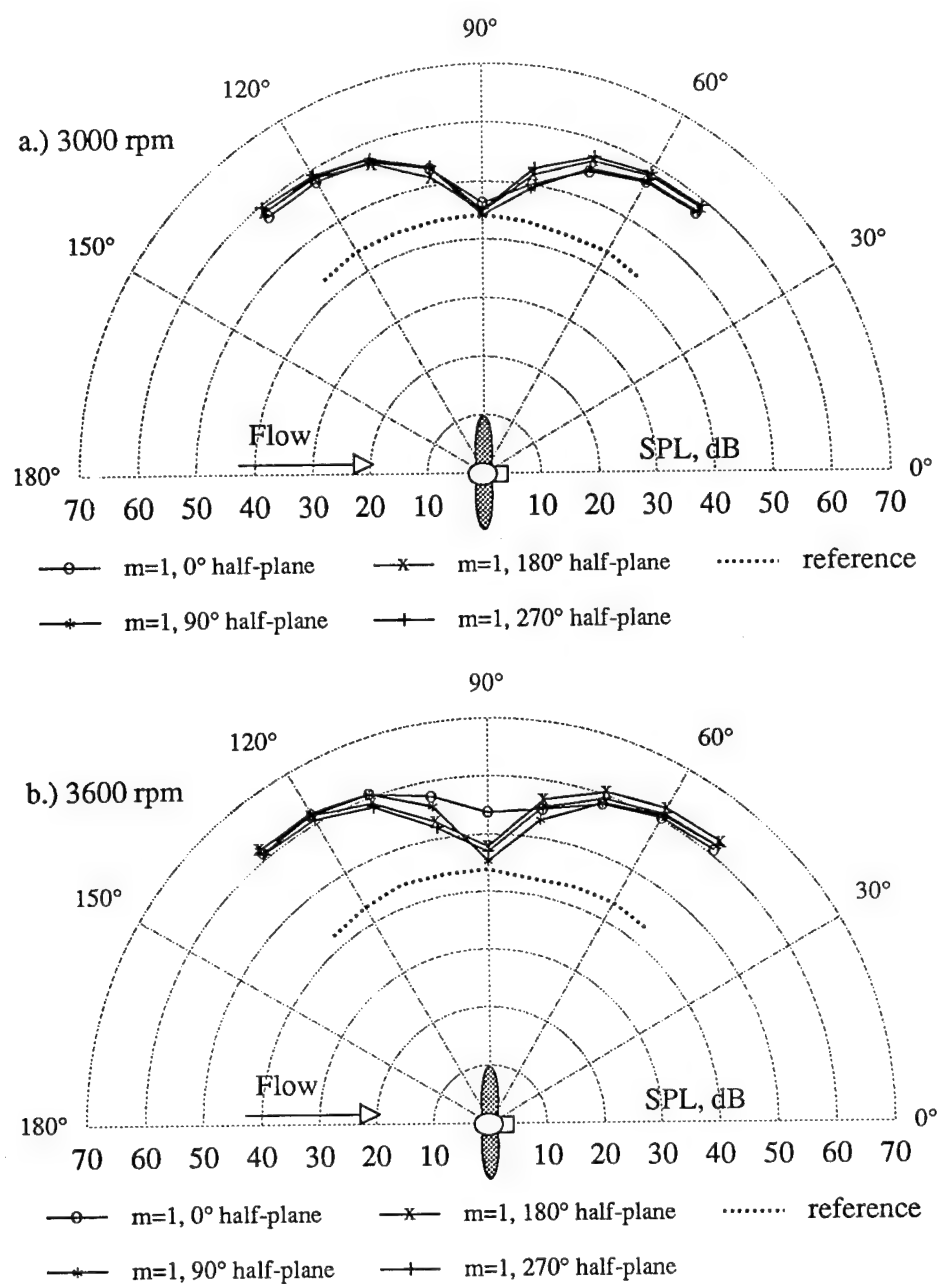
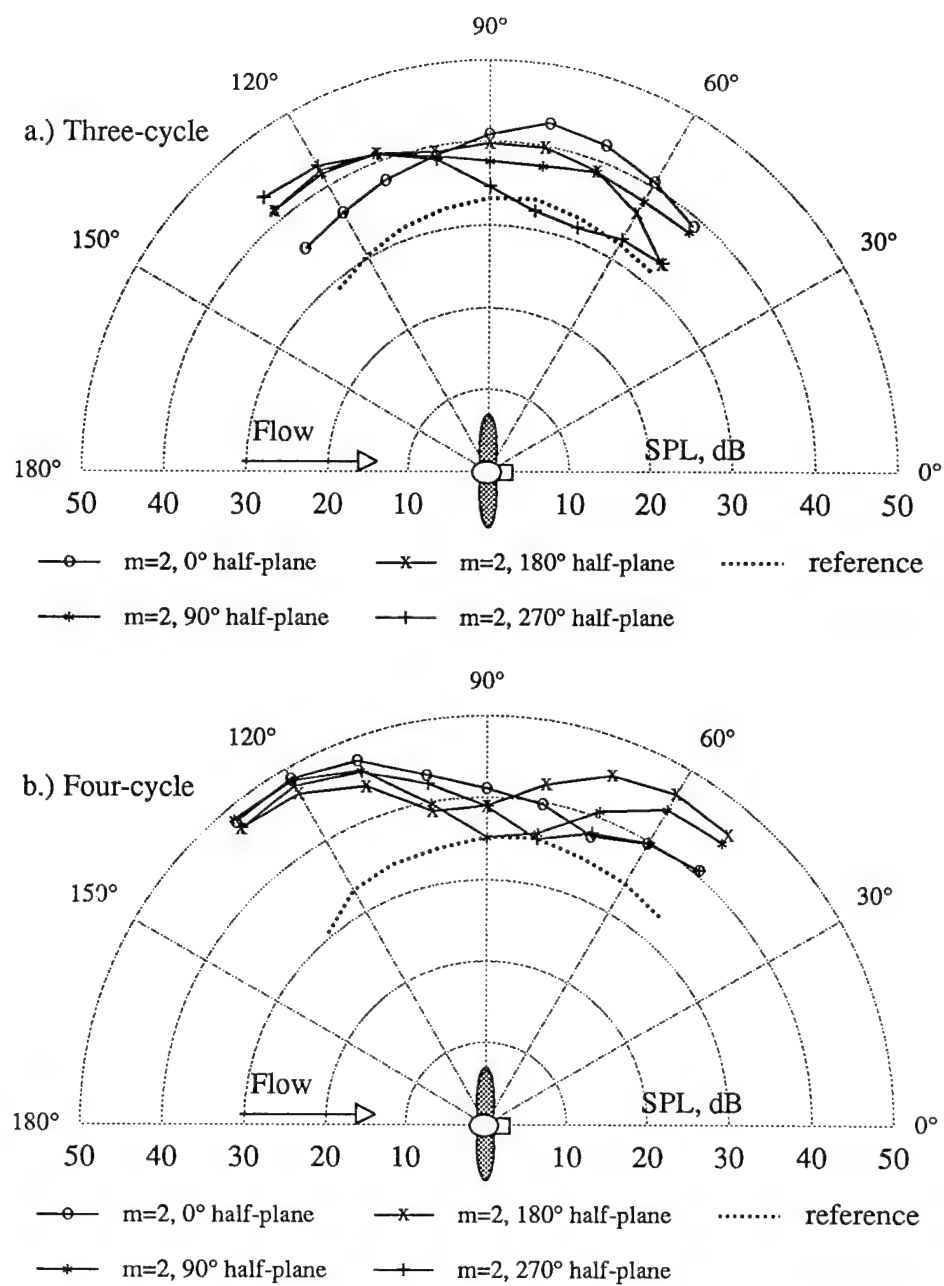Figure 10: First Harmonic Directivity due to Four-cycle Flow.   (a) 3000 RPM. (b) 3600 RPM.

Figure 11: Higher Harmonic Directivity from both screen flows. (a) Three-cycle Screen. (b) Four-cycle Screen.
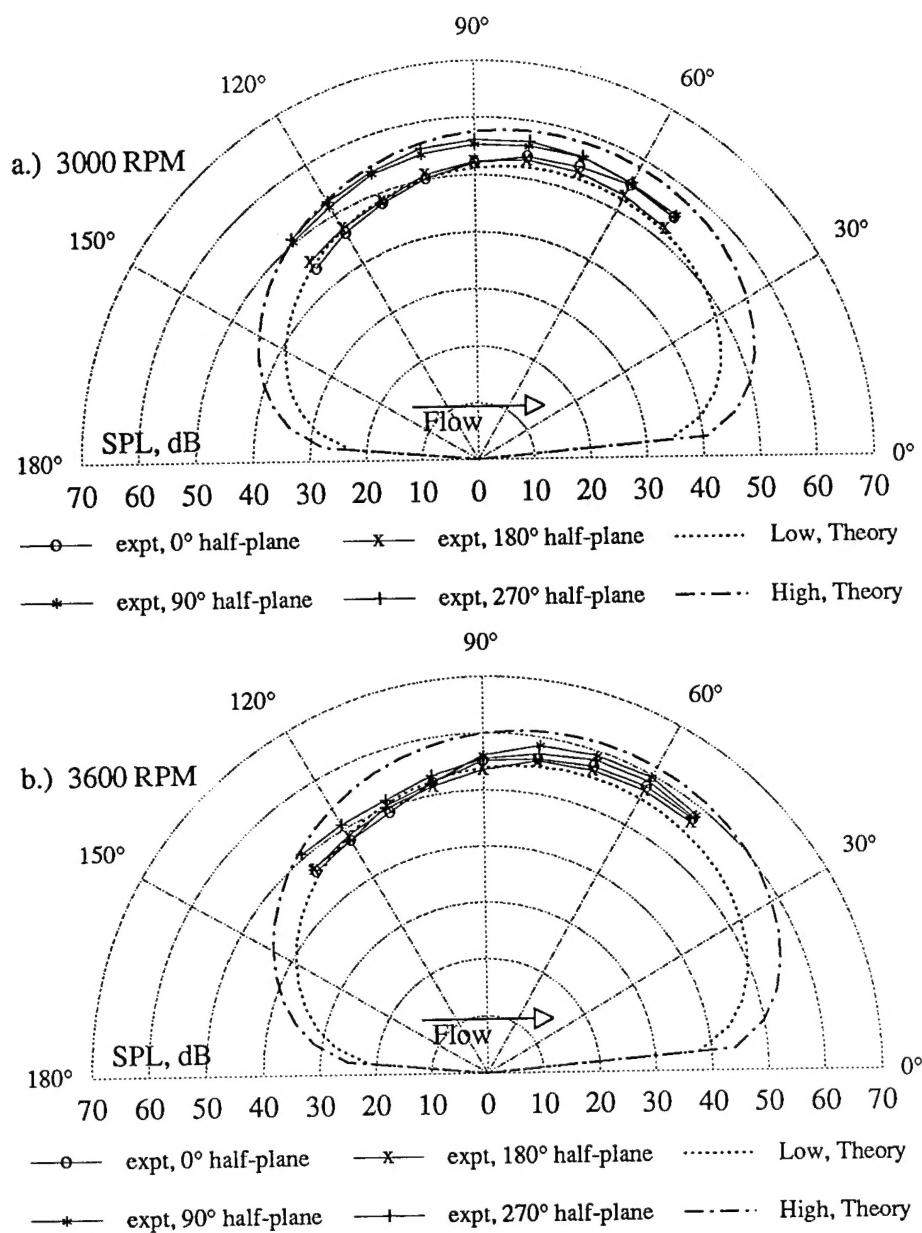
Figure 12: Comparison between Experiment and Theory for Three-cycle Flow. (a) 3000 RPM. (b) 3600 RPM.

r/R_t	c/D_t	P/D_t	t/Dt	g/D_t
0.2	0.1549	1.4600	0.0244	0.00020
0.3	0.1817	1.3850	0.0217	0.00460
0.4	0.2075	1.3425	0.0190	0.00580
0.5	0.2323	1.3055	0.0164	0.00620
0.6	0.2550	1.2790	0.0137	0.00610
0.7	0.2710	1.2620	0.0110	0.00569
0.8	0.2720	1.2555	0.0084	0.00471
0.9	0.2343	1.2525	0.0058	0.00333
0.95	0.1776	1.2510	0.0045	0.00216
1.00	0.0000	1.2500	0.0032	0.00000

Table 1: Geometry of DTRC Model Propeller 3714.

LIST OF LEGENDS

a_p amplitude of non-uniformities

c chord length of blade section

D diameter

dB decibels

EAR expanded area ratio for propeller

g section camber

Hz Hertz, unit of frequency

m harmonic number

p aerodynamic mode for inflow distortion cycles

P propeller pitch, $2\pi r \tan\gamma$

r radius of propeller at the section location

R_t propeller tip radius

RPM revolutions per minute

SPL sound pressure level

t section thickness

V freestream velocity in inertial frame

θ azimuthal angle (see Figure 2)

ϕ spherical angle (see Figure 2)

a subscript for volume average velocity

m subscript for mean velocity

**IN REPLY
REFER TO**   DTIC-OCC

1995 1024 0098

SUBJECT: Distribution Statements on Technical Documents

TO:
OFFICE OF NAVAL RESEARCH
CORPORATE PROGRAMS DIVISION
ONR 353
800 NORTH QUINCY STREET
ARLINGTON, VA 22217-5660

1. Reference: DoD Directive 5230.24, Distribution Statements on Technical Documents, 18 Mar 87.

2. The Defense Technical Information Center received the enclosed report (referenced below) which is not marked in accordance with the above reference.

> **FINAL REPORT**
> **N00014-93-1-0003**
> **TITLE: DEVEL. OF EXP. ENVERSION**
> **AND SIMULATION TECHNIQUES TO**
> **STUDY PROPELLER BLADE**
> **RESPONSE TO INFLOW DISTORTION**

3. We request the appropriate distribution statement be assigned and the report returned to DTIC within 5 working days.

4. Approved distribution statements are listed on the reverse of this letter. If you have any questions regarding these statements, call DTIC's Cataloging Branch, (703) 274-6837.

FOR THE ADMINISTRATOR:

1 Encl

GOPALAKRISHNAN NAIR
Chief, Cataloging Branch

FL-171
Jul 93